


1-1-2014

Pedestrian Head Protection During Car To Pedestrian Accidents: In The Event Of Primary Impact With Vehicle And Secondary Impact With Ground

Vishal Gupta
Wayne State University,

Follow this and additional works at: http://digitalcommons.wayne.edu/oa_dissertations

 Part of the [Biomechanics Commons](#), and the [Other Mechanical Engineering Commons](#)

Recommended Citation

Gupta, Vishal, "Pedestrian Head Protection During Car To Pedestrian Accidents: In The Event Of Primary Impact With Vehicle And Secondary Impact With Ground" (2014). *Wayne State University Dissertations*. Paper 885.

This Open Access Dissertation is brought to you for free and open access by DigitalCommons@WayneState. It has been accepted for inclusion in Wayne State University Dissertations by an authorized administrator of DigitalCommons@WayneState.

**PEDESTRIAN HEAD PROTECTION DURING CAR TO PEDESTRIAN
ACCIDENTS: IN THE EVENT OF PRIMARY IMPACT WITH VEHICLE
AND SECONDARY IMPACT WITH GROUND**

by

VISHAL GUPTA

DISSERTATION

Submitted to the Graduate School

of Wayne State University,

Detroit, Michigan

in partial fulfillment of the requirements

for the degree of

DOCTOR OF PHILOSOPHY

2014

MAJOR: MECHANICAL ENGINEERING

Approved by:

Advisor

Date

Co-advisor

DEDICATION

Dedicated to my parents, my wife (Meenu Gupta) and my son (Hardik Gupta)

ACKNOWLEDGEMENTS

I would like to thank Dr. King H. Yang for his invaluable guidance and support for this study. I am also grateful to Dr. Albert I. King, Distinguished Professor in Biomechanical Engineering at Wayne State University, and Dr. Trilochan Singh, Professor in Mechanical Engineering at Wayne State University, since this study was originally inspired by the discussions with them. I am especially grateful to Dr. Albert King for inspiration and ideas to carry out the work related to pedestrian head-on ground impact. I gratefully acknowledge the 'Detroit Engineered Products' (DEP) for providing the access to their morphing software known as 'DEP Morpher' for FE model shape change to use in this research work. I am also grateful to TASS for providing the access to MADYMO software along with pedestrian models for use in this study.

TABLE OF CONTENTS

Dedication.....	ii
Acknowledgements.....	iii
List of Tables.....	vii
List of Figures.....	viii
Chapter 1: Introduction.....	1
Chapter 2: Epidemiology and Anatomy of Frequently Injured Body Regions.....	4
2.1: Anatomy and Injury types.....	8
2.2: Head Anatomy and Injuries	8
2.2.1 Brain Anatomy and Injuries.....	10
2.3: Knee Anatomy and Injuries	13
Chapter 3: Overall Impact Kinematics, Injury Mechanism and Injury Criteria.....	15
3.1 Overall Body Kinematics.....	16
3.2 Injury Criteria and Threshold	18
3.2.1 Head Injury Criteria.....	18
3.2.2 Lower Extremity Injury Criteria.....	21
Chapter 4: Testing Tools, Testing Regulations and Safety Standard.....	23
4.1: Physical Test Devices	23
4.1.1 Local Impactors.....	23
4.2 Pedestrian Test Dummies.....	27
4.3 Mathematical Models	31
4.3.1 Lower Extremity FE Models.....	31
4.3.2 Head FE Models.....	31

4.3.3 THUMS 'Total Human Body Model for Safety'.....	36
4.3.4 MADYMO Pedestrian Models.....	36
4.4 Brief History of Pedestrian Safety Test Procedures Research.....	38
4.5 European Union Directive Regulation.....	39
4.6 Global Technical Regulation.....	40
4.7 EuroNCAP Pedestrian Safety Rating System.....	44
Chapter 5 Current Pedestrian Safety Countermeasures.....	47
5.1 Passive Safety Countermeasures.....	47
5.2 Active Safety Countermeasures.....	53
Chapter 6 Aims of Study.....	56
Chapter 7 Aim 1 – Feasibility of new hood edge designs for pedestrian head safety improvements	60
7.1 Methods.....	60
7.2 Shape parameters along hood edges.....	63
7.3 Results.....	69
7.4 Discussion.....	75
Chapter 8 Aim 2 - Evaluating practicality of Pedestrian Head Safety Regulations.....	77
8.1 Method.....	77
8.2 Results.....	85
8.3 Discussion.....	95
Chapter 9 Aim 3 - Effect of vehicle front-end profiles leading to pedestrian secondary head-on impact to ground	105
9.1 Method.....	106

9.2 Results.....	108
9.3 Discussion.....	118
Chapter 10 Conclusions and Future Works	128
10.1 Future Works.....	131
Appendix A- Vehicle FE Model Details and validation.....	133
Appendix B – Glossary of Vehicle Structure.....	141
Appendix C – Head Acceleration Histories.....	143
Appendix D: MADYMO pedestrian model validation summary.....	148
Appendix E: Method for calculating vehicle lowering amount relative to ground.....	150
Appendix F: Effect of front-end profile changes on frontal crash performance.....	151
References.....	154
Abstract.....	165
Autobiographical Statement.....	167

LIST OF TABLES

Table 4.6.1: GTR Injury Criterion.....	42
Table 4.7.1: EuroNCAP Injury Criterion.....	45
Table 7.1.1 Preliminary results for Head Impact on vehicle Hood.....	61
Table 7.3.1: Effect of the shotgun to fender interface change on HIC.....	71
Table 7.3.2: Effect of the hood inner section changes on HIC.....	73
Table 7.3.3: Effect of important shape changes along hood periphery on HIC.....	74
Table 8.1.1: Parameters values for vehicle front end profiles.....	79
Table 8.2.1: Mid-size vehicle - simulation setups and results.....	93
Table 8.2.2: SUV - simulation setups and results.....	94
Table 8.2.3: Sensitivity of HIC and Head impact angle for variation in pedestrian Posture during impact with mid-size car (profile 2) at 40 km/h.....	95
Table 8.3.1: Comparison of HIC based on full scale pedestrian model (column G) against HIC based on free motion headform at 65 degree (column H) and HIC based on free motion headform at same angle as predicted by full pedestrian model (column I).....	102
Table 8.3.2: Comparison of HIC and Head impact angle based on PMHS test, Pedestrian FE model and free motion headform.....	103
Table 9.2.1: Mid-size vehicle - simulation setups and results for ground impact.....	114
Table 9.2.2: SUV - simulation setups and results for ground impact.....	115
Table A.1: Effect on HIC with missing details in the FE model at some locations.....	133
Table D.1: Car-pedestrian impact tests used for validation of the pedestrian models..	149

LIST OF FIGURES

Figure 2.1: Distribution of Road Accidents by Road Users.....	4
Figure 2.2: PCDS distribution of all pedestrian injuries by body region.....	6
Figure 2.3: Comparison of Injury Distribution due to light trucks and passenger cars.....	8
Figure 2.2.1: Lateral view of skull and brain.....	9
Figure 2.3.1: Knee Joint and Knee Ligaments.....	14
Figure 3.1.1: Overall body kinematics: Pedestrian impact to car at 40km/h.....	16
Figure 3.2.1: WSTC Head Injury Tolerance Curve.....	19
Figure 4.1.1: Physical Test Devices for Lower Legform a) TRL-LFI, b) Flex PLI.....	25
Figure 4.1.2: Headform Impactor for Euro NCAP-Pedestrian Testing Protocol.....	27
Figure 4.2.1: Full Body Pedestrian Dummies: from left to right; Polar II (adapted from Akiyama et al., 1999), Autoliv child pedestrian, Autoliv adult pedestrian..	29
Figure 4.3.1: Mathematical head models A) Strasbourg University finite element head model, B) Wayne State University finite element head model.....	32
Figure 4.3.2: The GHBMC FE head model developed by WSU. (a) isometric view of The head model (d) medium sagittal view of the head model; (g) skull and facial bones; (b) 11 bridging veins; (e) falx and tentorium; (h) brain; and (c),(f),(i) brain sectional views in three directions (horizontal, sagittal, and coronal).....	35
Figure 4.3.3: MADYMO Pedestrian family including 3yr old, 6 yrs old, small female, small male and large size male.....	37
Figure 4.6.1: GTR Test Procedure for pedestrian safety.....	41
Figure 4.6.2: Example of marking of HIC 1000 and HIC 1700 zone in GTR Test.....	42
Figure 4.6.3: Pedestrian Head Impact Legal Requirement.....	43
Figure 4.7.1: EEVC Test setups and impact zones	45
Figure 5.1.1: Hood Inner panel patterns for uniformed strength distribution (a) Ford	

Kuga 2.0 inner panel (b) Toyota Corolla 1.8 LE hood inner panel.....	48
Figure 5.1.2: (a) wave type hood panel (b) beam type hood panel (c) acceleration Curve comparison	50
Figure 5.1.3: Different hood hinge concept for better pedestrian safety.....	52
Figure 5.1.4: Exploded view of the sandwich design for main hood area (upside-down view of the hood assembly).....	53
Figure 5.1.5: Enlarged sectional view of sandwich hood assembly.....	53
Figure 5.2.1: Concept of active hood system.....	54
Figure 7.1.1 Selected head impact simulation points along various WAD lines	61
Figure 7.1.2: HIC values predicted by a computer model mimicking an ISO headform impacting a full size SUV vehicle hood at 35 km/h along various impact points on hood. Zone 1 indicates those points with HIC>1,300, Zone 2 indicates those points with HIC >1,000 and green portion represents those points with HIC <1000.....	63
Figure 7.2.1: Cross-section view showing the section cut for fender, hood panels and shotgun: a) original interface, b) fender flange lowered along with the shotgun, c) fender flange at original position with crushable bracket for fender to shotgun bolting, and d) flat flange for fender with crushable bracket for fender to shotgun bolting.....	64
Figure 7.2.2: Lateral view for shotgun to fender interface: a) fender directly bolted to shotgun, b) fender bolted to shotgun by means of crushable brackets....	65
Figure 7.2.3: a) Original shotgun b) morphed shotgun (lowered by 90mm).....	65
Figure 7.2.4: cross-section view with section cut for fender, hood panels and shotgun showing hood inner panel's section changing in width and height. a) Original cross-section b) Section width reduced by moving section Inward c) Section height reduced by moving section upwards.....	66
Figure 7.2.5: cross-section view with section cut for fender, hood panels and shotgun a) hood inner panel cross section, and b) hood inner cross section with b) shear panel (highlighted in the circle).....	67
Figure 7.2.6: styling surface with penetrating under hood structure.....	68
Figure 7.3.1: Bracket buckling behavior a) 60 mm shotgun lowering- desirable bracket	

deformation resulting in more deformation space, b) 90 mm shotgun lowering-bad bracket buckling mode, resulting in lower deformation.....	70
Figure 7.3.2: Proposed fender to shotgun interface.....	70
Figure 7.3.3: Concept of raised hood using passive raised hinge design to create deformation space between hood and shotgun.....	71
Figure 7.3.4: HIC variation as a function of design variables along different impact locations.....	75
Figure 7.4.1: Head performance along hood top and edges after implementing hood shape parameters.....	76
Figure 8.1.1: Vehicle parameters morphed to develop different front-end profiles.....	79
Figure 8.1.2: Different front end vehicle profiles for the mid-size car with respect to a 50 th percentile male.....	80
Figure 8.1.3: Different front end vehicle profiles for the SUV with respect to a 50 th percentile male.....	80
Figure 8.1.4: Cross-section cut showing clearance change between hood panel and under hood packaging when vehicle front-end profile changed.....	81
Figure 8.1.5: Ramp angle for lowered front-end profile and raised front-end profile.....	81
Figure 8.1.6: (a) front view of pedestrian positioning along the vehicle front end (b) pre-impact position of pedestrian in the simulation setup.....	83
Figure 8.1.7: Pre-impact position of pedestrian (a) left leg back, right leg front, Impacting on left side, (b) left leg front, right leg back, impacting on left side, and (c) left leg back, right leg front, impacting on right side.....	83
Figure 8.1.8: Head Impact angle definition based on GTR.....	84
Figure 8.1.9: Free motion head-form simulation setup (a) at actual impact angle of Simulation number 8 on SUV as in Table 3 (b) at 65 degrees impact Angle as per safety regulation.....	85
Figure 8.1.10: Free motion head-form setup on windshield (a) at an actual impact angle obtained from test number 20 on mid-size car as listed in Table 2 (b) at 65 degrees impact angle as per EuroNCAP rating standard.....	85

Figure 8.2.1: Pedestrian kinematics of a small female (5 th percentile) pedestrian striking with the SUV (profile2) at 40 km/h	87
Figure 8.2.2: Pedestrian kinematics of small female striking with mid-size vehicle profile1 (raised front end) at 40 km/h.....	88
Figure 8.2.3: Pedestrian kinematics of the mid-size male striking with SUV profile3 (lowered front end) at 40 km/h.....	89
Figure 8.2.4: Pedestrian kinematics of the mid-size male striking with mid-size vehicle profile 2 at 40 km/h.....	90
Figure 8.2.5: Pedestrian kinematics of a 6 year old child pedestrian striking with the mid- size vehicle (profile3) at 40 km/h.....	91
Figure 8.2.6: Pedestrian kinematics of a 6 year old child pedestrian striking with the mid-size vehicle (profile3) at 30 km/h.....	92
Figure 8.3.1: Pedestrian kinematics comparison (a) 6 year old child pedestrian striking with the mid-size vehicle (profile1) at 40 km/h, and (b) small female (5 th percentile) pedestrian striking with the mid-size vehicle (profile1) at 40 km/h.....	97
Figure 8.3.2: Pedestrian kinematics of a 6 year old child pedestrian striking with the SUV (profile1) at 30 km/h.....	97
Figure 8.3.3: Comparison of the head impact angles for various pedestrians striking with different front-end profiles of the midsize car at 30 km/h.....	98
Figure 8.3.4: Comparison of the head impact angles for various pedestrians striking with different front-end profiles of the midsize car at 40 km/h.....	99
Figure 8.3.5: Comparison of the head impact angles for various pedestrians striking with different front-end profiles of the SUV at 30 km/h.....	100
Figure 8.3.6: Comparison of the head impact angles for various pedestrians striking with different front-end profiles of the SUV at 40 km/h.....	101
Figure 8.3.7: Pedestrian kinematics comparison (a) 50 th percentile pedestrian striking with mid-size car profile2 at 40 km/h, and (b) PMHS test01	104
Figure 9.1.1: Front end profile for the mid-size car with and without simulated pop-up hood.....	106

Figure 9.2.1: Pedestrian kinematics during Impact with mid-size car (Profile2).....	109
Figure 9.2.2: Average HIC comparison during primary impact and secondary impact for pedestrian striking with various profiles of the mid-size car at 40 km/h.....	110
Figure 9.2.3: Average HIC comparison during primary impact and secondary impact for pedestrian striking with various profiles of the SUV at 40 km/h.....	110
Figure 9.2.4: Comparison of pedestrian kinematics (a) mid-size male striking with SUV profile1 (raised front end) at 30 km/h (b) small female striking with SUV profile3 (lowered front end) at 30 km/h.....	112
Figure 9.2.5: Pedestrian kinematics (a) mid-size male with mid-size car profile1 (raised front end) at 40 km/h (b) mid-size male with mid-size car profile3 (lowered front end) at 30 km/h.....	113
Figure 9.2.6: Pedestrian kinematics of mid-size male striking with the mid-size car profile2 at 40 km/h.....	116
Figure 9.2.7: Pedestrian kinematics of mid-size male with mid-size car profile2 having pop up hood.....	117
Figure 9.3.1: Kinematics of 6 year old child pedestrian striking with the mid-size car profile1 at 40 km/h.....	120
Figure 9.3.2: Comparison of head CG trajectory for 50 th percentile pedestrian with Three different profiles of the simulated mid-size car.....	122
Figure 9.3.3: Comparison of head CG velocity for 50 th percentile pedestrian with Three different profiles of the simulated mid-size car.....	123
Figure 9.3.4: Kinematics of 6 years old child pedestrian striking with the mid-size car profile3 (lowered front-end) at 40 km/h.....	124
Figure 9.3.5: Kinematics of 6 years old child pedestrian striking with the mid-size car profile 3 (lowered front-end) at 30 km/h.....	125
Figure A.1: Velocity comparison- SUV FE simulation vs. test data.....	134
Figure A.2: Acceleration comparison- SUV FE simulation vs. test data.....	135
Figure A.3: SUV FE model energy balance.....	135
Figure A.4: Velocity comparison- Mid Size Car FE simulation vs. test data.....	137

Figure A.5: Acceleration comparison- Mid Size Car FE simulation vs. test data.....	137
Figure A.6: adhesives modeled between hood outer and inner panels.....	139
Figure A.7: Rear Hinges modeled in details with actual bolts.....	140
Figure B.1: glossary of vehicle structure terms- Surface A.....	141
Figure B.2: glossary of vehicle structure terms- Surface B.....	142
Figure B.3: adhesives between hood outer panel and hood inner panel.....	142
Figure C.1: comparison of head accelerations – the original model vs. final updated model.....	143
Figure C.2: comparison of head accelerations – the original model vs. final updated model.....	144
Figure C.3: comparison of section forces- original vs. modified shotgun (section Defined in middle of the shotgun).....	145
Figure C.4: comparison of section forces- upper vs. lower load path.....	146
Figure C.5: vehicle acceleration history- original model vs. modified model (measured at B-Pillar and Rocker Intersection).....	147
Figure C.6: Shotgun energy absorption capacity- original model vs. modified model..	147
Figure D.1: Different impactor test configurations used for model validation.....	148
Figure E.1: tire compression measurements.....	150
Figure F.1: Mid-size car acceleration comparison for different front-end profiles During frontal crash.....	151
Figure F.2: Mid-size car velocity comparison for different front-end profiles during Frontal crash.....	152
Figure F.3: SUV acceleration comparison for different front-end profiles during frontal crash.....	153
Figure F.4: SUV velocity comparison for different front-end profiles during frontal crash	153

Chapter 1: Introduction

Pedestrians are extremely vulnerable as road users, and pedestrian protection is becoming one of the major issues in traffic safety world-wide. It is estimated that approximately 1.2 million deaths occur worldwide every year due to road accidents (Lopez et al., 2001). Among these, 65% of the fatalities were due to pedestrian accidents and 35% of those pedestrian involved were children (The World Bank 2002). In the United States, pedestrian deaths constitute the second largest category of victims related to motor vehicle accidents (Ballesteros et al., 2004), though, they account for only 11% of all traffic fatalities (Zhang et al., 2004). Furthermore, pedestrian *fatalities* are only part of the problem, as the number of pedestrians surviving vehicle impacts with injuries far exceeds the number of fatalities. All these fatalities and injuries caused by traffic incidents led to significant economic and social costs.

In the last decade, lots of research efforts and measurements have been taken to reduce road accidents leading to pedestrian fatalities and these data have helped to reduce pedestrian fatalities significantly. Since 1997, the number of pedestrian fatalities has decreased by 10% to 4,784 from 5,264 in United States (NHTSA 2007).

There are several factors which have contributed towards improved pedestrian safety, such as enforced speed limits in residential areas and better traffic associated education for children. During the last 10-15 years, car designs have undergone significant changes like smoother front end shapes, shorter hoods, better energy absorbing hood and bumper designs, integrated headlamps, and anti lock brake system (ABS). Some of these changes originally implemented for some other purposes, such

as ABS, have benefited pedestrian protection (Matsui et al., 1998; Barrios et al., 2009) as well. Still in most developing countries such as India and China, due to expanding vehicle fleets and different types of road user involved, the situation of pedestrian accidents and fatalities has not improved (Mohan 2002; Li et al., 2008).

This thesis is separated into 10 chapters. Epidemiology of road accidents and pedestrian involved along with the injury distribution in different body regions in those accidents are presented in Chapter 2 by using a detailed accident data and other literature sources. In general, the head and legs are the two most frequently injured body regions in pedestrian accidents. Chapter 2 also presents head and legs anatomy and their injury types. Chapter 3 presents head and leg injury mechanism and injury tolerances along with pedestrian kinematics during pedestrian accident. A brief summary of different test devices used or proposed is described in Chapter 4 along with different mathematical models for subsystem level devices, full dummy models and different human body models. Chapter 4 also presents a detailed study of different safety regulations and tests designed by various organizations to counteract the problem of pedestrian safety. In pedestrian safety research, different test devices are proposed for pedestrian safety measurement such as subsystem level devices like lower legform, upper legform and free motion head or full pedestrian dummy. Chapter 5 presents some of the recent developments in the area of pedestrian safety such as Impact absorbing hood designs and impact absorbing bumpers as result of optimizations, collapsible hinges and latches, active hood system etc. Finally, aims of this dissertation are presented in Chapter 6.

Chapter 7 describes the effect of hood periphery shape parameters and hood-fender interface characteristics on pedestrian head injury measures. Chapter 8 discusses practicality of pedestrian safety regulation. Effect of vehicle front end profiles leading to pedestrian secondary head impact to ground are discussed in Chapter 9. Some of the conclusions of this study are described in Chapter 10.

Chapter 2: Epidemiology and Anatomy of Frequently Injured Body Regions

Approximately 1.2 million road traffic fatalities occur each year (The World Bank, 2002). The number of pedestrians surviving vehicle impacts with injuries far exceeds the number of fatalities. Figure 2.1 shows that, in Japan, among different types of road users, pedestrians are the second highest involved in road accidents after passenger car occupants.

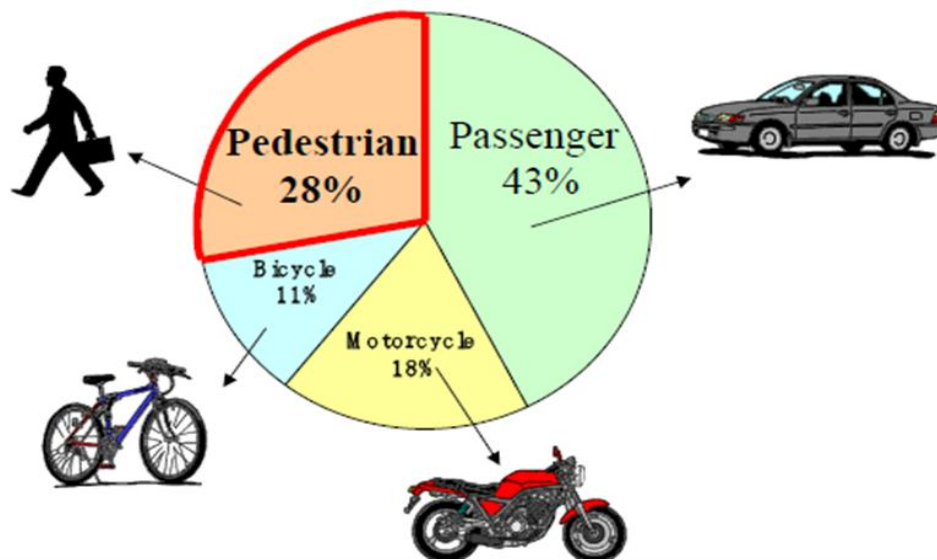


Figure 2.1: Distribution of road accidents incidents by road users [The traffic accident white paper 2002 edition, Japan]

In the year 2002, 4,808 pedestrians were killed in traffic crashes in the US. In addition, 71,000 pedestrians were injured in 2002, according to US traffic safety facts (NHTSA, 2003). This means that there is a pedestrian related fatality every 109 minutes and a pedestrian related injury every 7 minutes. In 2007, there are more than 13 injured pedestrians for every pedestrian fatality (NHTSA, 2007).

Pedestrian fatalities comprised 11.2 % of all traffic fatalities in the US in 2002 (NHTSA, 2003). In many other parts of the world the pedestrian fatality rate is much

higher; 27-32% in Japan (Matsui et al., 2002), nearly 30% in the United Kingdom (Stammen et al., 2001), 16 % in Australia (Anderson and Mclean, 2001) and up to 85% in urban areas of Ethiopia (Jacobs and Thomas, 2002). Based on traffic accident data from Japan, around 5,744 fatalities occurred and roughly 30% of them were pedestrian. Pedestrian accounted for 17% serious injuries and 58% of pedestrian fatalities sustained head injuries (ITARDA, 2007). It has been analyzed that there are fewer overall cases of road accidents involving pedestrians compared to car to car accidents. But still the rate of injuries and fatalities among pedestrians are more compared to passenger car occupants.

The most common method of defining the injury severity in road accidents is Abbreviated Injury Scale (AIS) with a scale from 1 to 6 where 1 represents a minor injury, 2 moderate, 3 serious, 4 severe, 5 critical and 6 fatal injuries. Additionally, AIS 9 is used to indicate unknown status of injury severity. Distribution of AIS 2+ injuries from the Pedestrian Crash Data Study (PCDS) database in the U.S. shows that the frequency of injuries to the lower extremities and head dominates as shown in Figure 2.2. Because injuries to the head often lead to death so head injuries are considered as the most serious injuries. Lower limb injuries are also important because they could lead to long-term impairments and result in high social costs.

Of the 552 pedestrian cases available in the PCDS database, 203 pedestrians sustained AIS2+ lower extremity injuries (Klinich and Schneider, 2003). Distributions of lower extremity injuries by severity level were provided based on their functional injury classification scheme rather than anatomical classification which means instead of

classifying femoral condyle fractures as femur fractures, and tibial plateau fractures as tibia fractures, they classified both injuries as knee joint fractures.

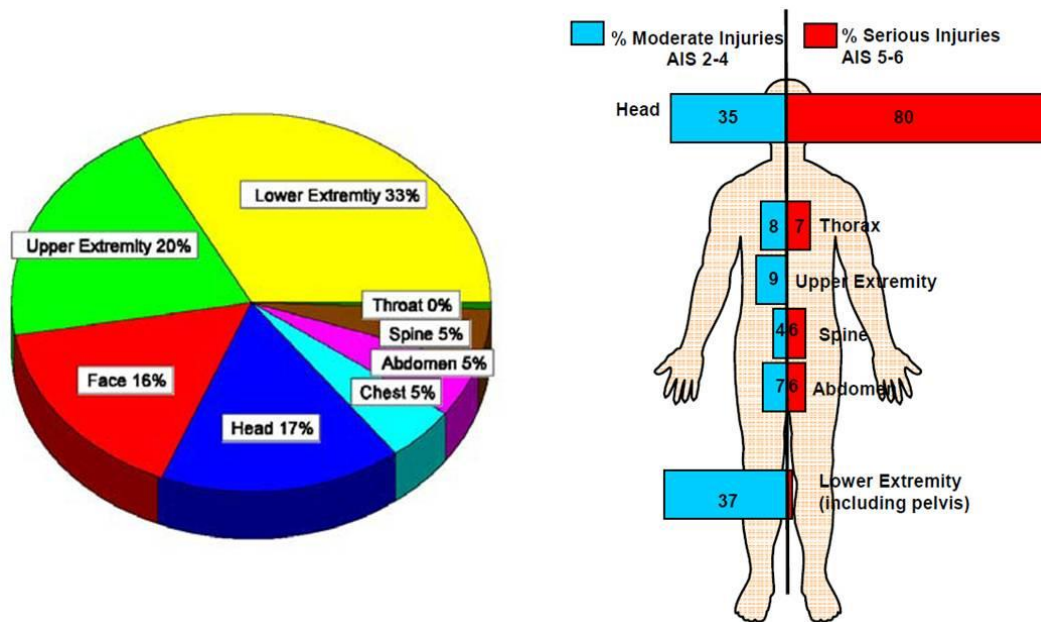


Figure 2.2: left: PCDS distribution of all pedestrian injuries by body region (Chidester and Isenberg 2001), and right: PCDS distribution of injuries by severity level and frequency.

While considering AIS 2 to AIS 4 level injuries (AIS 2+ and AIS 3+), leg (tibia and fibula) fractures were the most common injuries. When considering only the less severe injuries (AIS 2 and less), knee injuries (fractures and soft tissue injuries) are the second most common, followed by foot and ankle fractures, and pelvis/hip fractures (Klinich and Schneider, 2003). Examining the more severe AIS 3+ lower extremity injuries, injuries to the pelvis and hip are the second most common, followed by knee injuries (mostly fractures) and then thigh injuries (mostly femoral fractures) (Klinich and Schneider, 2003).

Teresinski and Madro (2001) performed detailed forensic autopsies of 357 fatally injured pedestrians, 214 (60%) of which had knee injuries. Among all pedestrians struck

laterally (165 cases), knee injuries were found in 94% of the cases. Bone bruises on the tibial plateau due to compression were found in a large proportion of the cases and femoral bruises were rare. Matsui et al. (1998) hypothesized that the distribution of lower extremity injuries will change as a result of changes in the trend of vehicle designs. Matsui et al. (1998) examined how the relative frequency of pedestrian injuries had changed over 10 years by comparing data sets compiled by the National Police Agency of Japan from 1987-1988 and 1993-1997. They found that despite decreases in femur (17% to 4%) and knee (10% to 1%) injuries, leg injuries increased (19% to 36%) considering the facts that lower leg injuries (tibia and fibula fractures) increased.

Ballesteros et al. (2004) revealed that compared to passenger vehicles, SUVs and pick-up trucks resulted in a higher percentage of injuries to the lower extremities above the knee. Longhitano (2005a) used the PCDS data to compare pedestrian injury distribution of light trucks with those of passenger car. It was found that light truck vehicles caused 43% AIS 3+ injuries to lower extremities and 81% AIS 3+ injuries to head and neck compared to 39% injuries to lower extremities and 71% injuries to head and neck caused by passenger cars as shown in Figure 2.3.

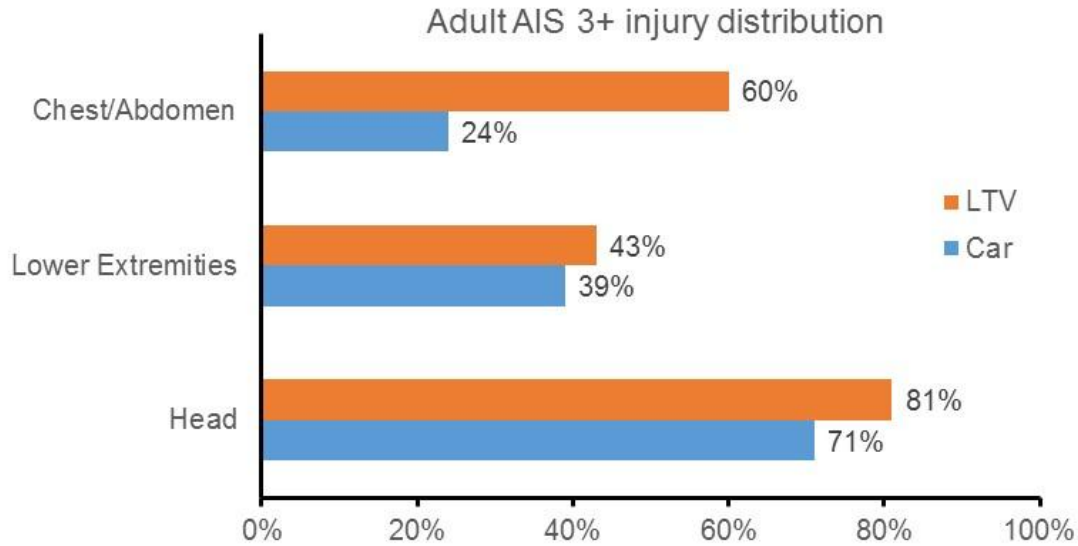


Figure 2.3: Comparison of injury distribution due to light trucks and passenger cars (Longhitano, 2005a).

2.1 Anatomy and Injury types

As previously described, the most frequently injured body region in pedestrian to car crashes is lower extremities followed by upper extremities and head. US data shows that for AIS 3 to AIS 5 injury types, head is most frequently injured body region (Longhitano et al., 2005b). Japanese data shows that for AIS 2 to AIS 3 injury types, lower extremities are the most injured (Matsui et al., 2002). The following sections briefly review the anatomy of head and lower extremity to better appreciate the complex nature of injuries in these two body regions.

2.2 Head Anatomy and Injuries

A brief overview of head anatomy and head injury types help to understand the head injury mechanism. In this study, the head is defined as the body region consisting of scalp, skull, cranium, meninges, and brain. A more detailed description can be found in Wisnans et al. (2000). The scalp is 5 to 7 mm thick layer consisting of hair, skin and

facial muscles. Scalp swelling and laceration are common types of injuries in pedestrian accidents when pedestrian head hits directly to car structure or ground. The skull is a strong box around the brain consisting of eight different bones: the unpaired frontal, occipital, sphenoid, ethmoid bones and the paired temporal and parietal bones as shown in Figure 2.2.1 (adapted from Gray's anatomy, 2000). Each bone has three different layers; Inner, Outer and Diploes.

Skull fracture can occur with or without brain damage. Skull fractures by themselves are not life threatening (Genneralli, 1985). Skull fractures are categorized as linear or depressed. In a linear skull fracture, the skull is cracked only in the form of single line. The linear fracture is not severe itself but it can cause the rupture of dural arteries under the skull resulting in extradural hematoma. A depressed fracture is defined as depression of a bone fragment larger than the thickness of skull. In this type of fracture the depressed fragment can be pushed into cranial cavity and can damage brain tissue and blood vessels (Genneralli, 1985).

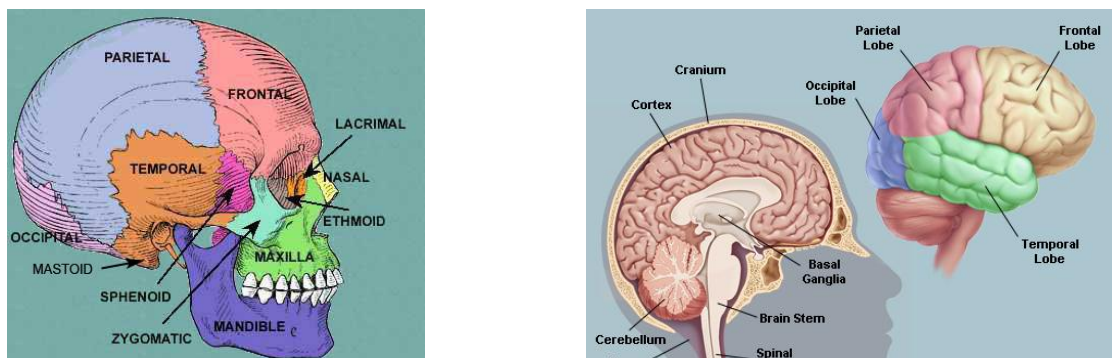


Figure 2.2.1: Lateral view of skull and brain (adapted from WebMD, LLC)

Underneath the skull there are three layers of soft tissues called meninges which cover and protect the brain and spinal cord. First layer below skull is dura mater which

is attached to skull and consists of outer and inner layers. Attached to the inner layer of the dura mater is the spider web like arachnoid mater. Third layer is pia mater which is thin membrane below arachnoid mater and it intimately adheres to the surface of the brain. Between the arachnoid and the pia mater is the subarachnoid space containing the cerebrospinal fluid (CSF). The CSF acts as shock absorber to cushion the brain from injury when jolted or hit (adapted from Gray, 2000).

2.2.1 Brain Anatomy and Injuries: The most part of brain anatomy and brain injury written in this dissertation is adapted from Melvin et al., 1994. The brain is the most complex and important organ of human body. It can be divided into three major parts, the cerebrum, brainstem and cerebellum. The cerebrum is the largest part of brain accounting for almost 85% of brain's mass. It is made up of left and right hemispheres which are separated by falx cerebri. Each hemisphere is divided into four lobes which are frontal, parietal, temporal and occipital lobes as shown in Figure 2.2.1. These lobes are named after the nearest cranium bone. The exterior surface of cerebrum is called cortex and is composed of gray matter. Under the cerebral cortex is a thick layer of white matter which connects the cerebral hemispheres with other parts of brain. The brainstem is made up of midbrain, pons and medulla oblongata. The brainstem contains fibers which connect the brain to spinal cord. These fibers provide the functionality for sensory and motor control. The cerebellum is composed of two lobes which are connected by bundle of white fibers called vermis. The name cerebellum is from Latin meaning the little brain. Cerebellum is situated at the base of the skull beneath the occipital lobes of the cerebral cortex and just behind the pons and medulla oblongata. The cerebellum is comprised of white matter and a thin outer layer of densely folded

gray matter. The folded outer layer of the cerebellum has smaller and more compact folds than those of the cerebral cortex. The cerebellum contains hundreds of millions of neurons for processing data. The cerebellum is involved in several functions of the body like fine movement coordination, balance and equilibrium and muscle tone etc.

Brain Injuries sometimes referred as Traumatic Brain Injury (TBI) lead to approx 50,000 deaths annually in US and motor vehicle accidents are the leading cause for that followed by sports, falls and intentional violence (Langlois et al., 2006). Brain injury happens due to translational and/or rotational forces caused by acceleration or deceleration of brain. When head hits a stationary object, like pedestrian head hitting windshield or hood, causes the head to decelerate and generating forces on brain. Brain injury can happen by force directly applied to head or force applied to head via neck as in whiplash injuries (McLean and Anderson, 1997). Both cases can set head in motion resulting in translational and rotational acceleration change. This can result in deformation of the brain tissue. If the magnitudes of deformation are great enough the tissue will fail, either in a physiological sense or a mechanical sense. There is a debate whether most of these deformations are produced by translational acceleration, rotational acceleration or both. Brain injuries can be either focal or diffuse. Focal injuries are due to localized damage to blood vessels and/or tissues. Focal brain injuries (Melvin et al. 1994) are Epidural Hematomas (EDH), Subdural Hematomas (SDH), Intracerebral Hematomas (ICH) and Contusions. Epidural Hematomas (EDH) is due to rupture of blood vessels between the skull and dura mater and it can occur with or without skull fracture. Subdural Hematomas (SDH) is due to rupture and tearing of the veins and arteries between the dura mater and the arachnoid mater. Intracerebral Hematomas

(ICH) is referred to homogeneous loss of blood within the cerebral cavity due to rupture of large vessels located inside brain. Contusion also called bruise is caused when blood vessels are damaged or broken as the result of a blow to the skin (bumping against something or hitting with a hammer). The raised area of a bump or bruise results from blood leaking from these injured blood vessels into the tissues as well as from the body's response to the injury. Contusion could occur at the site of impact called coup contusion and/or at the opposite side of impact called countercoup contusion. Countercoup contusion occurs mainly in frontal and temporal poles, where brain impacts against irregular bony floor of skull.

Diffuse injuries consist of concussion and diffuse axonal injury (DAI). Concussion is a disturbance of function of the nerve cells in the brain as a result of a blow to the skull. This means that parts of the brain's functions are temporarily 'on hold.' The symptoms include temporary unconsciousness, headache and, often, a loss of memory concerning the critical incident. Diffuse axonal injury is mechanical disruption of many axons in the white matter and it may extend into the midbrain and brainstem. Diffuse axonal injury occurs in about half of all severe head traumas, making it one of the most common traumatic brain injuries. Unlike a focal brain injury, it occurs over a more widespread area. In addition to being one of the most common types of brain injuries, it's also one of the most devastating. As a matter of fact, severe diffuse axonal injury is one of the leading causes of death in people with traumatic brain injury (Vik et al., 2006). Diffuse axonal injury isn't the result of a blow to the head. Instead, it results from the brain moving back and forth in the skull as a result of acceleration or deceleration. Automobile accidents, sports-related accidents, violence, falls, and child abuse such as

Shaken Baby Syndrome are common causes of diffuse axonal injury (Vik et al., 2006). When acceleration or deceleration causes the brain to move within the skull, axons, the parts of the nerve cells that allow neurons to send messages between them, are disrupted. As tissue slides over tissue, a shearing injury occurs. This causes the lesions that are responsible for unconsciousness, as well as the vegetative state that occurs after a severe head injury. A diffuse axonal injury also causes brain cells to die, which cause swelling in the brain. This increased pressure in the brain can cause decreased blood flow to the brain, as well as additional injury. The shearing can also release chemicals which can contribute to additional brain injury. The main symptom of diffuse axonal injury is lack of consciousness, which can last up to six hours or more.

2.3 Knee Anatomy and Injuries

The most of knee anatomy and injuries is adapted from (Kaneta et al., 2010). Among the most injured lower extremities during pedestrian crashes are lower leg, upper leg and knee. Injuries related with knee ligament shearing and tearing are the most common type of injuries associated with pedestrian accidents. Knee joint is made up of three bones and a variety of ligaments. The knee is formed by the femur (the thigh bone), the tibia (the shin bone), and the patella (the kneecap). Several muscles and ligaments control the motion of the knee and protect it from damage at the same time.

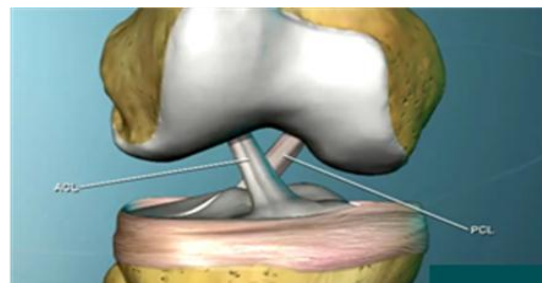


Figure 2.3.1: Knee joint and knee ligaments (adapted from WebMD, LLC)

There are 4 major ligaments that stabilize the knee as shown in Figure 2.3.1. Medial Collateral Ligament (MCL) is on the inner side of knee and Lateral Collateral Ligament (LCL) is on the outer side of knee. Collateral ligaments give sideways stability to knee. Two ligaments cross in the center of the knee. The ligament towards the front is anterior cruciate ligament (ACL) and one towards the back is posterior Cruciate Ligament (PCL). ACL prevents the tibia from moving forward and PCL prevents it from moving backward. If ACL tears occurred, then tibia can have too much forward motion and knee can be unstable.

Chapter 3: Overall Impact Kinematics, Injury Mechanism and Injury Criteria

Accident analysis shows that majority of pedestrian are impacted by the vehicle in a lateral direction. It is generally accepted that in the most representative pedestrian to car crash, the pedestrian is in normal walking posture, meaning that the pedestrian is standing sideways to the vehicle, and is struck by the vehicle from the side (Chidester and Isenburg, 2001). Further PCDS data shows that 75 (14%) pedestrians are impacted on their anterior face, 42 (8%) on their posterior face, 228 (41.3%) on their left side, 178 (32%) on their right side, and 29 (5%) were unknown. When anterior and posterior impacts are grouped together and left and right side impacts are grouped with lateral impacts, it can be seen that the lateral impacts account for almost 74% of pedestrian collisions.

Along with the body orientation, it is necessary to specify a leg orientation (stance) representative of impacted pedestrians in a pre-crash orientation. The PCDS data shows that 31 (6%) of the pedestrians impacted were standing with legs together, 27 (5%) were impacted with legs apart laterally, 362 (65%) were found to be in a gait stance at the time of collision, and 132 (24%) were in some other unknown stance. A total of 127 (23%) pedestrians were struck laterally with the struck-side limb back and 143 (26%) pedestrians were struck laterally with the struck-side limb forward. Chidester and Isenburg (2001) found that prior to crash, physical motions of 289 (55%) pedestrians were reported as walking and that 376 (72%) of the pedestrians had one limb forward and apart from the other limb at the time of impact.

3.1 Overall Body Kinematics

The nature of the injuries sustained by impacted pedestrians depends critically on the victim's body kinematics. The overall body kinematics of an adult pedestrian struck by a vehicle is shown in Figure 3.1.1. The first impact is generally between the pedestrian knee region and the vehicle's front bumper. Because this initial contact is usually below the pedestrian's centre of gravity, the upper body in such a case begins to rotate toward the vehicle. The second contact is usually between the upper part of the grille or front edge of the hood and the pedestrian's pelvic area. The pedestrian's legs and pelvis have reached the linear velocity of the vehicle at this point and the upper body (head and thorax) are still rotating toward the vehicle. The final phase of the collision involves the head and thorax striking the vehicle with a linear velocity approaching that of the initial striking velocity of the vehicle.

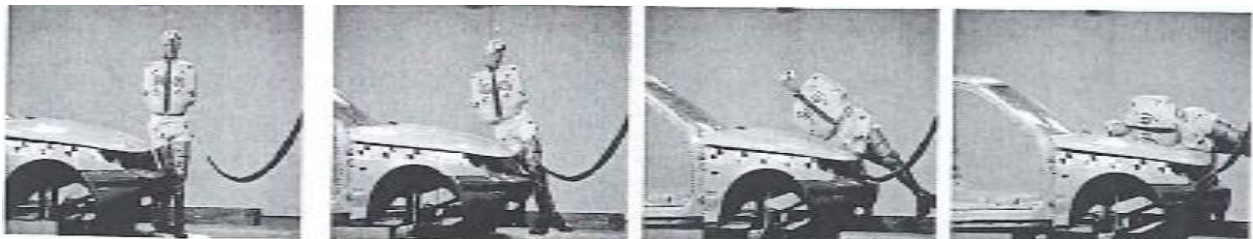


Figure 3.1.1: Overall body kinematics: Pedestrian impact to car at 40km/h (Kerrigan et al., 2007a)

The overall body kinematics depends on several factors such as pedestrian size, initial posture, car front shape and car speed etc. Pedestrian accident data shows that the cumulative frequency of the crash speeds up to 40 km/h can cover more than 75% of total pedestrian injuries (AIS 1+) in all body regions. Based on IHRA (International

Harmonized Research Activity) injury data, it was found that hood/wing contacts caused 41% of child head injuries of AIS2+ and 19% of the adult AIS2+ head injuries. Bumper contacts lead to 64% of adult AIS2+ leg injuries. So, the major source of child head injuries is the top surface of the hood/wing, while adult head injuries result from impacts to the top surface of hood/wing and windscreen area. For adult leg injuries, the major source is the front bumper of vehicles.

Four full scale PMHS tests were conducted by Masson et al. (2007) to simulate the impact conditions during pedestrian crash. Two tests were conducted with a compact sedan and the other two were conducted with a full size sedan. Results showed that head impact speed to car impact speed ratio was 0.66 for a PMHS hit by compact sedan and head impact speed to car impact speed ratio was 1.1 for a full size sedan. Seven full scale PMHS impact tests were conducted by Kerrigan et al. (2007). The seven PMHS subjects included three small sized, two medium sized and two large sized cadavers. Results showed that when all pedestrian impact happened at 40 km/h, the head impact speed varied between 27 to 51 km/h depending on the size of pedestrian involved. The medium sized PMHS's showed the lowest average head impact speed and large sized PMHS's showed the highest average head impact speed.

A pedestrian body versus hood sliding effect can also be seen during pedestrian impact with sedan type cars. The pelvis slides up on the hood surface after thigh impacts the hood leading edge.

3.2 Injury Criteria and Threshold

During pedestrian crashes, head and lower extremities are most injured regions, so injury criteria for only head and lower extremities are discussed in this thesis.

3.2.1 Head Injury Criteria: A logistic regression analysis and field injury data suggests that intracranial pressure is largely a function of the translational acceleration of the head while the maximum shear stress is more sensitive to rotational acceleration (Zhang et al., 2004). Although these intracranial responses are better injury predictors, they cannot be directly measured. No single injury criterion is able to predict all injury types. Still some injury criteria have been proposed based on theories and hypotheses. All these criteria have some limitations and criticisms due to insufficient biofidelity.

Wayne State Tolerance Curve (WSTC) was the first proposed head injury tolerance to assess the risk of head injuries. This criterion was developed based on combinations of cadaver test data, animal test data and non injury related volunteer data (Lissner et al., 1960). WSTC as shown in Figure 3.2.1 shows the relationship between acceleration level and impulse duration necessary to produce skull fracture. Short pulses of high acceleration can produce injury and lower accelerations require longer pulses to produce injury. A combination of magnitude and duration which lies above the curve in WSTC can cause AIS 3+ head injuries.

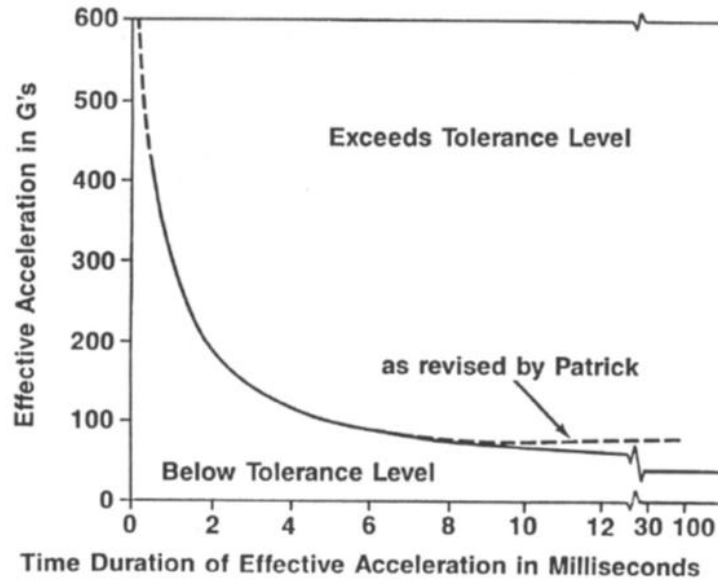


Figure 3.2.1: WSTC head injury tolerance curve (adapted from Yao, 2010)

Ono et al. (1980) used primate and cadaver skulls impacts that further reinforced the WSTC. Cerebral concussion was produced by pure translational acceleration of the skull. A tolerance curve for cerebral concussion to humans was developed by scaling the monkey data and it was called the Japan Head Tolerance Curve (JHTC). The difference in the WSTC and the JHTC between 1 and 10 ms was negligible. However there are minor differences for longer durations. Ono et al. (1980) showed that the threshold for skull fracture is slightly higher than that for cerebral concussion. Gadd proposed a weighted impulse criterion called Gadd Severity Index to account for shape of acceleration pulse.

$$\text{Gadd Severity Index (GSI)} = \int_0^{\tau} a^{2.5}(t) dt$$

Where $a(t)$ is the acceleration pulse and t is the duration. It was suggested that if GSI exceeded 1,000, there was a threat to life. GSI was highly criticized because it

deviates considerably from the WSTC criterion. NHTSA suggested a modified injury criterion, the Head Injury Criterion (HIC) based on paper published by Versace (1971):

$$\text{HIC} = \max \left\{ \left[\frac{1}{t_2 - t_1} \int_{t_1}^{t_2} a(t) dt \right]^{2.5} (t_2 - t_1) \right\}$$

Where $a(t)$ is the resultant head acceleration and $t_2 - t_1$ is the time period which maximizes the HIC value for duration of 15 msec at present. The main drawback of HIC is that it doesn't take angular acceleration into consideration. For adult pedestrians, a HIC value of 1,000 with a time period of 15 msec has been proposed as an injury tolerance level for severe head injury (IHRA 2001; EEVC 2002) as HIC of 1,000 represented a 16% risk of AIS 4 or greater brain injury.

Brain injury mechanism due to angular acceleration is not fully understood but many tolerance levels are recommended based on biomechanical data obtained from human surrogates. Ommaya and Hirsch (1971) predicted that a head rotational acceleration during whiplash in excess of $1,800 \text{ rad/sec}^2$ would have a 50% probability of resulting in cerebral concussion in man. Margulies and Thibault (1992) proposed a criterion for diffuse axonal injury based on animal studies and physical model experiments that below 5% critical shear strain there should not be any axonal injury and below 10% critical shear strain mild injury such as concussion could happen and above 10% critical shear strain diffuse axonal injury could happen.

There are few other Head Injury Criteria proposed like "3 ms criteria (a_{3ms})" based on WSTC and Generalized Acceleration Model for Brain Injury Threshold (GAMBIT) proposed by Newman (1986). None of these criteria are used in any

governmental regulations. The current study is limited to commonly used head injury criteria.

3.2.2 Lower Extremity Injury Criteria: To assess loading of the pelvis and lower extremities in crash tests, few criteria are established in existing regulations.

One of the criteria is compression force limit on femur and tibia. To protect the hip-thigh-knee complex, a maximum compression force of 10 KN for axial loading of the femur is defined in FMVSS 208. Tibia Compression Force Criterion (TCFC) states that to protect tibia under compression loading, the maximum compression force should not exceed 8 KN.

Tibia acceleration is used as an injury parameter in legal and consumer tests. The consumer test has the strict requirement for upper tibia acceleration not to exceed 150 g's. This requirement is to assess the risk of tibia fracture. The upper legform force and bending moment are assessed as the injury parameter for thigh and pelvic injury and these are not to exceed 5 KN and 300 Nm, respectively.

Femur Force Criterion (FFC) as defined in ECE R94 assesses the compression force acting on the femur as well as the duration [ms] for which the force is applied. The FFC is determined by the compression force [kN] that is transmitted axially on each femur. Axial compression force on femur for first 10 ms ranged from 9.07 KN at 0 ms to 7.58 KN at 10 ms and after 10 ms the force should not exceed 7.58 KN.

The Tibia Index (TI) involves the bending moments as well as the axial force in the tibia. The underlying idea of the TI is to prevent tibia shaft fractures. The TI is calculated according to the following equation:

$$TI = (M/ M_{crit}) + (F/ F_{crit})$$

with M being the bending moment and F the compressive force. M_{crit} and F_{crit} represent critical intercept values and read 225 Nm and 35.9 KN, respectively, for the 50th percentile male. These critical values were obtained in static bending tests of the tibia [Yamada 1970]. As per ECE R94 regulation, the maximum TI measured at the top and bottom of each tibia shall not exceed 1.3 at either location. As a further restriction, a maximum compression force has to be smaller than 8.0 kN.

Based on work done by Cesari and Ramet (1980), load tolerance to pelvic fracture was found to be mass dependant. The fracture load was 5 KN for a 50 kg subject and 10 KN for 76 kg subject. Zhou et al. (1995) performed sled tests to get injury tolerance of pelvis and femur. A load of 7.3 KN showed a 25% probability of fracture and 8.78 KN showed a 50% probability of fracture. The average force was seen to be a better predictor of pelvic fracture than peak force. An average force of 5 KN predicted a 25% probability of fracture.

Knee bending and shearing are used as injury parameters in legal and consumer tests. The consumer test has the strict requirement for knee bending as 15 degrees and knee shearing not exceeding 6 mm. These requirements are to assess knee ligament injury. There are some other injury criteria for lower extremities such as Pubic Symphysis Peak Force (PSPF), but this thesis is limited to commonly used injury criteria for pedestrian safety.

Chapter 4: Testing Tools, Testing Regulations and Safety Standard

For research in pedestrian safety as well as in regulatory work, a number of test devices; both physical test devices as well as numerical models are used.

4.1 Physical Test devices

One of the physical test surrogates is whole body Post Mortem Human Subject (PMHS). PMHS impacted with car can be used to reconstruct kinematics and, to some levels, injuries of pedestrian, but it is difficult to evaluate the modifications in vehicular frontal structure to reduce risk of pedestrian injury using PMHS. Another physical test device is local Impactors (legform and headform) as used in European New Car Assessment program (EuroNCAP) and Global Technical Regulation (GTR) tests. These impactors are effective in evaluating the effect of front end structure changes on pedestrian injuries in local body region but these local impactors cannot be used to reconstruct the kinematic of whole pedestrian. Apart from local impactor, there are full scale pedestrian dummies to represent different size of human (POLAR, Autoliv).

There are different physical test devices designed to simulate the kinematics of pedestrian body regions such as lower extremities and upper extremities and to measure injury risks.

4.1.1 Local Impactors: The lower legform known as TRL-LFI used in pedestrian safety regulation was developed by EEVC WG17 as the pedestrian legform impactor to study pedestrian kinematics and used as an injury assessment tool. In TRL-LFI, tibia and femur are represented as rigid, knee is made up of bending plate and shear spring, and

flesh is made up of neoprene and confor foam (EEVC WG 17 Technical Report). In physical test, the bending plate and confor foam can be used only once and confor foam is very sensitive to humidity. The design is intended to partially replicate the *in-vivo* situation where the flesh covered femur is constrained at the distal end by knee and at the proximal end by hip and is free to bend in the middle. There are load cells at upper and lower supports of the legform and strain gauges are used to measure the peak bending moment in the middle of impactor. The measurements done on lower legform to detect the potential risk of injury are the knee shear displacement, knee bending angle, and upper tibia acceleration. There is no measurement done in the tibia and fibula regions. Some of the limitations of TRL-LFI are that difference of the long bones stiffness between the TRL-LFI and human lower limb generates a different kinematics during car impact and the only allowable measurements in the knee and upper part of tibia regions lead to insufficient injuries assessment capability (Atsuhiro, 2008).

In 2000, JAMA-JARI decided to develop a more appropriate legform impactor Flex PLI which could provide better pedestrian kinematics and better injury assessment. This impactor has simulated human-like flexible long bones in its femur and tibia parts, knee is represented with ligaments, and flesh is made up of neoprene and rubber (Atsuhiro, 2008). In physical test, flesh made up of rubber can be used for multiple times. The proposed measurements are tibia bending moment, and knee MCL elongation. Figure 4.1.1 shows the details of lower legform impactors TRL-LFI and Flex PLI for their respective construction details and placements of some of the injury measurement sensors. In full human body model, lift up motion of lower limbs is large

due to higher upper body inertia compared to Flex PLI lower legform. So there is a need to have a lift up impact height for Flex PLI to correlate well with full human body model. Only MCL elongation is proposed as knee injury assessment criteria for Flex PLI. More works need to be done to validate Flex PLI impactor.

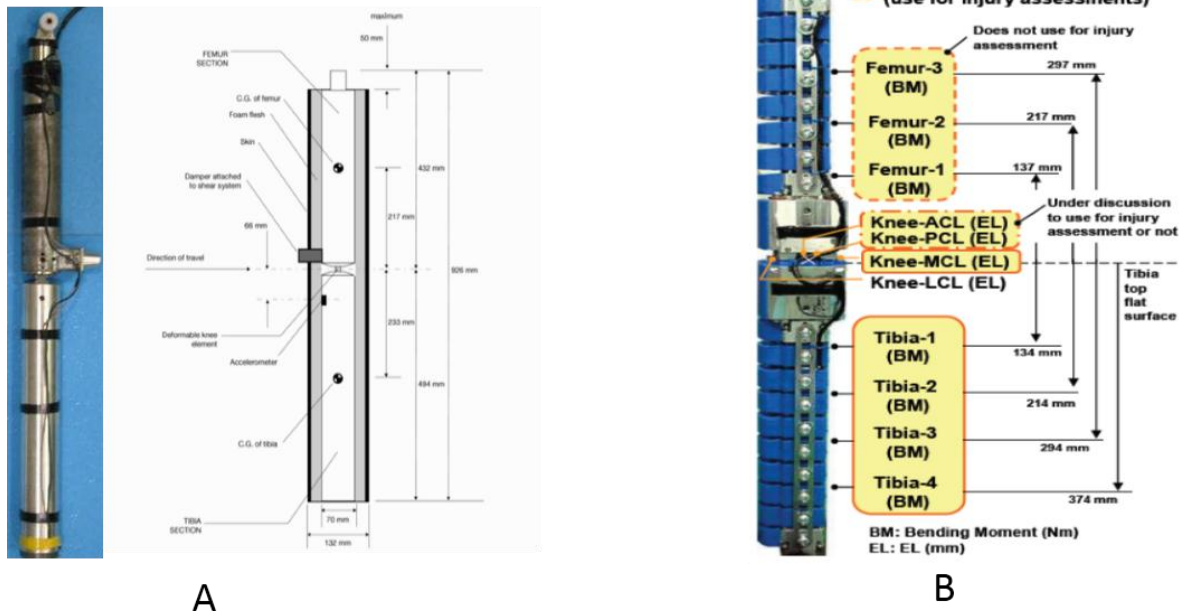


Figure 4.1.1 Physical Test Devices for Lower Legform a) TRL-LFI, b) Flex PLI (Atsuhiro, 2008)

The total mass of the upper legform impactor, including propulsion and guidance components which are effectively part of the impactor is around $9.5 \text{ kg} \pm 0.1 \text{ kg}$. Two load transducers are fitted to measure the individual forces applied at either end of the upper legform impactor front member. Three strain gauges are located on the impactor to measure the bending moments of each front member using a separate channel. The two outer strain gauges are located $50 \pm 1 \text{ mm}$ from the impactor's symmetrical axis. The middle strain gauge is located on the symmetrical axis with a $\pm 1 \text{ mm}$ tolerance.

Sum of forces on the upper and lower portions of femur and femur bending moment are measured to assess the risk of upper leg injury.

The EEVC WG17 developed headform impactors for pedestrian safety tests of passenger cars for the European Commission. Earlier two different headform impactors for adult head and child head were developed with different size (165 mm in diameter for adult and 135 mm in diameter for child). New headform impactors are developed with both headform of the same size with the adult head-form impactor of 4.5 kg and child head-form impactor of 3.5 kg. Construction of the headform consists of an inner hollow sphere made of aluminum, an end plate made of aluminum and a skin constructed by PVC (polyvinyl chloride) and has mount for accelerometer to track head accelerations in three mutually perpendicular directions. These headform impactors are tested for biofidelity (skin stiffness) using a drop test with a test corridor of 225-275 G for adult headform impactor and test corridor of 240-300 G for child headform. Figure 4.1.2 shows the construction details for the headform impactor. These headform impactors are good for parametric study in initial vehicle front-end design and to get some idea of head acceleration and HIC number in early phase. But these impactors being free motion headform can't predict the actual kinematics of neck-head response during impact and thus limited in actual level of injury prediction.

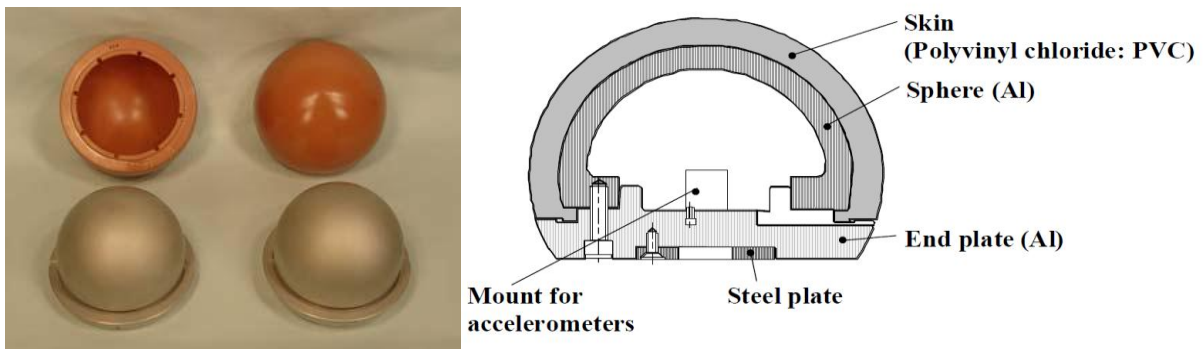


Figure 4.1.2: Headform Impactor (Euro NCAP-Pedestrian Testing Protocol Version 5.2.1)

Because of the complexity of pedestrian kinematics during vehicle impact, subsystem test procedures using local impactors are insufficient to evaluate the comprehensive level of protection potentially afforded by vehicle countermeasures. Subsystem tests are not effective for evaluating active safety systems such as pedestrian airbags or pop-up hood systems. These countermeasures usually include sensors that detect pedestrian contact with the vehicle which cannot be evaluated by subsystem testing.

4.2 Pedestrian Test Dummies

One of the pedestrian test dummy called POLAR II was designed, developed, manufactured and tested under funding from Honda R&D, Tochigi, Japan. POLAR II represents a 50th percentile male pedestrian. The second-generation POLAR II pedestrian dummy enables researchers to perform more precise accident testing. POLAR II has instruments throughout the body to measure the risk of injury. In the injury prone lower leg area, it has a detailed knee design that incorporates femoral condyles, meniscus, tendons and ligaments (Akiyama et al., 1999).

During the design and development phase of POLAR II, a series of computer simulations were performed to verify the placement of the origin and insertion points for the four knee ligaments, and the general force-deflection characteristics of the ligaments and the meniscus. The femoral condyles were represented using ellipsoids and the tibial plateau was simplified using planes. The ligaments were modeled as spring-dampers. The input stiffness characteristics of ligaments and the force-deflection characteristics of the meniscus were based on published values (Yang, 1995). The output from the simulation was compared with the output from an average high-speed shear test. It was seen that the maximum stretch was generated in the ACL and MCL, which are generally the ligaments liable to be damaged.

The design requirements for a deformable tibia were chosen such that it should have human-like force-deflection characteristics up to the point of fracture in quasi-static lateromedial loading response as seen in PMHS testing performed by Yamada (1970). It should have human-like force-deflection characteristics up to the point of fracture in dynamic lateromedial loading response as seen in PMHS testing performed by Nyquist (1985) and it should be a reusable component.

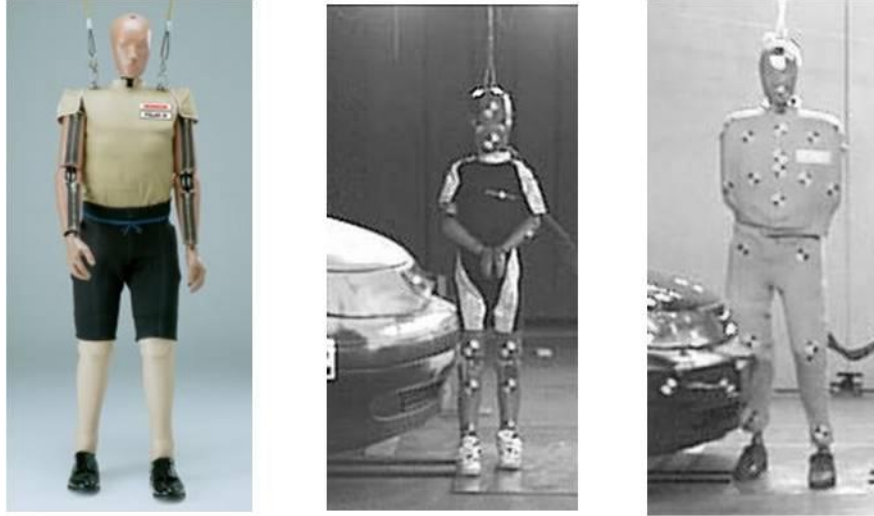


Figure 4.2.1: Full Body Pedestrian Dummies: from left to right; Polar II (adapted from Akiyama et al., 1999), Autoliv child pedestrian, Autoliv adult pedestrian

The Chalmers-Autoliv adult dummy (Figure 4.2.1) was developed as a combined project of Chalmers University and Autoliv Research. The head and neck are adapted from Eurosid-1, thorax and lumbar spine from US-SID, pelvis from Hybrid II and lower extremity parts are taken from Hybrid III. A standing position pelvis was added and the knee joints were redesigned and assigned the bending characteristics corresponding to the EEVC WG17 legform impactor to achieve humanlike lateral bending. The dummy was validated against mathematical human body pedestrian model and showed comparable results (Bjorklund and Zheng, 2001; Yao, 2010). It was concluded that this dummy is capable of measuring the injury parameters such as head acceleration, chest deformation, spine acceleration, pelvic acceleration, knee acceleration and knee bending angle.

The 6 years old (6YO) pedestrian dummy was developed in co-operation between Autoliv Research and Chalmers University of Technology based on a 6YO Hybrid III dummy which was equipped with a standard neck originally designed for frontal impact tests (Hayamizu et al., 2002). The neck was modified to provide higher biofidelity to the neck in lateral bending. The reason for developing a child dummy neck was the high involvement of child pedestrians in car-to-pedestrian impacts and the neck affects notably the head kinetics and kinematics. The neck design is made up of three rubber segments which provide bending stiffness and a rubber strap which controls the rotational stiffness. The dummy was validated against mathematical child pedestrian model. The static stiffness of the prototype neck satisfied human data in flexion, extension and lateral bending with a significant improvement.

Another physical test device in pedestrian safety is Hybrid III pedestrian dummy. Hybrid III pedestrian dummy is updated from occupant dummy by making modification in the pelvis, lower torso and knee region.

4.3 Mathematical Models

Based on different physical test devices, there are their mathematical counterparts to simulate the kinematics of pedestrian body regions such as lower extremities and upper extremities and to measure injury risks. Some models have the ability to simulate only particular region (segment based models) whereas some has the ability to simulate whole body (full body models). The segment based models can be categorized as lower limb models (lower leg, upper leg, knee joint) and upper limb models (head and neck).

4.3.1 Lower Extremities FE Models: In the past, several finite element (FE) lower limb models have been developed in order to reproduce lower limb injuries in the car to pedestrian accidents. In the initial models, the surrounding muscles and the skin were neglected, and the knee ligaments were modeled using spring elements (Bermond et al., 1994). In the recent models, due to high computational power and speed available, more detailed FE lower limb models have been developed. These models derive accurate geometry from CT and MRI scans of human volunteers (Beillas et al., 2001; Takahashi et al., 2003) and the flesh and knee ligaments were meshed with shell and solid elements. Still the accuracy of FE models depend not only on the quantity and quality of the model geometry (e.g. anatomical surfaces, the number of components modeled, or mesh quality), but also depends on the biofidelity of the material properties assigned to the FE components.

4.3.2 Head FE Models: Kang et al. (1997) developed the Strasbourg University finite element head model (Figure 4.3.1 A). The inner and outer surface geometry of the skull was digitized from a human adult male skull. The main anatomical features modelled

were the skull, falx, tentorium, subarachnoid space, scalp, cerebrum, cerebellum, and the brainstem. Material properties of the cerebral spinal fluid, scalp, facial bones, tentorium and falx were used as isotropic, homogenous and elastic with material types as *MAT_ELASTIC and the brain was assumed to be visco-elastic with material type as MAT_VISCOELASTIC. The skull was modeled by a three layered composite shells representing the inner table, the dipole and the outer table of human cranial bone. The head model was validated against Nahum's (1977) impact experiments (in order to validate brain response) and against Yoganandan's (1994) impact tests (in order to validate the skull behaviour and bones failure). The neck was not included in this model and a free boundary condition was used to simulate Nahum's impact. This hypothesis is based on the justification that the time duration of the impact is too short (6 ms) for the neck to influence the kinematics of head response impact. For Nahum's Impact, a good agreement was found for the impact force vs. time of impact. The maximum difference of pressure peak under 10% was reported. For Yoganandan's Impact, The numerical force-deflection curves are compared to the average dynamical response of experimental data. The dynamical model responses agreed closely with the experimental results.

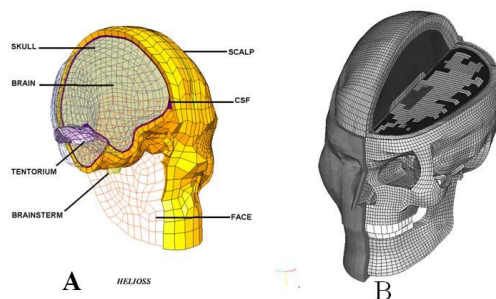


Figure 4.3.1: Mathematical head models A) Strasbourg University finite element head model, B) Wayne State University finite element head model.

WSUBIM version I (1993-1997) simulated essential anatomical compartments of the head (Ruan et al., 1993; Zhou et al., 1995). This model represented a 50th percentile male human head. It had 32,898 nodes and 41,354 elements with a total mass of 4.3 kg. By differentiating the material properties of gray matter from those of white matter, the model was capable of predicting the location of diffuse axonal injury (DAI) in the brain. WSUBIM version II (1998-1999) (Figure 4.3.1 B) was developed by introducing a sliding interface between the skull and brain surface. With this skull/brain interface, the model was able to match most of the pressure data by Nahum et al. (1977) and brain/skull relative displacement data measured from cadaveric impact tests conducted at WSU. The new version of WSUBIM was modeled with a finer mesh approximately 2 mm element size. The intracranial cisterns, dorsal and ventral surfaces of the brainstem had very few details in the previous versions but in current version, the cisterns were modeled and the brainstem was distinguished from the cerebellum with more detailed structural characteristics. The neuroarchitecture of brain tissues is naturally inhomogeneous and anisotropic. To incorporate the different material compositions of white and gray matter, it was assumed that the shear modulus of the white matter was 25% higher than that of the gray matter due to the fibrous nature of the white matter. The brain was modeled as isotropic in this study because anisotropic properties of the brain are not available at present. Brainstem shear modulus was assumed to be 80% higher than that for the cerebral white matter. An elastic-plastic material model was used for cortical and cancellous bones of the face. A Young's modulus of 560 MPa was assumed for the cancellous bone of the face and Young's modulus of 6 GPa for cortical bone was used based on literature data. An ultimate strain of 1.6 % and ultimate stress

of 4.5 MPa were defined for the cortical bone (Giesen et al., 2001). An ultimate strain of 4.5% and an ultimate stress of 4.9 MPa were defined for cancellous bone (Yamada 1970).

WSUBIM was validated against experimental data for intracranial and ventricular pressure, brain motion, force deflection for facial impact and stability. Model was simulated for comparison with experimental data from cadaveric frontal head impact tests conducted by Nahum et al. 1977. The results for contact force, intracranial coup and countercoup pressures were compared. Predicted coup and countercoup pressures correlated reasonably well with tests data except for one case. Model was simulated for comparison of intracranial pressure in the frontal and occipital lobes based on experimental data obtained by Trosseille et al., 1992. In this simulation, the skull was assumed to be rigid in order to impose a prescribed linear and angular accelerations to the CG of the head. The calculated pressure matched well in terms of magnitudes and trends with intracranial and ventricular pressure measurements for up to 14 ms. After 14 ms, predicted ventricular pressures approached zero while experimentally obtained pressures remained at a high level towards the end of the impact.

Mao et al. (2013) developed GHBM (Global Human Body Model Consortium) head model (Figure 4.3.2). The geometry of the model was developed based on computed tomography (CT) and magnetic resonance imaging scans of an average American adult male. Brain including cerebrum, cerebellum, brainstem, corpus callosum, ventricles, and thalamus, was modeled using hexahedral meshes. Bridging veins, cerebrospinal fluid, skull, facial bones, flesh, skin, and membranes—including falx, tentorium, pia, arachnoid, and dura were modeled using conventional meshing

methods. The head model has 270,552 elements in total. Thirty five loading cases were selected from a range of experimental head impacts to check the robustness of the model predictions based on responses including the brain pressure, relative skull-brain motion, skull response, and facial response. The brain pressure was validated against intracranial pressure data reported by Nahum et al. (1977) and Trosseille et al. (1992). Studies from 35 loading cases demonstrated that the FE head model could predict head responses which were comparable to experimental measurements in terms of pattern, peak values, or time histories.

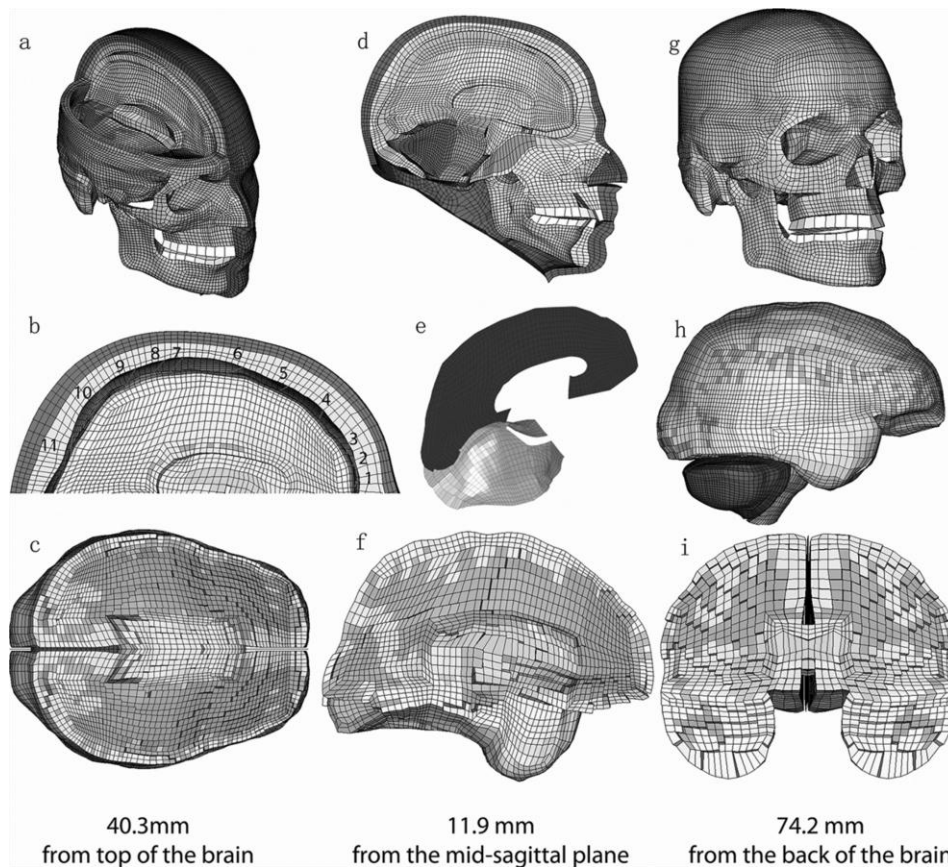


Figure 4.3.2: The GHBMC FE head model developed by WSU. (a) isometric view of the head model (d) medium sagittal view of the head model; (g) skull and facial bones; (b) 11 bridging veins; (e) falx and tentorium; (h) brain; and (c), (f), (i) brain sectional views in three directions (horizontal, sagittal, and coronal) (Mao et al., 2013).

4.3.3 THUMS: The 'Total Human Body Model for safety' (THUMS) is developed by Toyota Motor Corporation and Toyota Central Research & Development Laboratory. In THUMS, lower extremities model consists of the pelvis, femur, tibia, fibula, patella, foot bones. Bone is modeled as two layers; outer hard layer called cortical bone is modeled as shell elements and inner soft layer-the cancellous bone (spongy bone) modeled as solid elements. The material properties for each layer are determined by test data (Yamada, 1970). Soft tissues such as the skin, muscle, ligaments and tendon are modeled. Knee joint and ankle joint is modeled in THUMS. In THUMS, knee structure is similar to human knee. MCL, LCL, ACL and PCL are modeled as membrane elements. If plastic strain in ligaments exceeds 11 %, the ligaments are considered to be ruptured. The bending moment, angle relationship was validated against PMHS tests. Tomoyuki and Junji (2001) did validation work for kinematics and risk of bone injury using THUMS and compared its results with PMHS results for impact with passenger car. THUMS has the ability to simulate lower legform bone fracture and knee ligament rupture however knee ligament rupture still need to be validated.

4.3.4 MADYMO Pedestrian Models: MADYMO has a family of different mathematical models (Figure 4.3.3). The different sets of mathematical models from MADYMO are known as ellipsoid model, facet model and finite element model. The main difference in three types of model is the technique used to represent the geometry and mechanical properties used for dummy parts (Happee et al., 2003). The difference between MADYMO occupant model and pedestrian model is their outer geometry definition. The outer geometry of occupant model is modeled by facet or FE elements to have proper contact interaction of occupant skin with belt/airbag. The outer geometry of the

pedestrian models is represented by ellipsoids, which provide a less accurate representation of the geometry but result in shorter computation times than facet models. The inertial properties of the pedestrian body parts are incorporated in the rigid bodies of the pedestrian models. Deformation of flexible components (elastic long bone bending as well as fracture in femur and tibia) is defined in kinematic joints in combination with dynamic restraint models. Deformation of soft tissues (flesh and skin) is represented by force-penetration based contact characteristics for the ellipsoids.

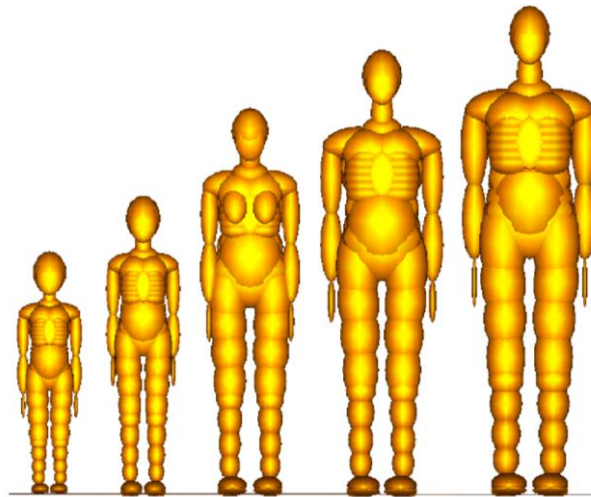


Figure 4.3.3: MADYMO Pedestrian family including 3 years old, 6 years old, small female, mid-size male and large-size male.

MADYMO pedestrian models do not have a detailed knee. The pedestrian knee is modeled by just one free joint. The knee flexion/extension stiffness has been implemented using volunteer data (Engin, 1979; Ma et al., 1995). Knee lateral shear stiffness of $6.7E5$ N/m has been applied to meet injury tolerance level of 4 KN force and 6 mm displacement. To account for leg bending and resulting bone fracture, bending and fracture properties are implemented at several locations in the femur and tibia using bending/fracture joints. Based on the work by Coley and De Lange, 2001, the model

prescribes the correct kinematics but in order to predict injuries correctly, a detailed vehicle model with correct contact stiffness characteristics or deformations is needed. The model predicted injury outcome is influenced (up to 40%) by change in contact stiffness of the vehicle front (Coley and De Lange, 2001).

4.4 Brief History of Pedestrian Safety Test Procedures Research

Four groups have or had been working to develop test procedures for pedestrian protection. NHTSA did some work during 1980 but suspended after 1992 and presently contributing towards the work of IHRA PS (International Harmonized Research Activity for Pedestrian Safety). EEVC (European Experimental Vehicle Committee) now renamed as European Enhanced Vehicle-safety Committee, played a major role in developing pedestrian safety test procedures through WG 7, 10, and 17. In 1983, ISO (International Organization for Standardization) started working towards pedestrian safety, in 1990 ISO working group activity for pedestrian safety shifted toward IHRA program. IHRA program proposed in 1996 to harmonize the technical pedestrian safety regulations.

EEVC has proposed different tests for pedestrian safety. Four main tests proposed by EEVC are: 1. Lower legform to bumper test for bumper height up to 500 mm, above that height, there is an alternate test of upper legform to bumper impact, 2. Upper legform to hood leading edge, 3. Child headform impact to hood top, and 4. Adult headform to hood top (EEVC proposed higher priority to child headform test). EEVC proposed an impact speed of 40 km/h and the impactor used are the EEVC child headform with a mass of 2.5 kg, EEVC adult headform with a mass 4.8 kg, EEVC lower legform and EEVC upper legform. EEVC proposed an injury criterion as a HIC of 1,000

for child and adult headform and maximum dynamic lateral knee bending angle of 15 deg, max knee shear displacement of 6 mm, maximum acceleration of 150 g at the top of tibia for the lower legform and bending moment not to exceed 220 N-m for the upper legform.

Work program of ISO is very similar to EEVC working group but ISO proposed a different headform impactor compared to EEVC which are the ISO child headform with a mass of 3.5 kg and ISO adult headform with a mass of 4.5 kg. The headform are of the same size (diameter 165 mm) compared to EEVC headforms. Test procedures developed by IHRA are also very similar to EEVC test procedures. But the headform specifications are the same as those of ISO headform. IHRA test procedures are developed to be suitable for vehicle speed ranging from 30 to 50 km/h.

There are different regulations for pedestrian safety and some rating systems for consumer rating of vehicles. Some of the regulations are European Union Directive also known as European Legal, Japan Technical Standard (Japan Legal) and Global Technical Regulation (GTR). Apart from these regulations for pedestrian safety there are some rating tests developed by EuroNCAP (European New Car Assessment program), Japan NCAP and Australian NCAP.

4.5 European Union Directive Regulation

The initial proposal for the European Union Directive relating to pedestrian protection was based on EEVC WG17. The directive implemented requirement in two phases. Phase 1 covers the tests for the lower legform to bumper and child headform to hood top, while other two tests to be conducted are for monitoring purpose only. Phase 2 requires all tests to be conducted for more stringent requirements (EEVC working

Group 17 Report). The EEVC procedure uses a legform impactor developed by the Transport Research Laboratory (TRL). A legform impactor is imposed on the bumper at a velocity of 40 km/h in a direction parallel to the longitudinal axis of the vehicle, and the lower leg acceleration, knee shearing displacement and knee bending angle are measured (EEVC/WG17). The lower leg acceleration is used to evaluate the tibia crack risk, while the knee shear displacement and bending angle are used to evaluate the ligament injury risks.

4.6 Global Technical Regulation

Based on IHRA data, each of critical body regions, i.e. head of child/adult and adult leg, covers more than 30% of total fatal and severe injuries. Thus GTR focuses on protecting these body regions. The test procedures proposed in GTR have been developed on the basis of current light vehicles, taking into account the pedestrian kinematics when impacted by such vehicles. For this reason, the scope of application is limited to passenger cars, sport utility vehicles (SUV), light trucks and other light commercial vehicles. This GTR would improve pedestrian safety by requiring vehicle hoods and bumpers to absorb energy more efficiently when impacted in a 40 km/h vehicle-to-pedestrian impact, which accounts for more than 75% of the pedestrian injured accidents (AIS 1+) reported by IHRA.

The GTR consists of two sets of performance criteria applying to the hood top and wings and the front bumper. Test procedures have been developed for each body region using sub-system impacts for adult and child head protection and adult leg protection. (Global Technical Regulation No.9)

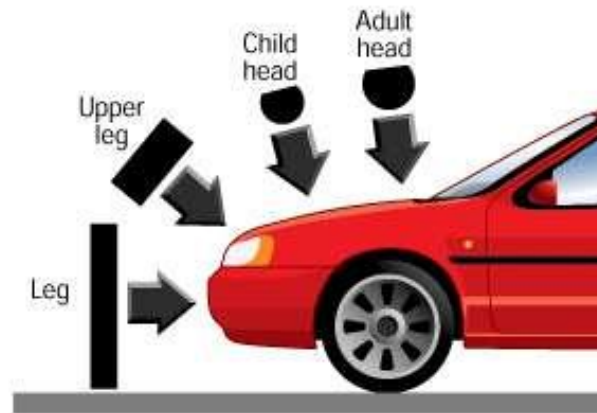


Figure 4.6.1: GTR test setups for pedestrian safety

Briefly, GTR test procedures are:

- **Legform Test to Bumper:** Vehicles with a lower bumper height of less than 425 mm are tested with a lower legform, while vehicles with a lower bumper height of more than 500 mm are tested with an upper legform test device. Vehicles with a lower bumper height between 425 and 500 mm are tested with either legform chosen by the manufacturer. Vehicle bumper is struck at 40 km/h with a legform that simulates the impact response of an adult's leg. The bottom of the impactor shall be at 25 mm above ground reference plane at the time of first contact with the bumper with a ± 10 mm tolerance.
- **Child Headform Test to Hood:** The child headform test area is bounded in the front by a boundary determined by a wrap around distance (WAD) of 1,000 mm, and at the rear by a WAD of 1,700 mm line. The hood top and wings would be impacted with a child headform at 35 km/h. The direction of impact shall at an angle of $50 \pm 2^\circ$ to the horizontal.
- **Adult Headform Test to Hood:** The adult headform test area begins in the front at a WAD of 1,700 mm, and ends at the rear with a boundary determined by a WAD of

2,100 mm (or the rear edge of the hood for shorter vehicles). The hood top and wings would be impacted with an adult headform at 35 km/h. The direction of impact shall be at an angle of $65^\circ \pm 2^\circ$ to the horizontal.

Table 4.6.1: GTR Injury Criteria

Body Form Impactors	Injury Assessment Parameter	Limit
Lower Legform	Knee Bending Angle	19 deg
	Knee Shear Displacement	6 mm
	Upper Tibia Acceleration	170 g's
Upper Legform	Sum of Impact Forces	7.5 KN
	Bending Moment	510 Nm
Child Headform	HIC	Should not exceed 1,000 for 2/3 of test area and should not exceed 1,700 for remaining 1/3 area
Adult Headform	HIC	

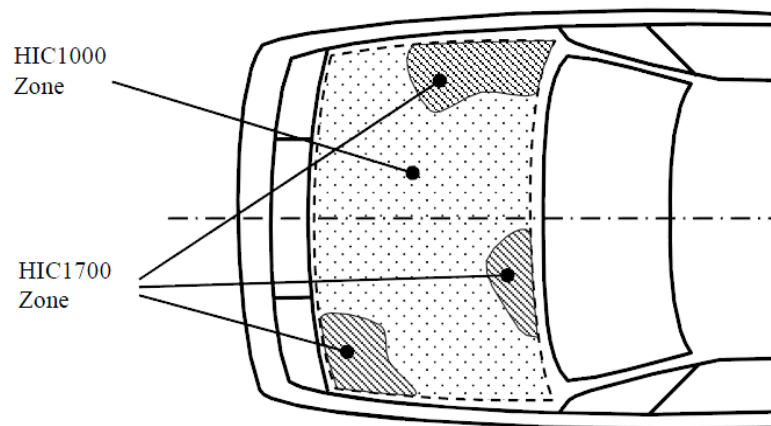


Figure 4.6.2: Example of marking of HIC 1,000 and HIC 1,700 zone in GTR tests

ISO	ISO
Child Head	Adult Head
V = 35 km/h	V = 35 km/h
M = 3.5kg	M = 4.5kg

Limit:
 (Whole test area)
 1/3 : HIC \leq 1700
 2/3 : HIC \leq 1000

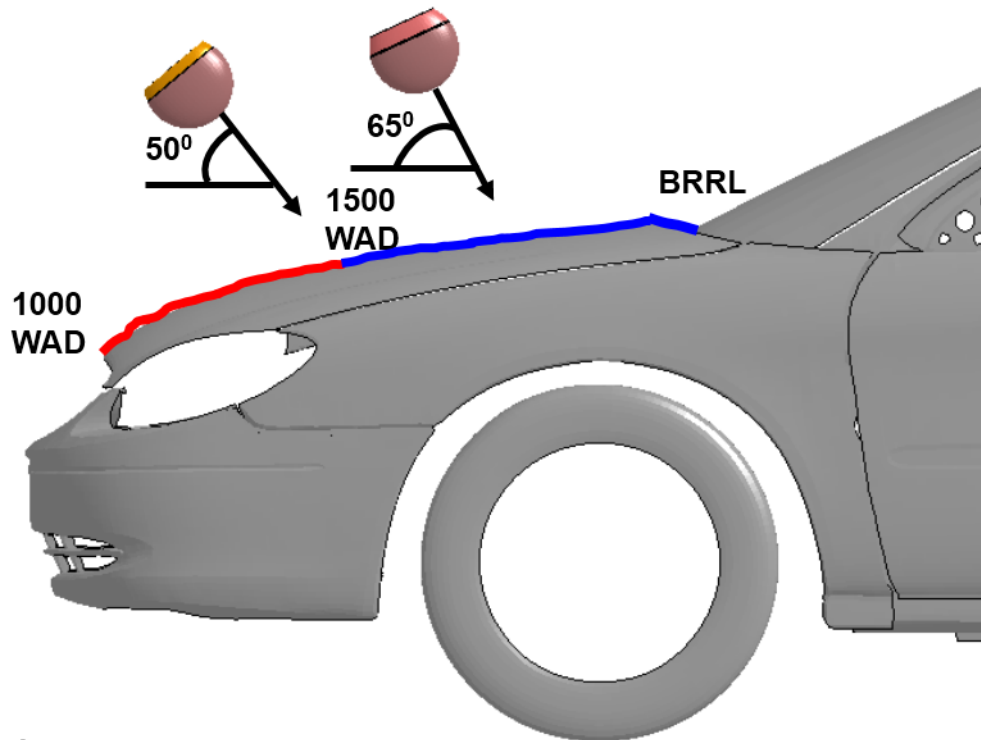


Figure 4.6.3: Pedestrian Head Impact Legal Requirement

In determining the angles of impact, the informal group considered the findings of IHRA and the EEVC. EEVC's decisions concerning head impact angles for child and adult tests were based on the work done by Glaeser K.P. (1991) which showed a peak of the distribution of adult head impact angles to be 60 degrees, with all the results falling between 50° and 80°. In contrast, EEVC concluded that one set of angles (50 degrees for the child headform test and 65 degrees for the adult headform test) for all vehicles is

reasonable, simplifying any head test procedure dramatically (Global Technical Regulation No.9, Pedestrian Safety, ECE/TRANS/180/Add.9)

4.7 EuroNCAP Pedestrian Safety Rating System

The EuroNCAP rates a car's overall safety performance out of five stars, taking into account pedestrian protection along with performance during other crash event such as frontal, side, rear and rollover crashes. Before 2009, each car was awarded three individual star ratings based on adult, child and pedestrian protection. This was replaced in 2009 with one overall rating, simplifying the comparison process and placing a greater emphasis on pedestrian protection. Euro NCAP carries out a series of tests at 25 mph (40 km/h) to replicate crashes involving child and adult pedestrians: a legform test assesses the protection afforded to the lower leg by the bumper; an upper legform assesses the leading edge of the hood, while child and adult headform are used to assess the risk of head injury impacting the hood top area. If the leg is impacted low down and away from the knee, a car will score more highly if it features pedestrian friendly bumpers (which deform when they hit a pedestrian's leg). If the forces are spread over a longer length of leg, the hood top area needs to be able to flex to protect the head.

The vehicle is marked by following the marking guidelines given by EuroNCAP (Euro NCAP Pedestrian Testing Protocol Version 5.2.1). The various marking lines used are bumper reference lines, bumper corners, hood leading edge reference line, hood side reference lines and hood top WAD lines. 1,000-1,500 WAD lines mark as child head impact zone and 1,500-2,100 WAD lines mark as adult head impact zone. Head

impact speed of 40 km/h, child headform impact angle of 50° and adult headform impact angle of 65° is used.

Table 4.7.1: EuroNCAP Injury Criteria

Body Form Impactors	Injury Assessment Parameter	Limit
Lower Legform	Knee Bending Angle	15 deg
	Knee Shear Displacement	6 mm
	Upper Tibia Acceleration	150 g's
Upper Legform	Sum of Impact Forces	5 KN
	Bending Moment	300 Nm
Child/Adult Headform	HIC	Should not exceed 1000

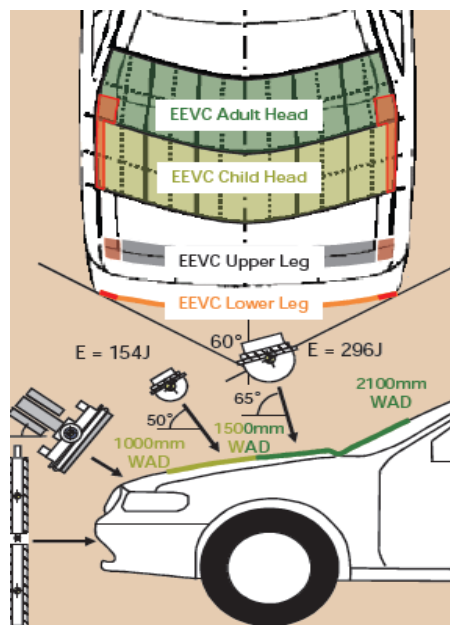


Figure 4.7.1: EuroNCAP test setups and impact zones

In 2012, EuroNCAP head injury assessment has been revised to be reported as overall performance score value (Euro NCAP Pedestrian Testing Protocol Version 6.0). Based on this new assessment criterion, Manufacturer must provide the head impact test data for all grid points tested and should be presented based on color scheme as:

Green	$HIC < 650$	1.00 point
Yellow	$650 \leq HIC < 1000$	0.75 point
Orange	$1000 \leq HIC < 1350$	0.50 point
Brown	$1350 \leq HIC < 1700$	0.25 point
Red	$1700 \leq HIC$	0.00 point

A maximum of 24 points is available for head impact test zone. Total score of all grid points is calculated as percentage of maximum achievable score and then multiplied by 24. For e.g. if 190 grid points are tested which resulted into total points of 96. Then percentage achievable score is $96/190 = 50.5\%$, which multiplied by 24 gives 12.12 points.

Chapter 5: Current Pedestrian Safety Countermeasures

Two different strategies have been used to protect pedestrians. One strategy is to prevent fatalities and injuries when pedestrian collision can't be prevented. Another strategy is to prevent pedestrian accidents by means of better traffic system and by employing the devices which can detect pedestrian, warn the driver and trigger autonomous braking. Here more focus is given for countermeasures developed during crash events. These countermeasures can be divided into two categories namely passive safety countermeasures and active safety countermeasures.

5.1 Passive Safety Countermeasures

Car front-end structure designs have great influence on the severity of injuries in pedestrian impact. Car-front designs have changed significantly over the past two decades. Some of these changes are smoother shapes of hood and fender, reduced hood length, reduced hood leading edge and reduced bumper leading edge. Some of these shape changes were not intended for pedestrian safety but more for styling but these changes have contributed toward better pedestrian protection performance. As an example, a smooth fender and hood edge help reduce the local stiffness in these areas and thus help in better pedestrian head protection.

Based on pedestrian kinematics during impact, vehicle hood is the critical area where pedestrian head hits and thus causes head injury. Hood performance demands energy absorption capacity and more clearance space between hood and under hood packaging. Over time, hood is optimized for better energy absorption capability during pedestrian head impact thus leading to lower HIC. Various shape changes, hood inner patterns and even different materials such as aluminum and carbon fiber composites

are utilized to improve hood performance. Various hood inner patterns are developed for pedestrian protection. But these hood optimization studies have one basic limitation that other structural performances of hood such as hood beaming, oil canning etc. are not considered during hood optimization process. Figure 5.1.1 shows different hood inner panels for uniform strength distribution.

Different hood materials (steel and aluminum) have been tested to meet structural requirement as well as pedestrian head impact protection. Steel hood is chosen based on cost and material properties and aluminum hood is chosen based on its low specific weight. Based on stiffness testing, steel hood provides much better stiffness over aluminum but also cause much higher mass (Schwarz et al., 2004). Few critical impact points were selected to test the feasibility of hood material. Typical under hood package was used without any changes. For impact points without any significant

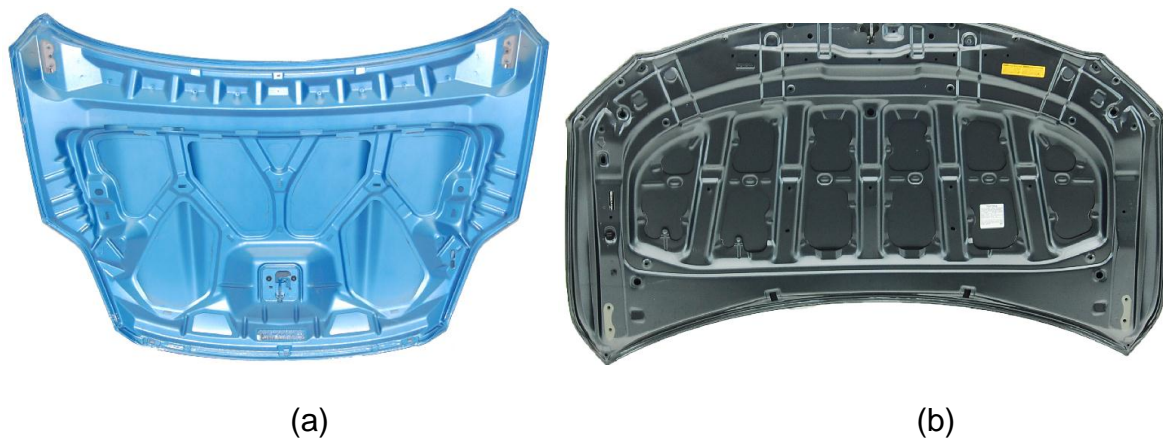


Figure 5.1.1: Hood Inner panels with uniformed strength distribution (a) Ford Kuga 2.0 inner panel (b) Toyota Corolla 1.8 LE hood inner panel

under hood structure, head acceleration and HIC for an aluminum hood was lower as hood deformation was higher and there was no secondary peak (Schwarz et al., 2004). For impact points with under hood structure like engine, air filter box etc. there was a

secondary peak which results in a higher HIC in case of aluminum hood (Schwarz et al., 2004). It was concluded that in addition to material changes, some constructive optimization to hood for both types of materials (steel and aluminum) can lead to reduction of injury severity.

The hood inner panel was suggested to be redesigned to meet pedestrian safety performance. For identical HIC value, head acceleration with a higher first peak needs less headform displacement (only 58 mm), whereas head acceleration with a lower first peak and higher second peak involves more headform displacement (around 150 mm) (Cheng and Wang, 2002). Thus HIC could be reduced by increasing the first peak of the acceleration curve and by eliminating or reducing the second peak. Increase in the first acceleration peak can be achieved by increase in inertia mass which in turn could be achieved by increasing mass per unit area or by increasing the effective area. Hood inner panel was redesigned to increase effective area. A wave type of hood inner panel structure was preferred over beam pattern (Figure 5.1.2) (Ikeda and Ishitobi, 2003) because it increased effective area without weight increase. The wave-type hood structure increased the amount of energy absorption and achieved HIC values under 1,000 with less space.

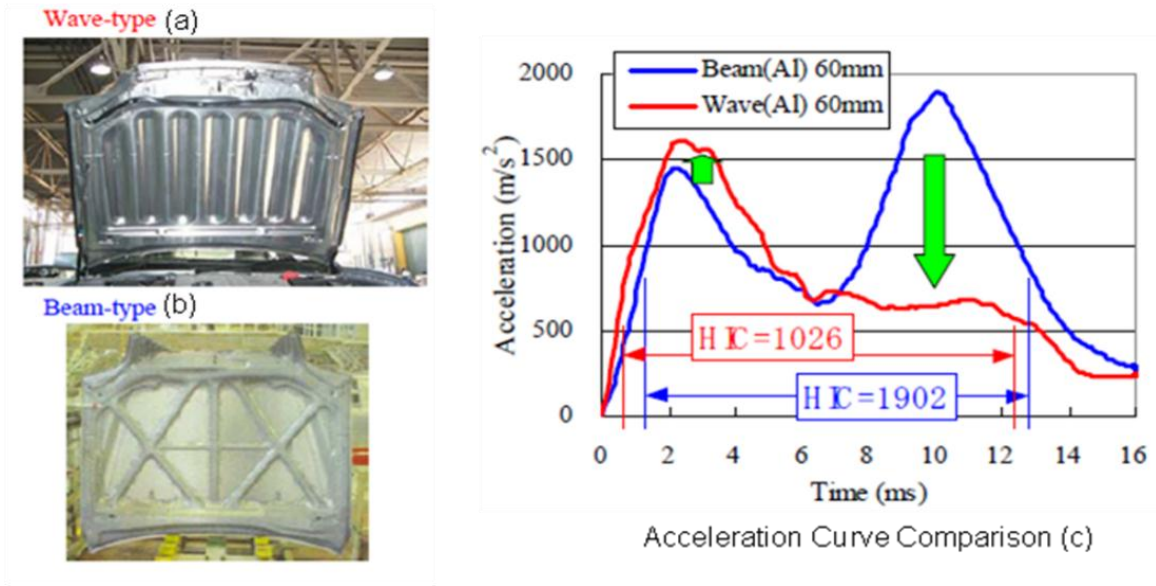


Figure 5.1.2: (a) wave type hood panel (b) beam type hood panel (c) acceleration curve comparison (Ikeda and Ishitobi, 2003)

To lower HIC, two main principles are necessary: provision of sufficient deformation space and provision of a low stiffness of the impacted vehicle body parts. The acceleration of the first few milliseconds is defined by the initial active mass. Therefore the type of material, the gages of initial struck components are of major influence. The later acceleration is defined by the stiffness of the structure so the component sizes, their design, their mountings and secondary contacting component are of increasing influence at this stage. To meet the sufficient deformation space requirement, the component under hood should be packaged by following certain clearance space criteria. A styling surface should be generated based on defined minimum clearance (for e.g. min 60-70 mm vertical gap between hood inner and top surface of any packaged components), package components that penetrate the generated deformation space need to be considered as critical and need to be relocated or tuned (Kerkeling et al., 2005).

The hood edges are more critical for pedestrian safety compared to hood inner structure because surrounding components such as fender and the hood mountings are within the deformation zone. These components have more significant influence than that of the hood itself. Some suggested design concepts for hood edges are reduced section height for brace wheelhouse to provide additional deformation space, designing weak fender mountings, inlaid hood compared to wrap around hood and vertical flanges compared to hem flanges (Kerkeling et al., 2005). These suggested design concepts need to be verified for their effect on pedestrian safety.

Next critical area of hood to meet pedestrian protection requirement is hood hinges, latches and bump stops etc. These mounting points are usually the most difficult to fulfill head impact requirement. Hood hinges are needed to transfer forces from hood to vehicle and vehicle to hood under handling and driving conditions. Hood mount requirements are also conflicting for vehicle durability load cases and pedestrian protection. For vehicle durability load cases, hood mounts need to be strong so that acceleration forces caused by driving conditions does not result in visible hood movements, force applied by somebody leaning against the hood in the open position or leaning on the hood in the closed position cannot cause plastic deformation, hood movement at the hinges in the low speed tests need to be minimum to avoid any damage at the hood and the fenders, the hood does not intrude into the windscreen under high speed frontal crash.

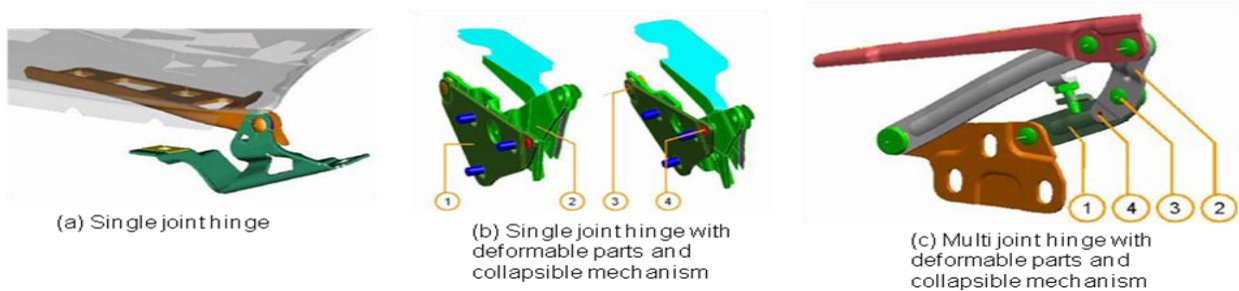


Figure 5.1.3: Different hood hinge concept for better pedestrian safety (Kerkeling et al., 2005).

For pedestrian safety requirement, hood mounts should provide enough deformation space to provide constant lower acceleration for longer duration. Some of concept designs for hinges are: single joint hinges with joints located outside the impact area (Figure 5.1.3 (a)), single joint hinges designed with deformable parts and a collapsible mechanism (Figure 5.1.3 (b)) (Kerkeling et al., 2005). But limitation for single joint hinge with joint far away is that it needs to be designed very stiff for larger distance of the hood hinge mounting to the pivot point. These concept designs need to be verified in more details for their validity for pedestrian safety and other structural requirement.

Liu et al. (2009) developed a sandwich hood to meet pedestrian head safety requirements. This sandwich hood design consists of three aluminum substructures, the outer hood as an upper layer, the ripple plate as a middle layer, and the support plate as a lower layer (Figure 5.1.4). The ripple plate is bonded to the outer hood with glue strips (Figure 5.1.5)

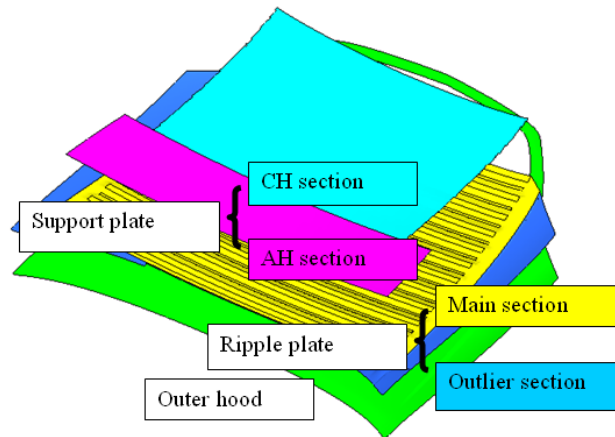


Figure 5.1.4: Exploded view of the sandwich design for main hood area (upside-down view of the hood assembly) (Liu et al., 2009)

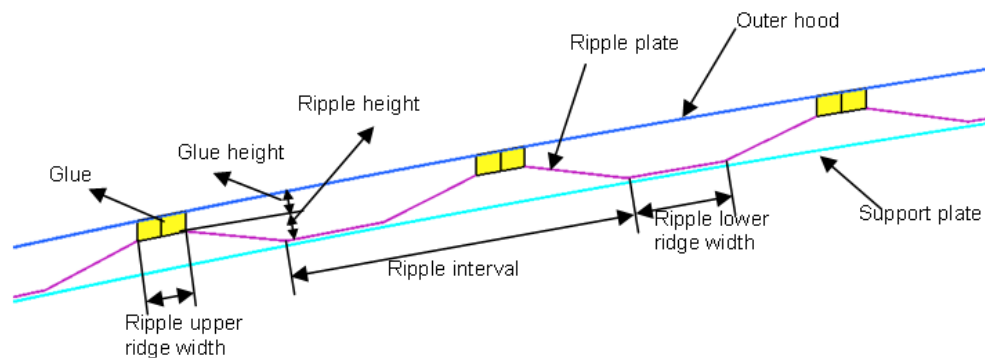


Figure 5.1.5: Enlarged sectional view of sandwich hood assembly (Liu et al., 2009)

5.2 Active Safety Countermeasures

During pedestrian accident, the pedestrian's head can collide with the stiff points of the hood (such as the hood hinge, washer reservoir, battery terminal, cowl, and air cleaner housing, engine etc.). These impact areas do not have enough deformation space to absorb the impact energy. During impact with such stiff points, the injury level of the pedestrian's head is relatively higher than that at the other points. Active hood system has been developed where hood hinges pop up to lift the hood at

the rear to provide more deformation space during head impact (Huang and Yang, 2009). The active hood lift system (Figure 5.2.1) consists of the hinge and the actuator, under the hood. When a pedestrian collides with the frontal structure of a vehicle, a sensor attached to the bumper detects the collision and sends a signal to an electronic central unit (ECU). The ECU determines whether or not a pedestrian accident occurs and the gunpowder within the actuator is fired and the actuator lifts the hood using the firing pressure of the gunpowder in the actuator.



Figure 5.2.1: concept of active hood system (Huang and Yang, 2009)

Based on preliminary work done on active hood system, it was shown that a lifted hood can reduce the HIC significantly (Bae et al., 2007). Some optimization work was done to optimize the active hood concept design and it was further seen that by optimizing the lift speed and lift height, HIC could be further improved. But success of an active hood system depends on the ability of sensor system to detect the pedestrian and trigger the hood deployment and the speed of hood lifting. The drawback of these presented active hood optimization studies lies in that they were conducted on lifted hoods (by varying lift height, hood design etc.). Moreover only head was used as

impactor during active hood impact but when pelvic and thorax hit the hood front, overall body kinematics will change the raised hood behaviour.

A Reversible Bumper System (RBS) for protecting the lower limbs of pedestrian need to be designed as a movable system (Huang and Yang, 2010). When a risk of pedestrian collision is detected, the RBS can be deployed before the occurrence of the crash to absorb impact energy more efficiently and better protect pedestrian lower limbs. In case the crash is avoided, the RBS can be moved back into place to protect against future accidents. Influencing parameter for the design of RBS will be: bumper deployment speed, bumper deployment distance, bumper stiffness. The work done in this field by Huang and Yang (2010) needs to be carried out more carefully. In their paper it is shown that there is huge difference in results between tests carried out using lower limb model and lower legform model. The lower limb model and legform model used by them need to be validated more closely before carrying out this study for effect of RBS which in their case is around 20% lower than test results.

Chapter 6: Aims of Study

Based on literature reviews presented in previous chapters, the following specific aims are selected to partially improve pedestrian safety:

1. Feasibility of New Hood Edge Designs for Pedestrian Safety Improvement

Hood and windshield are critical vehicle parts involved in pedestrian-car accidents. Improper designs of these two components may increase the risk of head injuries during primary impact. A number of studies have focused on optimizing vehicle front end structure involved in pedestrian interface, such as bumper and hood, for better energy absorption capability during pedestrian impact. These studies focus on developing different patterns for hood inner panel (beam or wave type patterns etc.) or using combination of different materials (steel, aluminum, and carbon fiber) for hood structure. But the main limitation with these studies is that these hood pattern designs are applied only to the central region of the hood. But in most cases, the central region of the hood structure is of lower risk to head injuries if proper packaging methodology for under hood structure is used. On the other hand, the hood edges that are supported by other vehicular structures (such as fender and shotgun) have higher stiffness. Upon impact along hood edges, higher head acceleration could be expected. This aim focuses on investigating several key shape parameters along hood edges and along hood to vehicle interface to reduce the vehicle stiffness in that region. So that it could help in reducing the head injury risk during primary impact thus improving pedestrian safety.

2. Evaluating practicality of pedestrian safety regulations

Most studies of pedestrian injury focus on reducing traumatic injury due to the primary impact between the vehicle and pedestrian. The critical vehicle parts involved in pedestrian-car incidents for primary head impact are the hood and the windshield. Inadequate designs of these two components may increase the risk of head injury. Most studies of pedestrian safety are based on the head impact tests defined by the Global Technical Regulation (GTR) or European New Car Assessment Program (EuroNCAP). These test setups utilize a free motion headform impacting the hood or windshield at a fixed angle of 50° (for a child headform) or 65° (for an adult headform) and at a constant speed of 35-40 km/h. These test setups do not consider variations in the vehicle front-end profile, such as a lower front-end or raised front-end. The purpose of this study is to evaluate how various front-end vehicle profiles affect pedestrian kinematics and head impact angle during primary impact.

3. Effect of vehicle front-end profiles leading to pedestrian secondary head impact to ground

The cause of head injury is still under debate that whether head injury leading to fatality is caused by the first impact with vehicle or second impact with ground. Most studies of pedestrian injury focus on reducing traumatic injuries due to the primary impact between the vehicle and the pedestrian. However, based on the Pedestrian Crash Data Study (PCDS), some researchers concluded that one of the leading causes of head injury for pedestrian crashes can be attributed to the *secondary impact*, defined as the impact of the pedestrian with ground *after* the

primary impact of the pedestrian with the vehicle. Krieger et al. (1976) conducted a series of ten experimental tests simulating pedestrian-vehicle impacts using cadavers and a 95th percentile dummy. The purpose of this study was to acquire data to describe pedestrian kinematics, injury patterns and effect of different vehicle front-end geometries. Two of these tests showed no head-on ground impact. Kendall *et al.* (2006) reconstructed vehicle-pedestrian impacts by performing multi-body simulations and showed that in most cases the vehicle would pose a greater risk of injury than the ground. However, they also noted that the ground impact can be one of the main sources of *head* injury in pedestrian impacts with vehicles having a raised front-end profile, such as sport-utility vehicle (SUV). Roudsari *et al.* (2005) investigated a total of 386 pedestrian crashes obtained from the PCDS database. They concluded that the leading cause of head injury for pedestrian-vehicle crashes involving raised front-end profile vehicle can be attributed to ground impact. Comparing pedestrian injuries from passenger cars and high front-end profile vehicles such as SUVs, mini vans, and light trucks (LTV), researchers have shown that for passenger cars the ground contact accounts for only 7% of head injuries compared to 39% for LTVs (Roudsari *et al.*, 2005). Head injuries are especially more frequent for Bonnet (Hood) Leading Edge (BLE) heights above 700 mm (Otte and Pohlemann 2001). Tamura et al. (2010) conducted a series of numerical simulations for pedestrian-SUV impact. Their study suggested the importance of accounting the effect of pedestrian ground impact because the pedestrian can be seriously injured when

landing head-on onto the road surface following primary impact with the striking vehicle.

The purpose of this aim is to understand if different vehicle front-end profiles can affect the risk of pedestrian secondary head impact with the ground and thus may help in reducing the risk of head injury during secondary head impact with ground. Previous pedestrian safety research work has suggested the use of active safety methods, such as 'pop up hood,' to reduce pedestrian head injury during primary impact. Accordingly, this aim presents some numerical simulations using a full pedestrian human model with raised hood to capture the effect of a pop-up hood on overall kinematics.

Chapter 7: Aim 1 – Feasibility of new hood edge designs for pedestrian head safety improvements

7.1 Methods

To test the feasibility stated in the first aim, finite element analysis is utilized by employing a full size SUV vehicle model (available at the National Crash Analysis Center at George Washington University) with a steel hood and free ISO headform FE model (developed and validated by Oasys (Solihull, UK), to simulate vehicle to pedestrian head Impact. For validation of the SUV model, full frontal crash simulations into a flat rigid wall were completed. Some model preparation work was done on vehicle front end to make it suitable for pedestrian safety work. The details of vehicle FE models along with their validation are shown in Appendix A. Details of head Impactor models are explained previously in Section 4.1.1. The hood of the FE car model is marked with different WAD lines, per guidelines of the GTR regulations, to divide the hood top area into child head impact zone and adult head impact zone. Child head impact points and adult head impact points are marked (Figure 7.1.1) along with different WAD lines on hood top for every 100 mm to fully evaluate the complete hood top. Only left half portion of hood top is analyzed in this study considering the hood symmetry and to reduce the computational costs. As the 2100 WAD was falling out of BRRL in this particular car model, another intermediate line is marked referred as 'b/w 1700-2100 WAD Line'. Some other impact points are evaluated based on critical under hood structure such as hood hinges to evaluate the HIC on those critical areas.

A series of preliminary numerical simulations were conducted mimicking an ISO headform impacting various points on a full size SUV vehicle FE model hood at 35 km/h based on legal requirements. Results as shown in Table 7.1.1 suggest that the highest model-predicted HIC points lie along the hood periphery region, not in the central zone of hood as shown in Figure 7.1.2. Zone1 (bound by solid line) indicates the regions with $HIC > 1700$, zone 2 (bound by dotted line) shows those with $1000 < HIC \leq 1700$, and remaining portion of hood forward of rear edge marks regions with $HIC < 1000$.



Figure 7.1.1 Selected head impact simulation points along various WAD lines

Table 7.1.1 Preliminary results for Head Impact on vehicle Hood

S.No	Impact Location	HIC
1	1000 WAD Pt1	3163
2	1000 WAD Pt2	1613
3	1000 WAD Pt3	955

4	1000 WAD Pt3_Frt	1177
5	1000 WAD Pt4	999
6	1000 WAD Pt5	1006
7	1000 WAD Pt6	910
8	1000 WAD Pt7	872
9	1000 WAD Pt7_frt	1195
10	1250 WAD Pt1	3713
11	1250 WAD Pt2	1287
12	1250 WAD Pt3	835
13	1250 WAD Pt3_Rear	870
14	1250 WAD Pt4	870
15	1250 WAD Pt5	957
16	1250 WAD Pt6	872
17	1250 WAD Pt7	808
18	1700 WAD Pt1	2921
19	1700 WAD Pt2	1219
20	1700 WAD Pt3	1080
21	1700 WAD Pt4	1275
22	1700 WAD Pt5	1671
23	1700 WAD Pt6	1703
24	1700 WAD Pt7	1608
25	1700-2100 WAD pt1	2616
26	1700-2100 WAD pt1_FRT	3645
27	1700-2100 WAD pt2	1371
28	1700-2100 WAD pt3	1100
29	1700-2100 WAD pt4	966
30	1700-2100 WAD pt5	900
31	1700-2100 WAD pt6	942
32	1700-2100 WAD pt7	772

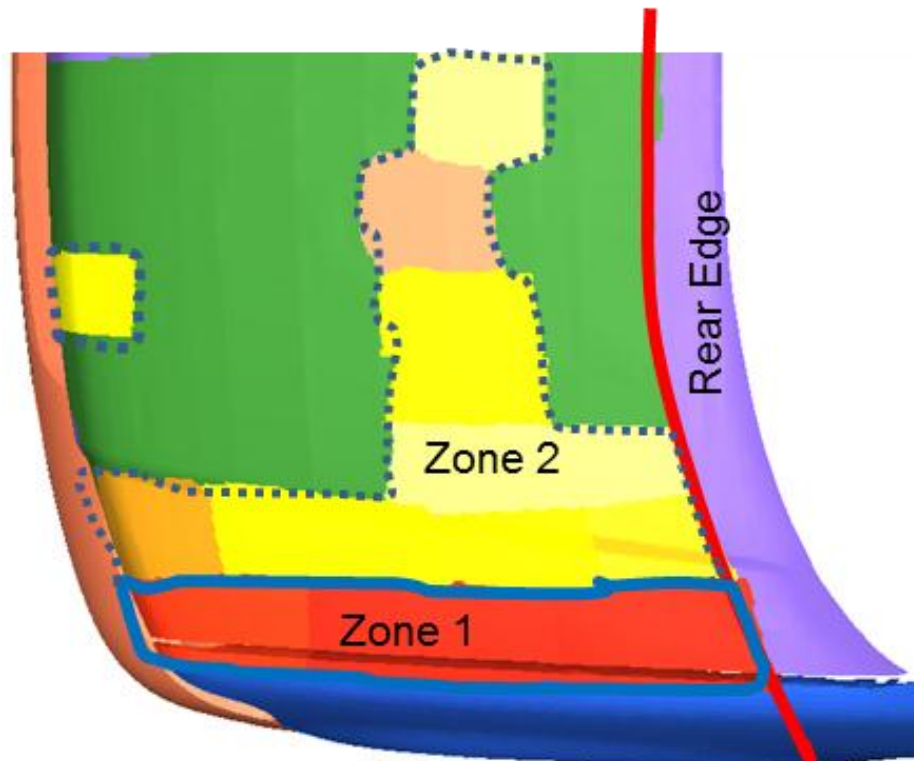


Figure 7.1.2: HIC values predicted by a computer model mimicking an ISO headform impacting a full size SUV vehicle hood at 35 km/h along various impact points on hood. Zone 1 indicates those points with $HIC > 1,300$, Zone 2 indicates those points with $HIC > 1,000$ and green portion represents those points with $HIC < 1000$.

Different shape parameters are studied by morphing the vehicle FE models using commercial morphing software, DEP Morpher version 5.1 (Troy, Michigan). A glossary of vehicle terminology is shown in Appendix B.

7.2 Shape parameters along hood edges

7.2.1 Shotgun to fender interface: One of the shape parameter along hood periphery is lowering the shotgun distal end in vertical direction by keeping the proximal end fixed to the hinge pillar. The shotgun was lowered in 3 different intervals (30-90 mm) to study the effect on hood-fender interface stiffness. While lowering the shotgun, the fender

interface with shotgun was maintained in three different ways to analyze the best possible scenario for fender to shotgun interface.

- lowering the fender flange along with shotgun and keeping fender directly bolted to shotgun (Figure 7.2.1 b)
- keeping the fender flange at original location and modeling a crushable bracket made of mild steel in between shotgun and fender flange (Figure 7.2.1 c and Figure 7.2.2 b)
- making the flat flange for fender and modeling a crushable bracket in between shotgun and fender flange (Figure 7.2.1 d)

Different interfaces for shotgun to fender are shown in Figure 7.2.1 (cross-sectional views). Figure 7.2.2 shows the lateral view for shotgun changes along with added crushable bracket between shotgun and fender. The original shotgun and modified shotgun are shown in Figure 7.2.3.

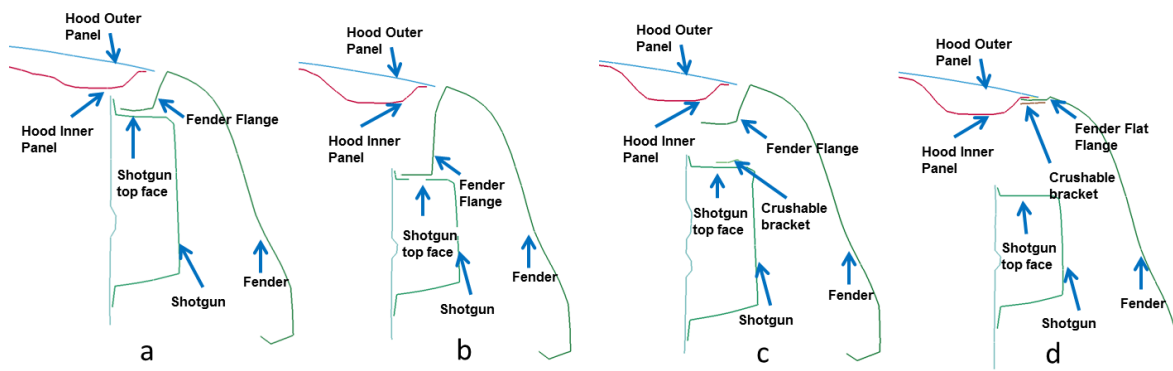


Figure 7.2.1: cross-sectional views showing the sectional cuts for the fender, hood panels and shotgun: a) original interface, b) fender flange lowered along with the shotgun, c) fender flange at original position with crushable bracket for fender to shotgun bolting, and d) flat flange for fender with crushable bracket for fender to shotgun bolting.

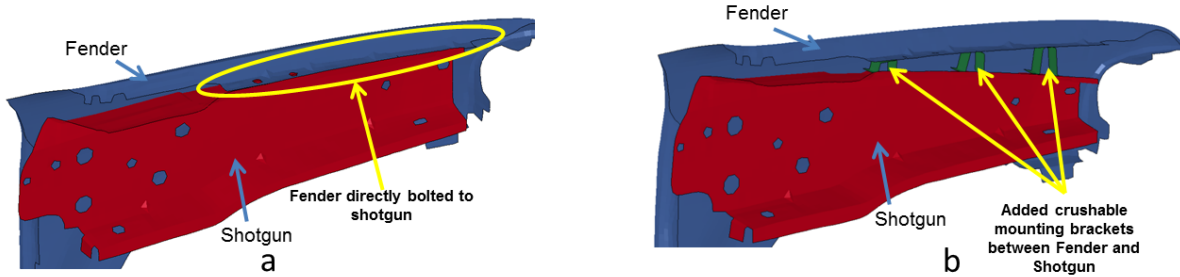


Figure 7.2.2: Lateral view for the shotgun to fender interface: a) fender directly bolted to shotgun, b) fender bolted to shotgun by means of crushable brackets.

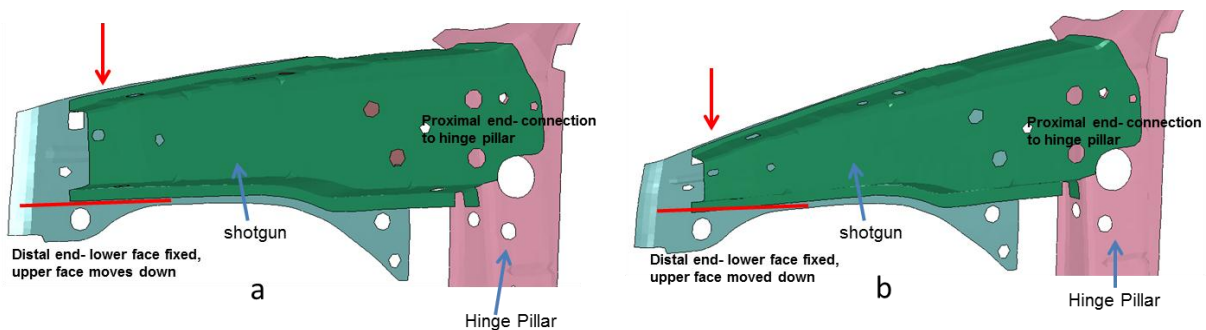


Figure 7.2.3: a) The original shotgun b) morphed shotgun (lowered by 90mm at the distal end)

7.2.2 Hood inner panel periphery cross section: peripheral cross-section of the hood inner panel is morphed for changing its width (inward/outward) and height (up/down) to analyze its effect on head impact severity along the hood periphery. These peripheral cross-sectional changes are analyzed one at a time. These cross sections changes are done in addition to shotgun to fender interface changes as described in section 7.2.1. Figure 7.2.4 shows the peripheral cross-section of the hood inner panel with the scope of morphing.

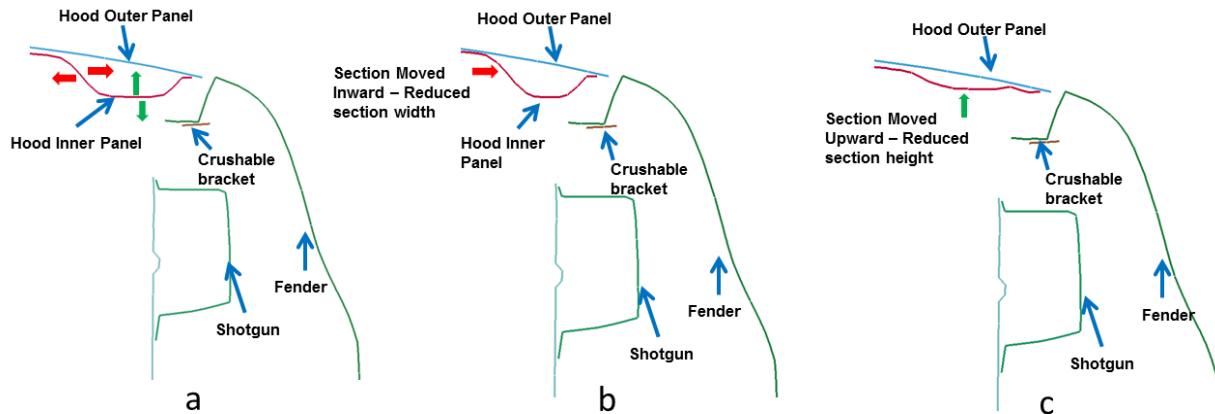


Figure 7.2.4: cross-sectional views with section cut for the fender, hood panels and shotgun- showing hood inner panel's section changing in width and height. a) The original cross-section b) section width reduced by moving section inward c) section height reduced by moving section upwards

7.2.3 Hood inner panel periphery shear panel: The periphery of hood inner panel is split into two parts as shown in Figure 7.2.5. The two pieces of hood inner panels are joined by adhesives of low strength so that adhesives will fail at a plastic strain of 5%. This result in detaching of outer piece of hood inner panel along the periphery from inner piece during head impact in that zone thus reduces the hood stiffness along the peripheral region. These changes are done on FE model where the shotgun is already morphed to a maximum allowable low position and has a flat flange for the fender with added crushable bracket in between the fender and shotgun as described in section 7.2.1 and shown in Figure 7.2.1 d.

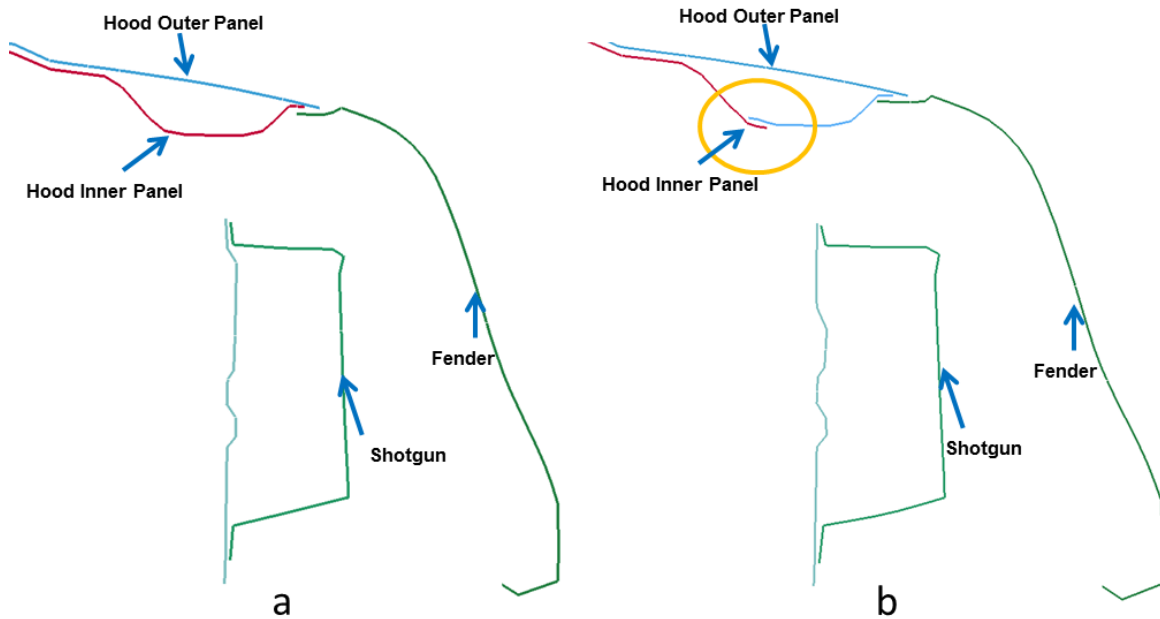


Figure 7.2.5: cross-sectional views with section cut for the fender, hood panels and shotgun: a) hood inner panel cross section, and b) hood inner cross section with shear panel (highlighted in the circle).

7.2.4 under hood packaging clearance: a certain amount of clearance space is required between the hood inner panel and under hood packaged structure. The interactions with the under hood packaged structure could lead to an increase in the secondary acceleration thus resulting in higher HIC (Kerkeling et al., 2005). We used a 50 mm clearance space to develop a styling surface. Any under hood packaging structure that penetrates into that styling surface is considered critical and is repackaged under the hood to analyze the head impact points for opportunity to improve head performance criteria. These changes are done on FE model where shotgun is already moved down to maximum allowable low position as described in section 7.2.1. Also this FE model has flat flange for fender with added crushable bracket in between the fender-shotgun as shown in Figure 7.2.1 d, and the hood inner panel is

split into two pieces along periphery as shown in Figure 7.2.5 b. Figure 7.2.6 illustrates the styling surface for proposed clearance with the penetrating under hood structure.

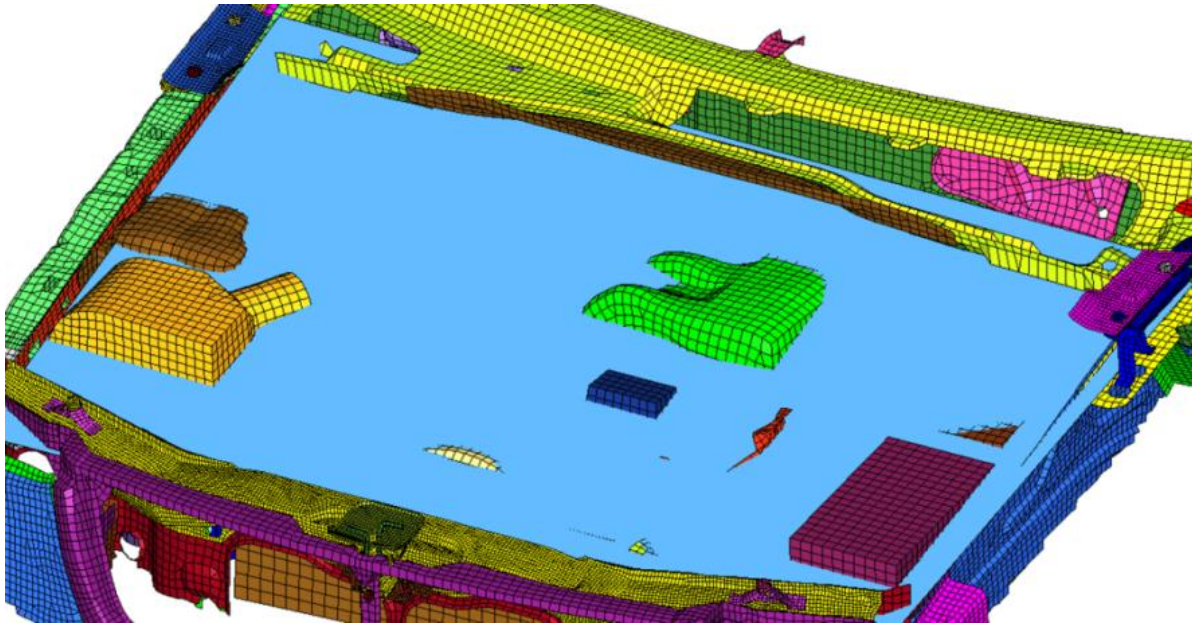


Figure 7.2.6: styling surface with penetrating under hood structure.

7.2.5 Fender and crushable bracket stiffness: another important parameter to reduce the hood periphery stiffness is to use low stiffness materials for hood-to-vehicle interface such as the fender and mounting brackets for fender to shotgun attachment. The fender does not contribute much to energy absorption during frontal crash scenario thus the fender material could be switched to a low stiffness material such as aluminum without the risk of deteriorating other crash impact performances. The fender and mounting brackets are switched to aluminum material in this study with proper gauge adjustment. Different head impact points on hood periphery along various WAD lines are analyzed.

7.3 Results

The shotgun to fender interface changes as described in section 7.2.1 showed significant improvement in the head performance criteria. Three impact points were tested along the hood periphery on different marked WAD lines. These changes for shotgun to fender interface made good improvement along the first two impact points along periphery thus showing the feasibility of this shape change for HIC improvement along the hood edge. The results showed an interesting solution for shotgun to fender interface. It suggests the best overall improvement for child impact zone in the case of shotgun lowered by 60 mm and developing a crushable bracket for fender mounting on shotgun as shown in Table 7.3.1. The bracket to support the hood over shotgun became unstable in case of 90 mm shotgun lowering due to more height of the bracket and bracket's buckling behavior changed (Figure 7.3.1). This bracket buckling behavior resulted in less total deformation in the case of 90 mm shotgun lowering. For adult impact zone, overall improvement is suggested by lowering the shotgun at the distal end by 90 mm and directly bolting the fender flange to shotgun. Based on a different fender to shotgun interface suggested by these outcomes for child and adult head impact zones, a combined proposed interface is shown in Figure 7.3.2 where for child impact zone, Shotgun is lowered by 60 mm and fender with flat flange is mounted to shotgun by means of crushable bracket. For adult impact zone, fender flange is lowered along with shotgun and directly bolted to shotgun.

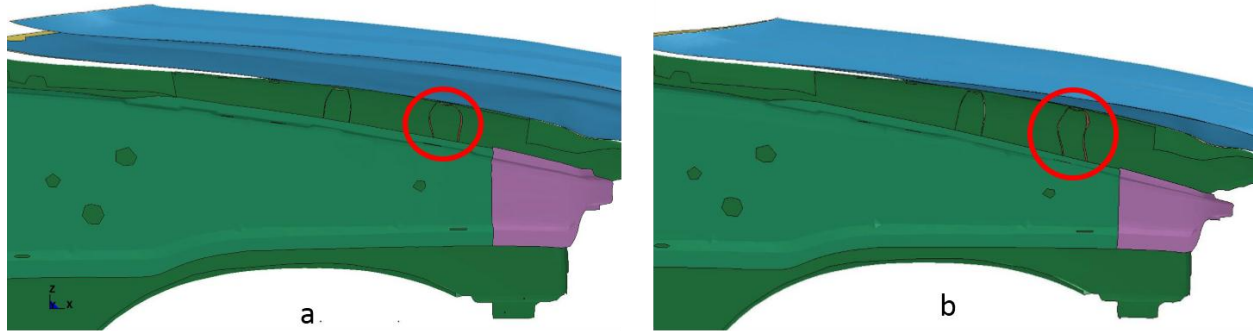


Figure 7.3.1: Bracket buckling behavior a) 60 mm shotgun lowering- desirable bracket deformation resulting in more deformation space, b) 90 mm shotgun lowering- bad bracket buckling mode, resulting in lower deformation.

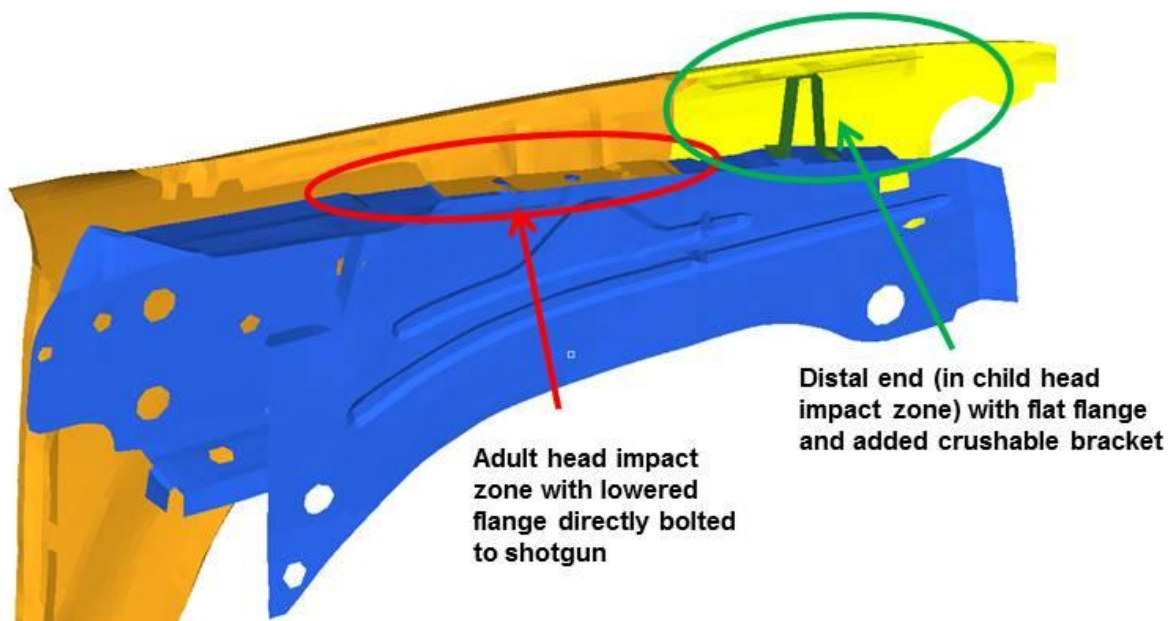


Figure 7.3.2: Proposed fender to shotgun interface.

Table 7.3.1: Effect of the shotgun to fender interface change on HIC

S.No	Impact Location	HIC	Shotgun Lowered 90 mm	Shotgun Lowered 60 mm Fender Flat flange and Brkt	% change (based on best options indicated)
1	1000 WAD Pt1	3163	2771	2019	36.17
2	1000 WAD Pt2	1613	1475	1632	-1.18
3	1000 WAD Pt3	955	955	968	-1.36
4	1250 WAD Pt1	3713	2878	1974	46.84
5	1250 WAD Pt2	1287	1285	1304	-1.32
6	1250 WAD Pt3	835	827	863	-3.35
7	1700 WAD Pt1	2921	1850	1584	36.67
8	1700 WAD Pt2	1219	1095	1239	10.17
9	1700 WAD Pt3	1080	1082	1082	-0.19
10	1700-2100 WAD pt1	2616	1786	1922	31.73
11	1700-2100 WAD pt1_FRT	3645	1763	1759	51.63
12	1700-2100 WAD pt2	1371	1159	1292	15.46
13	1700-2100 WAD pt3	1100	977	1033	11.18

Based on above results, it could be proposed that more crush space is needed between the hood and fender mounts which could also be achieved by raising the hood in terms of extended hinges as illustrated in Figure 7.3.3. But raising the hood could lead to different overall pedestrian kinematics and needs to be verified independently for overall pedestrian kinematics rather than just using free form head impacts.

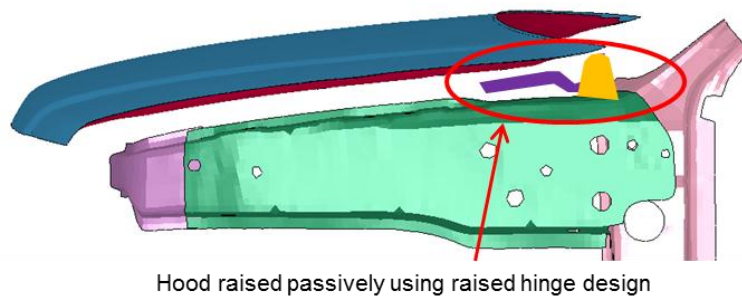


Figure 7.3.3: Concept of raised hood using passive raised hinge design to create deformation space between hood and shotgun.

Changes in periphery cross-section of the hood inner panel, as shown in Figure 7.2.4, did not make a significant improvement in HIC value except for localized impact points in the vicinity of that structural change. Among all peripheral cross-sectional changes, by moving the cross-section lateral showed some improvement in HIC as shown in Table 7.3.2. Changes in the hood inner panel as shown in Figure 7.2.5 showed significant improvement for impact point 2 and impact point 3 on all marked WAD lines (Table 7.3.3). Using the under hood clearance based on styling surface helped improve HIC significantly but this change did not help along the hood edges. Using a low stiffness material for the fender and crushable brackets helped to make HIC meet legal requirements along the overall hood as shown in Table 7.3.3. Each shape change was implemented in addition to previous shape change as discussed in Sections 7.2.1 to 7.2.5, thus Table 7.3.3 shows the cumulative effect of these shape changes.

Table 7.3.2: Effect of the hood inner section changes on HIC

S.No	Impact Location	Shotgun Lowered 90 mm Fender Flat flange and Brkt	Hood Inner _SectionMoved Out
1	1000 WAD Pt1	2147	2064
2	1000 WAD Pt2	1637	1630
3	1000 WAD Pt3	972	999
10	1250 WAD Pt1	2060	2024
11	1250 WAD Pt2	1314	1234
12	1250 WAD Pt3	862	881
18	1700 WAD Pt1	1738	1624
19	1700 WAD Pt2	1251	1319
20	1700 WAD Pt3	1088	1082
25	1700-2100 WAD pt1	2092	2099
26	1700-2100 WAD pt1_FRT	1693	1591
27	1700-2100 WAD pt2	1356	1375
28	1700-2100 WAD pt3	1067	1096

Also a histogram (Figure 7.3.4) highlights the variation of HIC values as a function of design variables. The results indicate that the shotgun to fender interface, splitting hood inner panel along periphery, under hood clearance and fender interface material are key players for reducing the overall hood stiffness. Lowered hood stiffness, in turn, could reduce the risk of head injury during primary head impact with the hood.

Some resultant head acceleration histories calculated from the original model are compared with the final improved model. These head acceleration histories are shown in Appendix C. Full frontal crash simulation was performed with final updated hood details and shotgun to fender interface changes to analyze the effect of these shape

changes on frontal crash performance. This analysis confirmed that changes in the upper load path didn't affect the frontal impact performance. Results and comparisons of original model performance versus modified model are also shown in Appendix C.

Table 7.3.3: Cumulative effect of shape changes along hood periphery on HIC

S. No.	Impact Location	HIC	Shotgun to fender Interface	Splitting Hood Inner panel along periphery	Under Hood Clearance	Fender Interface Material	% improvement
1	1000 WAD Pt1	3163	2147	na	1511	1202	62.0
2	1000 WAD Pt2	1613	1637	1394	1353	1313	18.6
3	1000 WAD Pt3	955	972	809	738	731	23.5
5	1000 WAD Pt4	999	na	na	669	669	33.0
6	1000 WAD Pt5	1006	na	na	742	742	26.2
7	1000 WAD Pt6	910	na	na	746	746	18.0
8	1000 WAD Pt7	872	na	na	690	690	20.9
10	1250 WAD Pt1	3713	2060	na	1482	1055	71.6
11	1250 WAD Pt2	1287	1314	1116	751	740	42.5
12	1250 WAD Pt3	835	862	725	572	556	33.4
14	1250 WAD Pt4	870	na	na	586	586	32.6
15	1250 WAD Pt5	957	na	na	557	557	41.8
16	1250 WAD Pt6	872	na	na	535	535	38.6
17	1250 WAD Pt7	808	na	na	536	536	33.7
18	1700 WAD Pt1	2921	1738	1473	1259	962	67.1
19	1700 WAD Pt2	1219	1251	1086	793	783	35.8
20	1700 WAD Pt3	1080	1088	944	609	611	43.4
21	1700 WAD Pt4	1275	na	na	741	741	41.9
22	1700 WAD Pt5	1671	na	na	928	928	44.5
23	1700 WAD Pt6	1703	na	na	949	949	44.3
24	1700 WAD Pt7	1608	na	na	904	904	43.8
25	1700-2100 WAD pt1	2616	2092	1804	1751	1535	41.3
26	1700-2100 WAD pt1_FRT	3645	1693	na	1320	1607	55.9
27	1700-2100 WAD pt2	1371	1356	1156	1005	972	29.1
28	1700-2100 WAD pt3	1100	1067	895	723	720	34.5
29	1700-2100 WAD pt4	966	na	na	630	630	34.8
30	1700-2100 WAD pt5	900	na	na	660	660	26.7
31	1700-2100 WAD pt6	942	na	na	673	673	28.6
32	1700-2100 WAD pt7	772	na	na	723	723	6.3

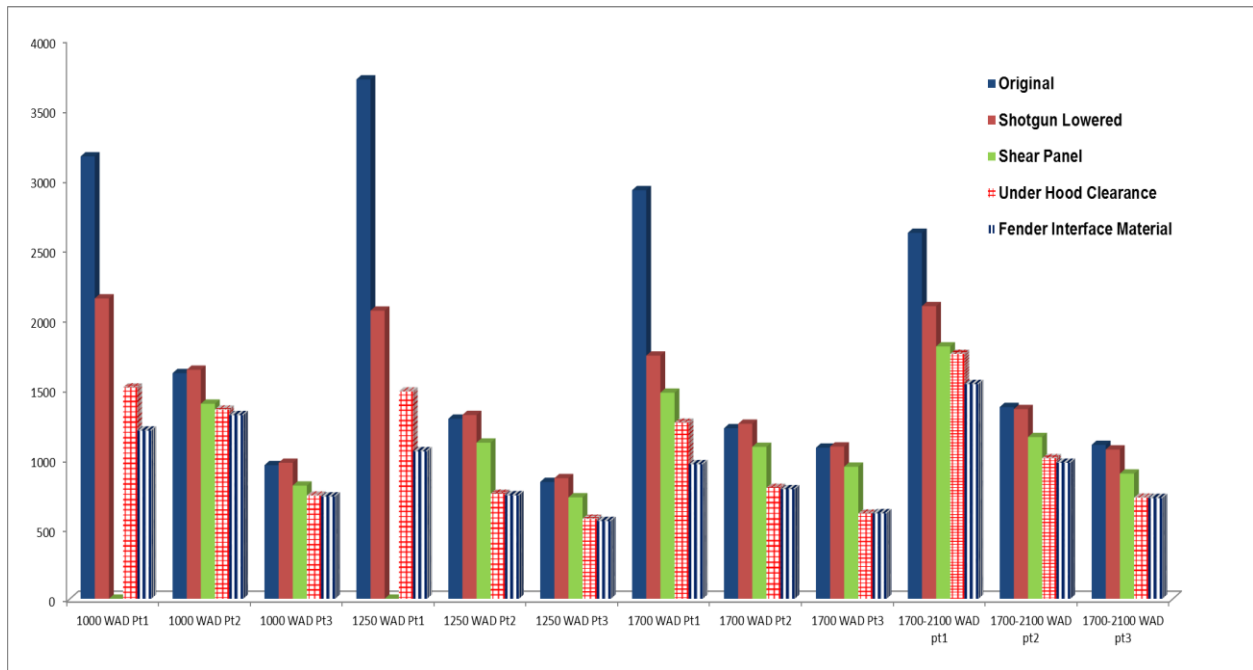


Figure 7.3.4: HIC variation as a function of design variables along different impact locations.

7.4 Discussion

Head Impact performance criterion is very critical in pedestrian to vehicle accidents. The proposed limited structural change for the hood edges and hood to vehicle interface showed a significant improvement in HIC on different impact points on the hood and along hood edges. The shape changes for the shotgun to fender interface, dividing hood inner panel into two pieces along their periphery, the under hood clearance, and fender interface low stiffness material proved to be promising structure redesigning alternatives to meet pedestrian crash safety legal requirement as illustrated in Figure 7.4.1. Overall, the hood top area with $1000 < \text{HIC} \leq 1700$ is shown as zone 1 (bound by dotted lines) and hood top area meeting legal requirement of $\text{HIC} \leq 1000$ is shown as zone 2 (remaining portion of hood forward of rear edge).

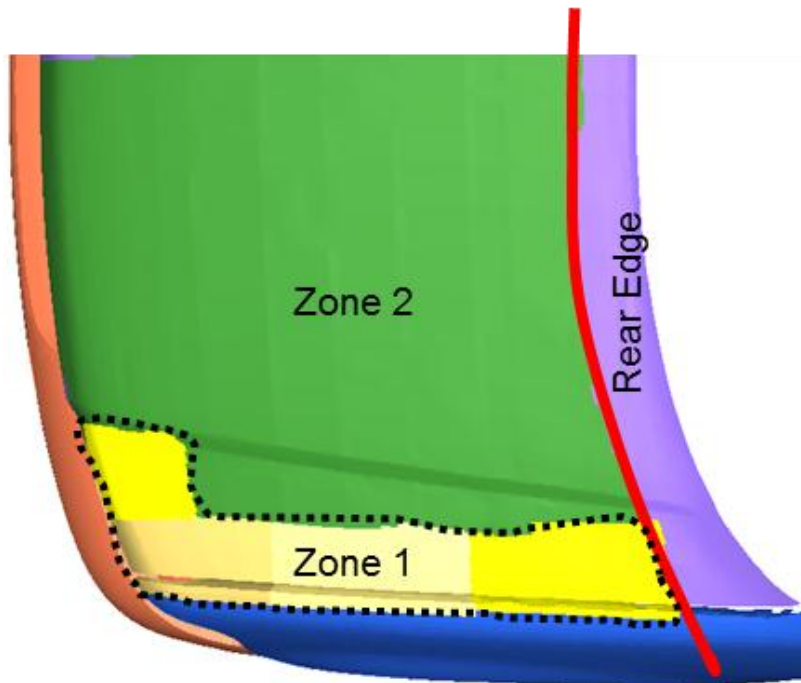


Figure 7.4.1: Head performance along hood top and edges after implementing hood shape parameters.

In this work, only one vehicle FE model is used to study the effect of shape changes for reducing head injury. Moreover, free motion headform is used to simulate the head impact which may not reflect the actual kinematics of pedestrian. HIC is used as the injury indication parameter which may not be a perfect variable to assess head injuries. Future work could be performed to validate the effect of these structural changes such as shotgun lowering on other structural performances such as bending and torsion stiffness, durability etc. Also, Future work could be performed to simulate the pedestrian impact using full human body models to verify the effect of these changes in reducing the risk of injuries. Also, frontal impact simulation could be performed after these structural changes to verify performance in event of front crash and to tune any gages for front load path if required.

Chapter 8: Aim 2 - Evaluating practicality of Pedestrian Head Safety Regulations

In this aim, pedestrian responses are studied using several front-end profiles based on a mid-size vehicle and an SUV that have been validated previously along with several MADYMO pedestrian models (50th, 5th and 6yr old child). Mesh morphing is used to explore changes to the bumper height, hood leading-edge height, and hood rear reference-line height. Numerical simulations leading up to pedestrian head impact with vehicle hood or windshield are conducted at impact speeds of 40 and 30 km/h.

8.1 Methods

While there have been other studies into the effect of vehicle front-end profile on pedestrian injury (Fisher and Hall, 1972; Pritz et al. 1975; Danner et al. 1979), these studies did not consider the high vehicle front-end profiles prevalent today. Moreover, because these studies were based on experimental data, they could not consider as many vehicle profile variations as we can consider with finite element (FE) simulations.

Finite element model simulation: In this study, pedestrian-vehicle crashes were simulated using finite element (FE) vehicle models representing a mid-size car and an SUV (available at the National Crash Analysis Center). MADYMO human pedestrian models were used which represented a mid-size male (50th percentile - standing height 1.74 m and weight 76 kg), small female (5th percentile – standing height 1.53m and weight 50 kg), and 6 year old child (standing height 1.17 m and weight 23 kg). Different pedestrian sizes were considered to ensure that any conclusions about vehicle front-end profile would be applicable to multiple sizes of pedestrians instead of one particular pedestrian size. The MADYMO human pedestrian models have been validated (Lange

et al., 2001; Hoof et al., 2003; MADYMO Human models manual release 7.2, 2010) against blunt impact tests and car-pedestrian impact tests. Summary of these validation tests is given in Appendix D. These validation tests concluded that the models accurately predict the global kinematics; they predict the impact points on the vehicle, especially for the head; and that they predict the shape and trends of the head, chest, and pelvis accelerations. In regard to the vehicle FE model validation, full frontal simulations of crash into a flat, rigid wall were completed. Some more work was done on vehicle front-end to make it useful for pedestrian safety work. Details of vehicle FE models along with their respective validations are already explained in Appendix A. The full vehicle model were used which includes engine and other under hood components but only main components of vehicle front-end profile are shown in most figures for easy viewing.

In this study, commercially available software of dynamic FE solver, LS-DYNA version 971 R5.1.1 (Livermore Software Technology Co., Livermore, CA) and MADYMO 7.2 (TASS International, Helmond, The Netherlands) were used as coupled tools to perform pedestrian-vehicle crash simulations. Different front-end profile shapes were obtained by morphing the vehicle FE models using commercial morphing software, DEP Morpher version 5.1 (Troy, Michigan). Front bumper, bonnet (hood) leading edge and bonnet (hood) rear reference line are the changed parameters (Figure 8.1.1) to obtain different front-end profiles of the vehicles.

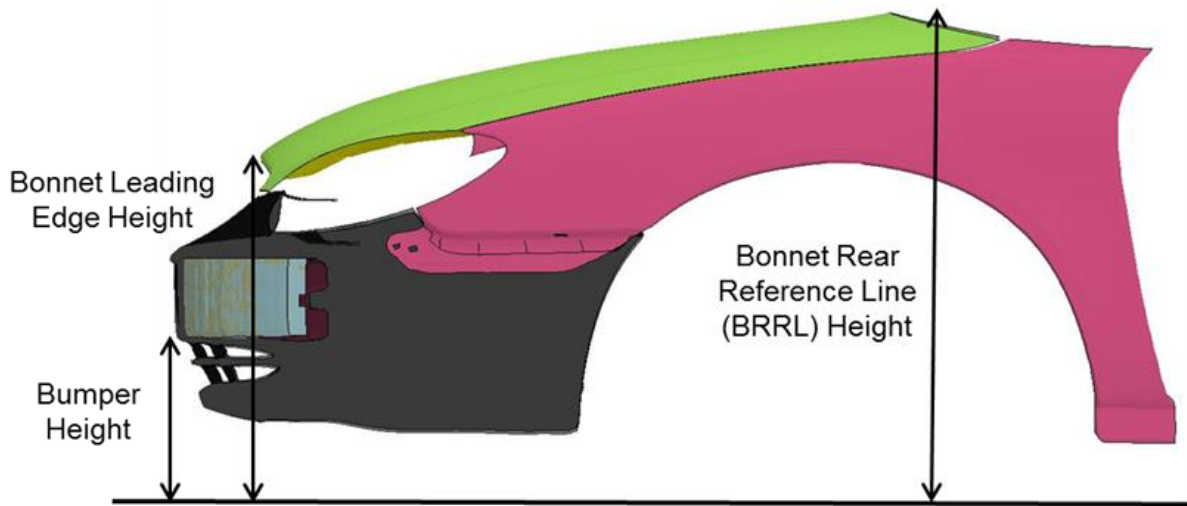


Figure 8.1.1: Vehicle parameters morphed to develop different front-end profiles (vehicle components morphed are: front bumper - shown in blue, hood panels - shown in green, fender - shown in red and fascia - shown in gray)

Four vehicle front-end profiles were used to represent the midsize sedan (Figure 8.1.2) and another four for the SUV (Figure 8.1.3). Profile1 in this study represents lowest hood slope, profile 4 represents maximum hood slope (Table 8.1.1) and profile 2 represents original profile of the vehicle.

Table 8.1.1: Parameters values for vehicle front end profiles

		Bumper Height	Bonnet leading edge	BRRL
Mid Size Sedan	Profile1	325	795	900
	Profile2	325	650	900
	Profile3	300	585	900
	Profile4	300	650	980
SUV	Profile1	375	1075	1150
	Profile2	360	980	1150
	Profile3	360	885	1150
	Profile4	360	980	1235

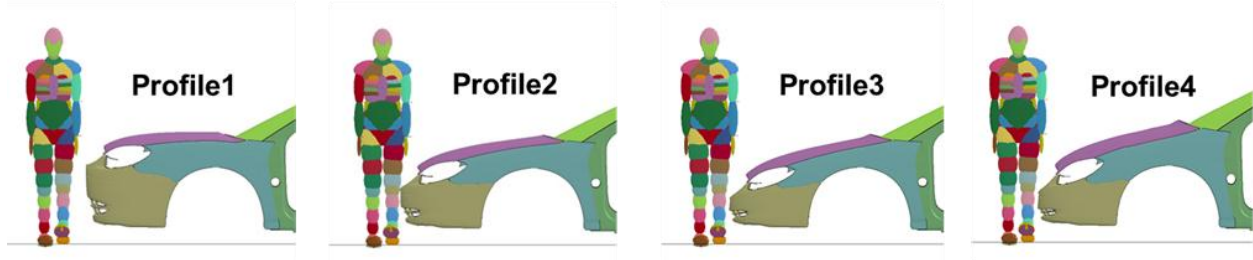


Figure 8.1.2: Different front end vehicle profiles for the mid-size car with respect to a 50th percentile male

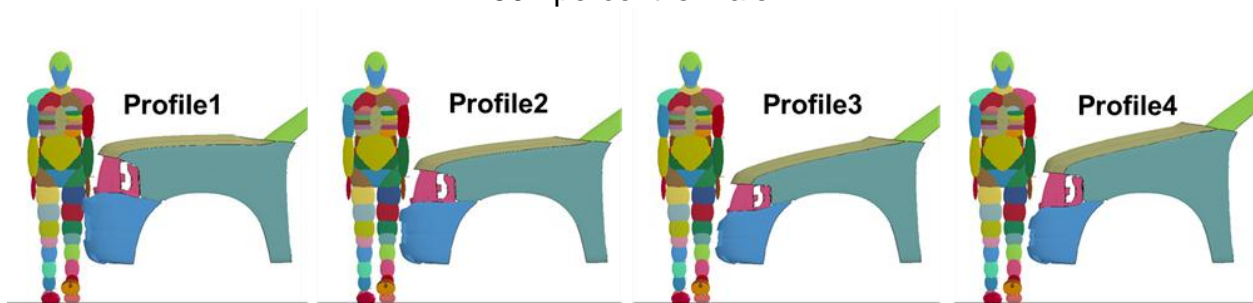


Figure 8.1.3: Different front end vehicle profiles for the SUV with respect to a 50th percentile male

As the hood slope changed for lowered or raised profile, the clearance between hood surface and engine also changed which resulted in overall stiffness change during pedestrian impact with hood. Head acceleration and HIC during impact with hood depends upon deformation space and overall hood stiffness, so there is some suggested clearance between hood panel and engine to achieve head impact targets (Kerklings et al., 2005). In this study, minimum clearance of 50 mm was maintained while developing all different front-end profiles. The fascia was morphed along with the bumper height changes. Ramp angle didn't change while changing the bumper height as we kept the lowest point of the fascia at the same height. Figure 8.1.4 illustrates the cross-section cut to show clearance change between hood inner panel and under hood packaging. Figure 8.1.5 shows the ramp angle for lowered and raised front end profile.

Ramp angle didn't change while changing the bumper height as the lowest point of fascia was kept at the same height.

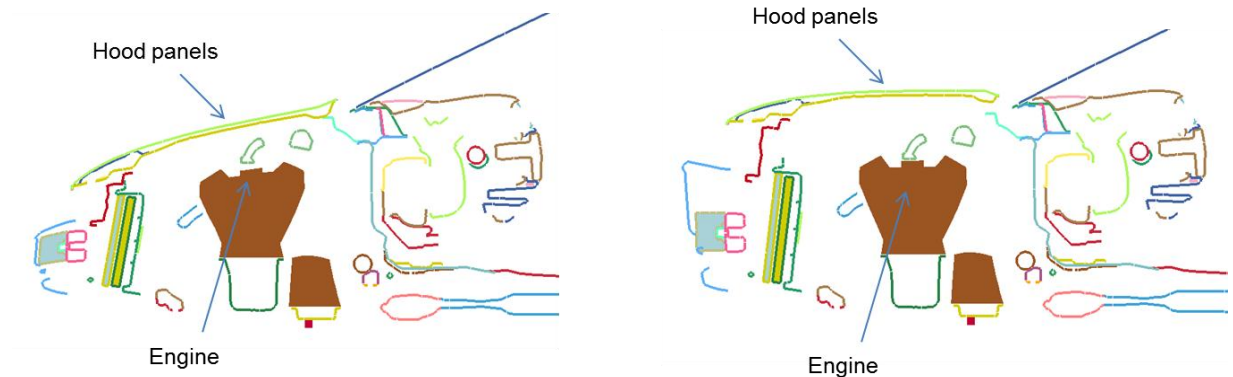


Figure 8.1.4: cross-section cut showing clearance change between hood panel and under hood packaging when vehicle front-end profile changed

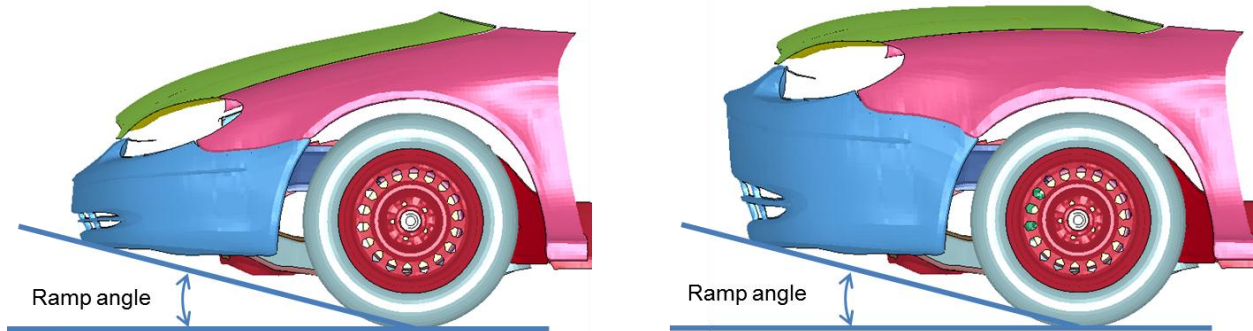


Figure 8.1.5: Ramp angle for lowered front-end profile and raised front-end profile

Boundary condition:

The Pedestrian models were configured to represent a walking pedestrian struck from the side at one leg stance through the gait cycle (Untaroiu et al., 2005). For each vehicle type and front-end profile (Figures 8.1.2 and 8.1.3), crash simulations were run with different combinations of the following factors: vehicle velocity at the moment of

impact (30 or 40 km/h), pedestrian-vehicle impact location (centerline of the vehicle or corner of the vehicle), and pedestrian size (50th, 5th or 6yr old child). Altogether, for the mid-size car, we simulated 29 factor combinations (Table 8.2.1); for the SUV, we simulated 26 factor combinations (Table 8.2.2). In all these simulations, pedestrian posture was kept constant (left leg back and right leg front) and Pedestrian model was positioned with its left side towards the striking vehicle to simulate a lateral impact (Figure 8.1.6). Apart from these, 6 more simulations were conducted to study the sensitivity of HIC and head impact angle due to variation in pedestrian postures (Figure 8.1.7). These simulations were conducted using same 3 pedestrian models striking with mid-size car profile2 at 40 km/h.

A contact function based on that reported by Rooij et al. (2003) was used to represent the contact between the MADYMO human models and vehicle front-end components. This contact function was kept constant for each pedestrian size during impact with different vehicle front-end profiles to capture the effect of only vehicle front profile changes. In pedestrian crashes, the driver tends to brake sharply before an impending impact, causing the front-end of the vehicle to slightly drop in height. To simulate the effect of braking, a constant deceleration pulse of 0.7 G was applied to impacting vehicle (Kendall *et al.*, 2006; Rooij et al., 2003; Meissener et al., 2004). In addition, the original vehicle FE model does not take into account that, due to the weight of the vehicle and compression of the tire, the tire will not be perfectly round. To take tire compression into account, the SUV vehicle model was lowered by 60 mm from pedestrian ground level and mid-size vehicle model was lowered by 40 mm from pedestrian ground level. Details for calculating the amounts of vehicle lowering are

described in Appendix E. The road surface was modeled using a plane element as rigid surface having a coefficient of friction of 0.7 to represent the stiffness and frictional characteristics of asphalt (Kendall *et al.*, 2006).

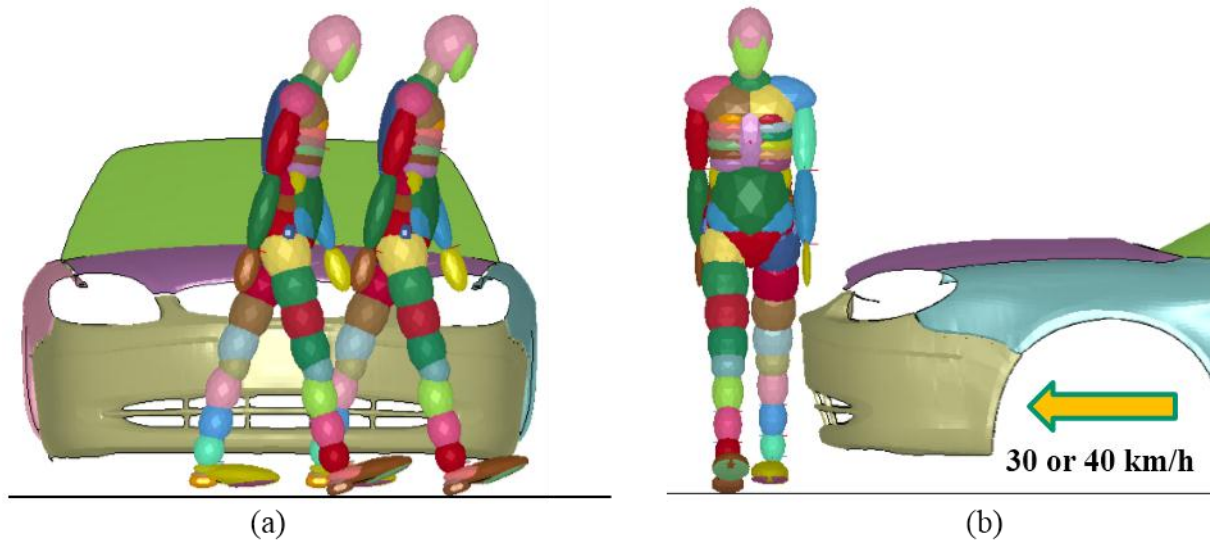


Figure 8.1.6: (a) frontal view of the positioning of pedestrian along the vehicle front-end and (b) lateral view of the pre-impact position of pedestrian in the simulation setup

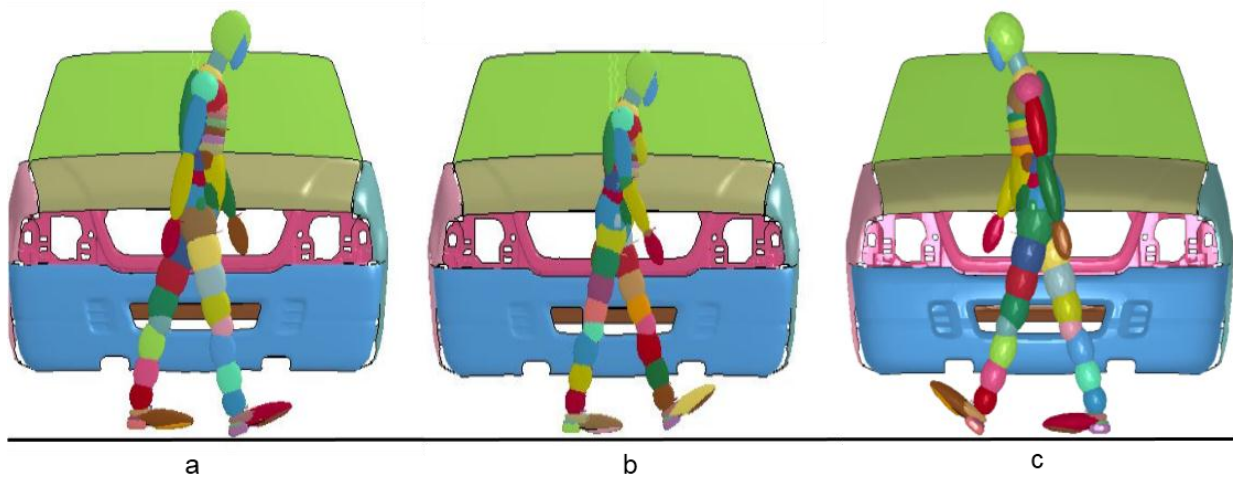


Figure 8.1.7: Pre-impact position of pedestrian (a) left leg back, right leg front, impacting on left side, (b) left leg front, right leg back, impacting on left side, and (c) left leg back, right leg front, impacting on right side

Head impact angles were calculated as described by GTR (Figure 8.1.8). Some simulations were conducted in the same way as the head impact test described by pedestrian safety regulation discussed in Section 4.7. Free motion headform was impacted at the impact location using actual impact angles (as measured from simulations using full pedestrian model) and at an impact angle of 65 degrees (Figures 8.1.9 and 8.1.10) as described by safety regulation [EuroNCAP Pedestrian Testing Protocol Version 5.2.1]. The purpose of this additional study was to compare the impact angles and injury response measurements using a free motion headform and a full scale pedestrian human body model.

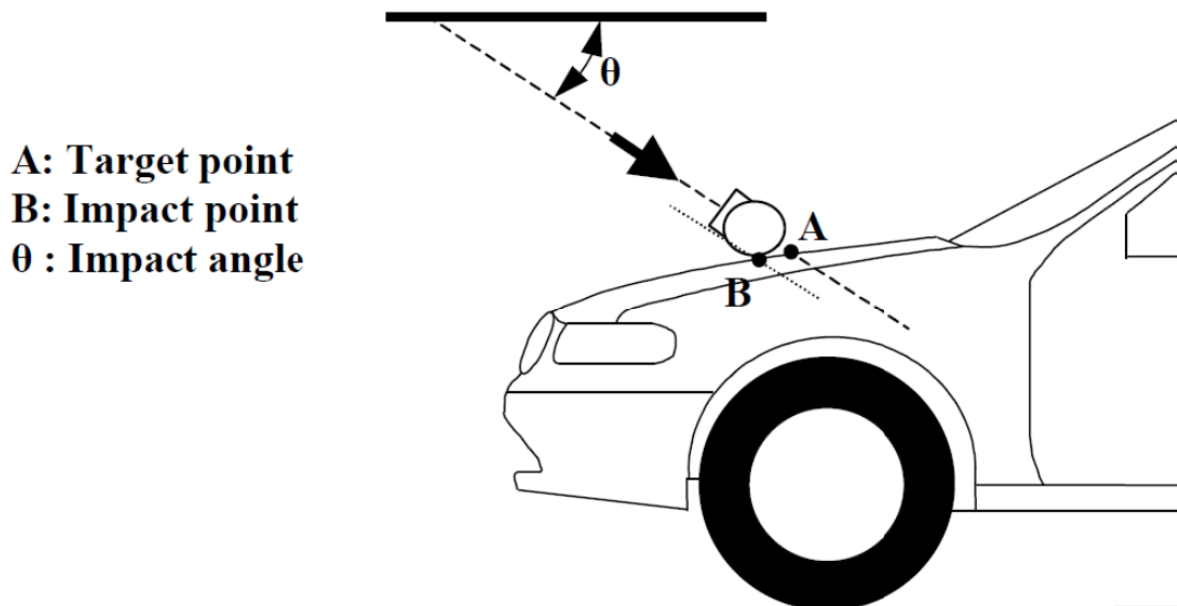


Figure 8.1.8: Head Impact angle definition based on GTR [Technical Report IHRA/Ps/200]

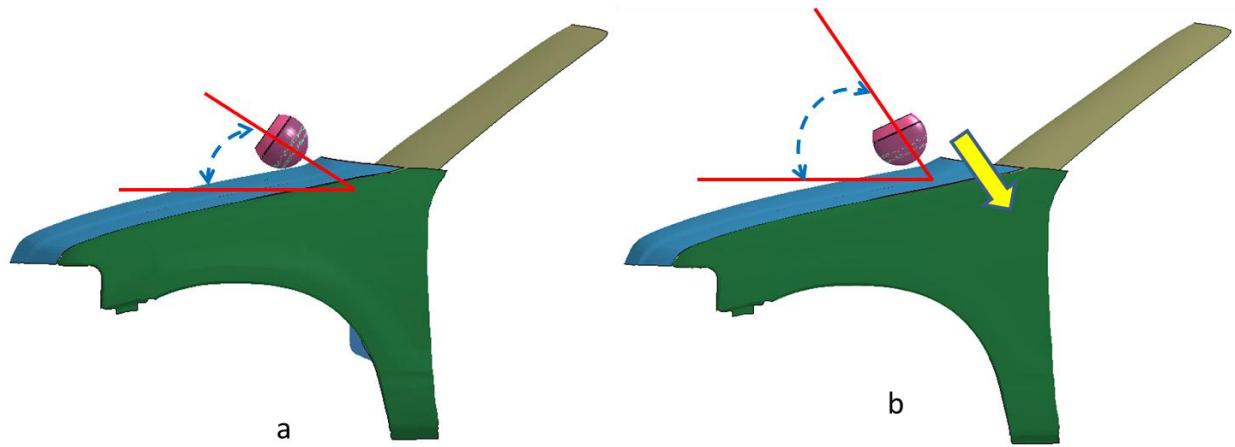


Figure 8.1.9: free motion head-form simulation setups (a) at impact angle as predicted by full pedestrian model on SUV (Run 8, Table 3) and (b) at impact angle of 65 degrees as per EuroNCAP standard.

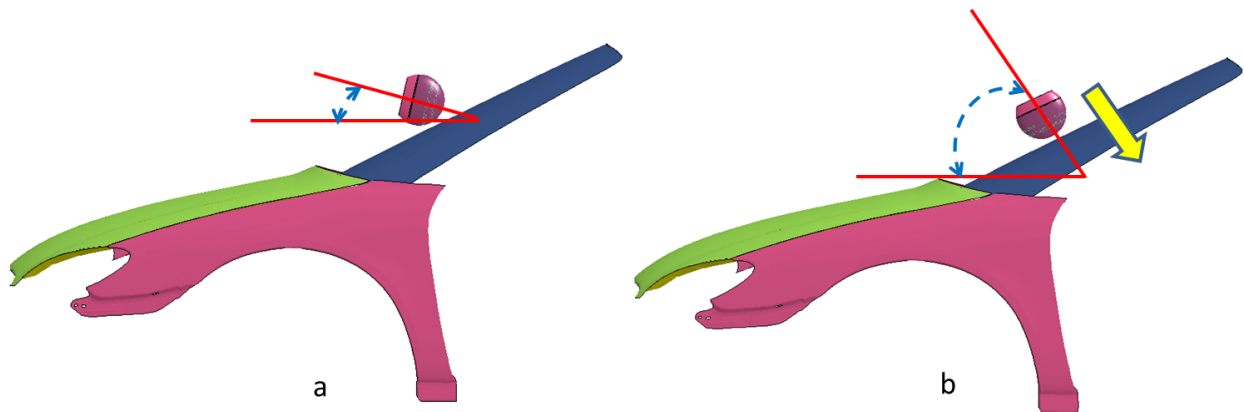


Figure 8.1.10: free motion head-form setup for impact simulations on windshield (a) at impact angle as predicted by full pedestrian model on mid-size car (Run 20, Table 2) and (b) at impact angle of 65 degrees as per EuroNCAP standard.

8.2 Results

Due to variation in pedestrian posture (left leg back-right leg front, left leg front-right leg back etc.) HIC and head impact angle changed by 4% - 40% (Table 8.2.3). HIC

and head impact angle didn't vary much for adult pedestrian (5th percentile and 50th percentile) when impacting on left side or right side but there were some difference in HIC and head impact angles for left leg forward compared to left leg backward.

Typical pedestrian kinematics of 5th percentile female striking the SUV profile2 at 40 km/h (Figure 8.2.1) shows that the bumper first hit the lower legs, causing both feet to leave the ground. Further, the hood leading edge hit the upper legs and pelvis, followed by the pedestrian body rotation towards the hood. The lower body wrapped around the vehicle front-end structure, and lateral head rotation caused the head to have a primary impact on the hood top surface or on the windshield. Pedestrian head impacted with hood top making a smaller angle with horizontal surface (Figure 8.2.1) compared to 65 degrees as described by safety regulations (GTR and Euro NCAP). Pedestrian kinematics for a small female striking with mid-size car of profile1 at 40 km/h (Figure 8.2.2) illustrates that pedestrian head impacted with vehicle hood but making higher impact angle compared to when striking with the SUV vehicle (Figure 8.2.1).

Pedestrian kinematics of a mid-size male striking the SUV of profile3 at 40 km/h (Figure 8.2.3) clearly demonstrates that the SUV with a lowered front-end, as described by profile3, lead to primary head impact with the hood top. Whereas pedestrian kinematics for a mid-size male striking the mid-size car of profile2 at 40 km/h (Figure 8.2.4) shows that pedestrian head impacted with windshield having impact angle almost zero (head almost parallel to horizontal surface). Kinematics of 6 year old child pedestrian striking with mid-size car profile3 at 40 km/h (Figure 8.2.5) and at 30 km/h (Figure 8.2.6) show that impact angle is less at lower impact speed (14° at 30km/h compared to 20° at 40

km/h). At lower impact speed, pedestrian head took longer duration to have first impact with vehicle hood.

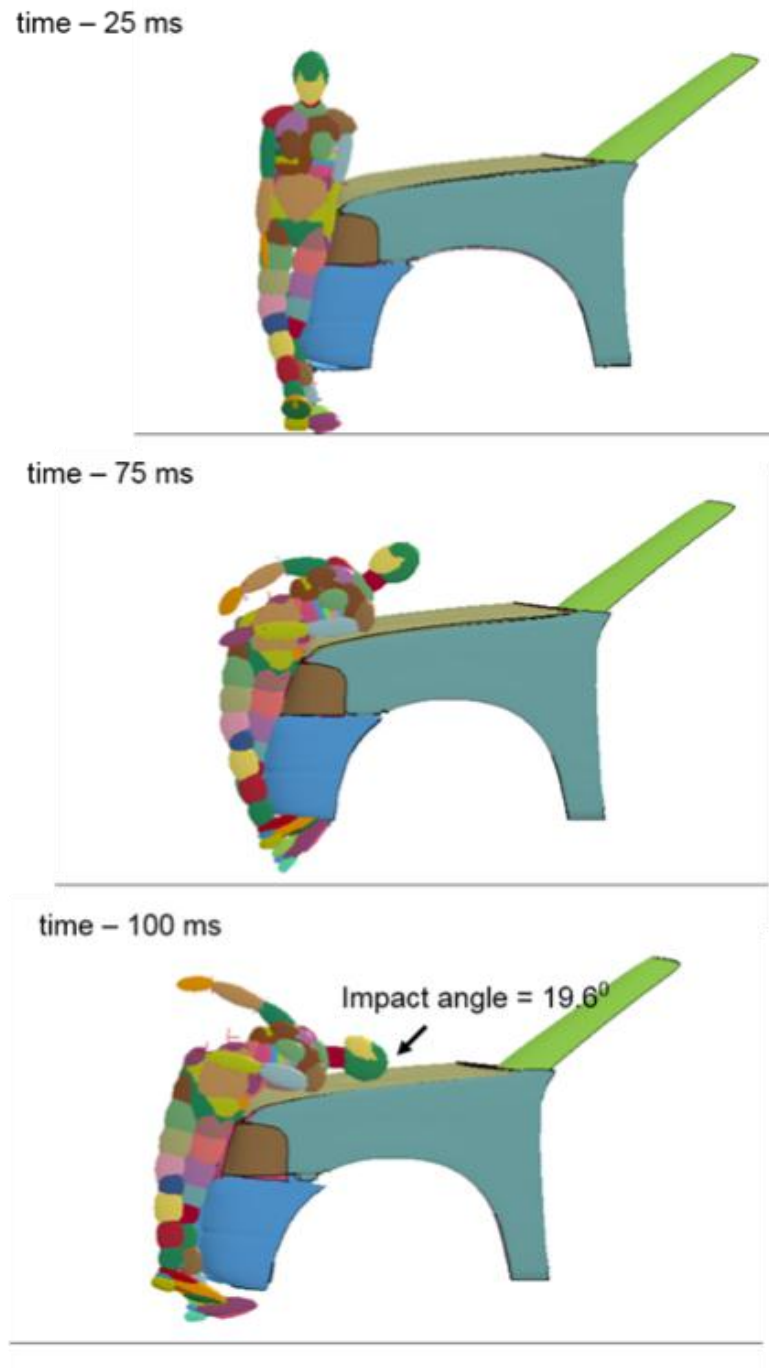


Figure 8.2.1: Pedestrian kinematics of a small female (5th percentile) pedestrian striking with the SUV (profile2) at 40 km/h

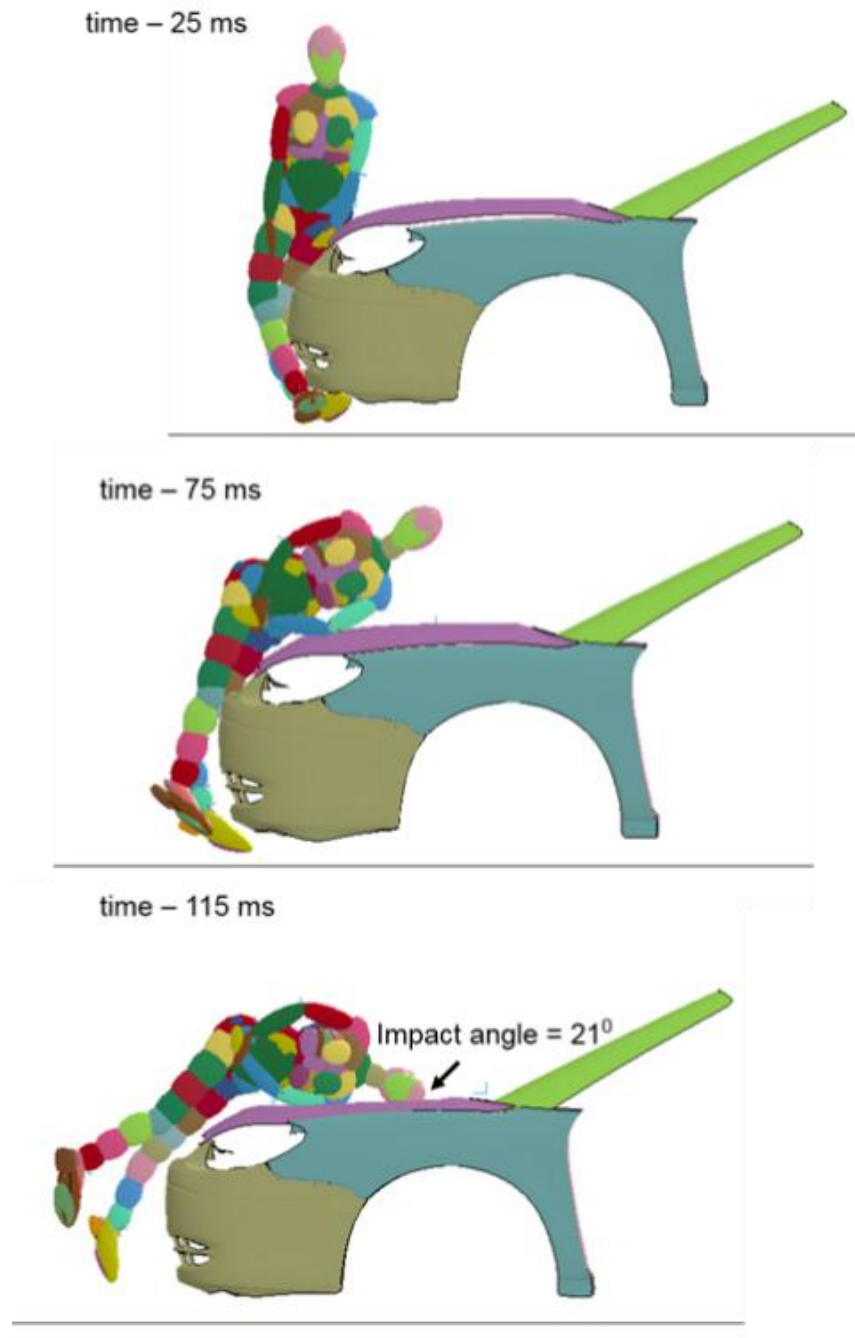


Figure 8.2.2: Pedestrian kinematics of a small female (5th percentile) pedestrian striking with the mid-size vehicle (profile1) at 40 km/h

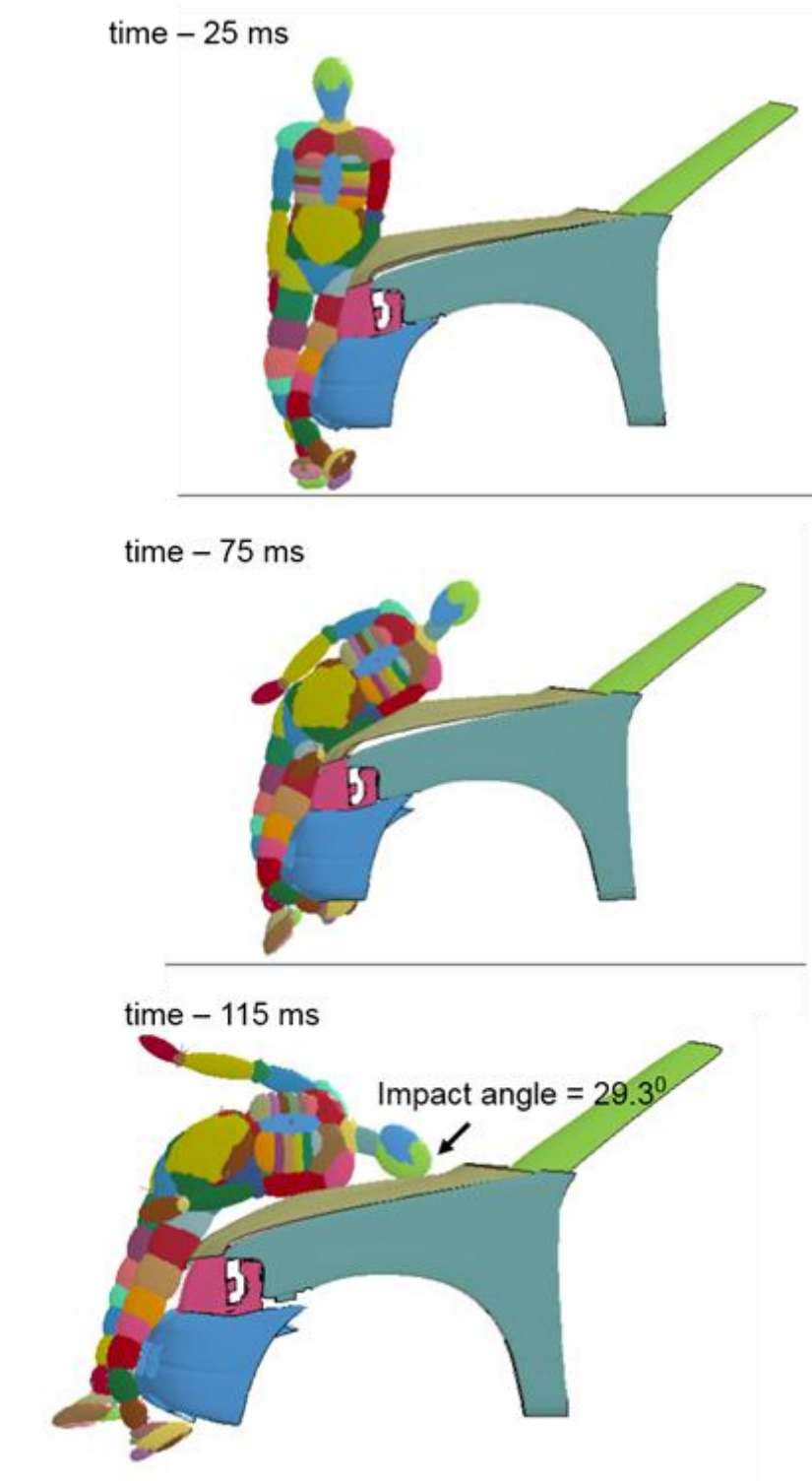


Figure 8.2.3: Pedestrian kinematics of a mid-size male (50th percentile) pedestrian striking with the SUV (profile3) (lowered front end) at 40 km/h

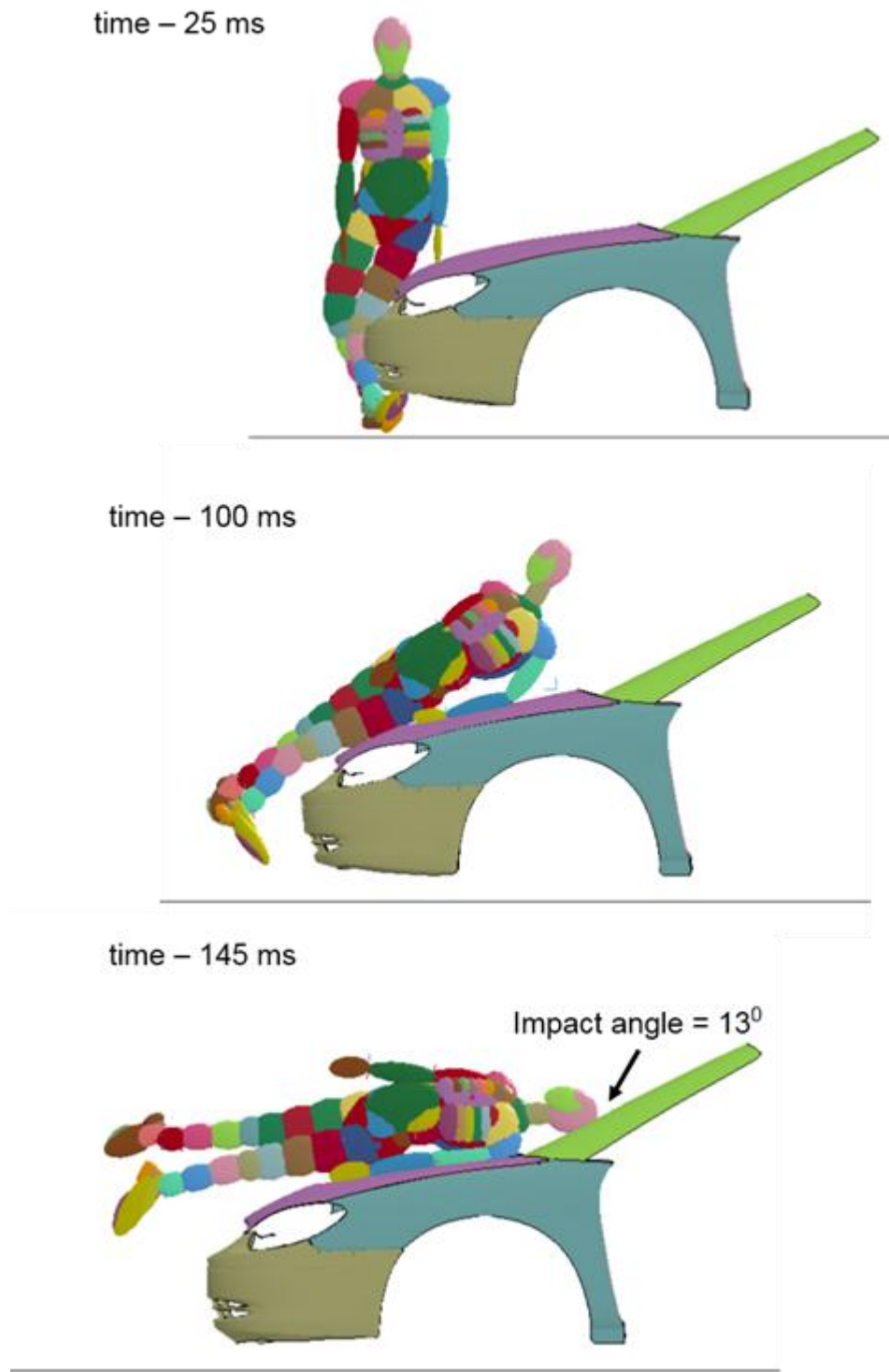


Figure 8.2.4: Pedestrian kinematics of a mid-size male (50th percentile) pedestrian striking with the mid-size vehicle (profile2) at 40 km/h

time – 0 ms



time – 50 ms



time – 100 ms

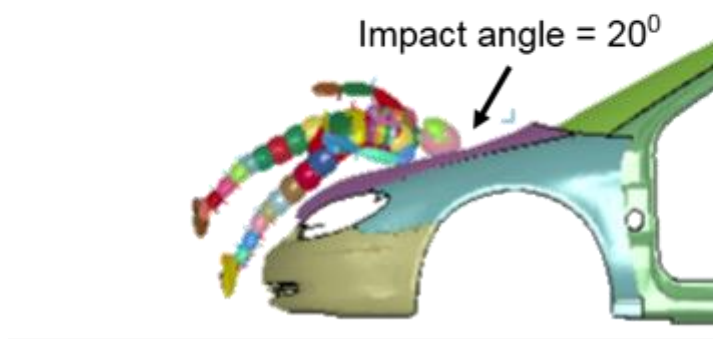
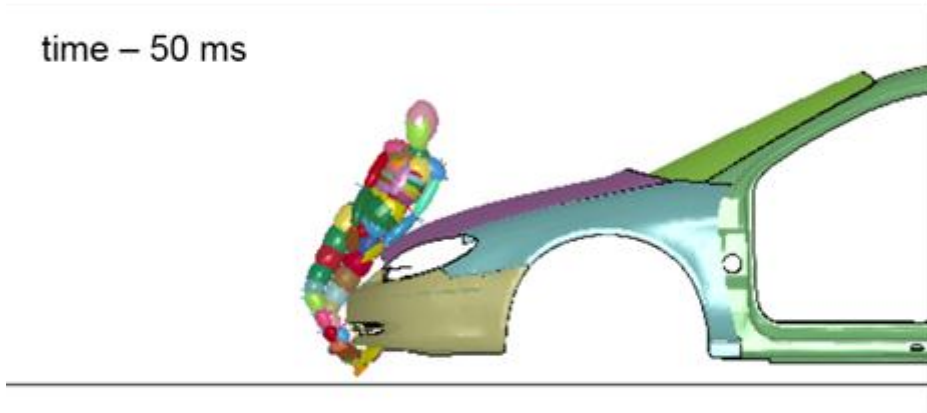


Figure 8.2.5: Pedestrian kinematics of a 6 year old child pedestrian striking with the mid-size vehicle (profile3) at 40 km/h

time – 0 ms



time – 50 ms



time – 110 ms

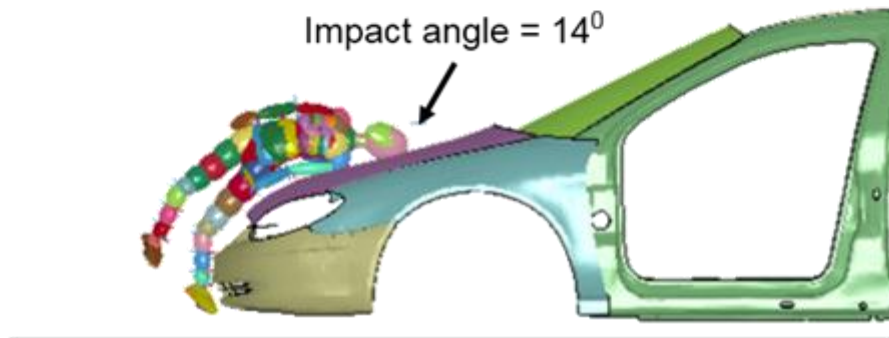


Figure 8.2.6: Pedestrian kinematics of a 6 year old child pedestrian striking with the mid-size vehicle (profile3) at 30 km/h

Table 8.2.1: Mid-size vehicle - simulation setups and results

Run no	Pedestrian Size	Vehicle Profile	Position	Speed (KPH)	Impact angle	HIC Primary Impact
1	6 yr Child	Profile2	Center	40	24.5	393
2	6 Yr Child	Profile2	Corner	40	2.6	796
3	6 yr Child	Profile1	Center	40	41	154
4	6 yr Child	Profile3	Center	40	20	1144
5	6 yr Child	Profile2	Center	30	17.4	174
6	6 yr Child	Profile1	Center	30	24.7	80
7	6 yr Child	Profile3	Center	30	14	236
8	6 yr Child	Profile4	Center	40	17.2	486
9	6 yr Child	Profile4	Center	30	16.1	177
10	5th Ped	Profile2	Center	40	12.5	1298
11	5th Ped	Profile2	Corner	40	10.1	302
12	5th Ped	Profile1	Center	40	21	361
13	5th Ped	Profile3	Center	40	4	3459
14	5th Ped	Profile3	Corner	40	0	302
15	5th Ped	Profile2	Center	25	0	358
16	5th Ped	Profile1	Center	30	22.2	244
17	5th Ped	Profile3	Center	30	0	1423
18	5th Ped	Profile4	Center	40	14.5	986
19	5th Ped	Profile4	Center	30	0	135
20	50th Ped	Profile2	Center	40	13	650
21	50th Ped	Profile2	Corner	40	0	557
22	50th Ped	Profile1	Center	40	33	838
23	50th Ped	Profile3	Center	40	1	420
24	50th Ped	Profile2	Center	25	22.7	244
25	50th Ped	Profile3	Center	30	10	104
26	50th Ped	Profile4	Center	40	10	660
27	50th Ped	Profile4	Center	30	3	200
28	50th Ped	Profile3	Corner	40	0	369
29	50th Ped	Profile3	Corner	30	3	125

Table 8.2.2: SUV - simulation setups and results

Run no	Pedestrian Size	Vehicle Profile	Position	Speed (KPH)	Impact angle	HIC Primary Impact
1	6 yr Child	Profile2	Center	40	-24.2	369
2	6 Yr Child	Profile2	Comer	40	-20	319
3	6 yr Child	Profile1	Center	40	-70	733
4	6 yr Child	Profile2	Center	30	-20	131
5	6 yr Child	Profile3	Center	30	0	68
6	6 yr Child	Profile1	Center	30	-72	314
7	5th Ped	Profile2	Center	40	30.5	170
8	5th Ped	Profile2	Comer	40	19.6	497
9	5th Ped	Profile3	Center	40	30.9	161
10	5th Ped	Profile1	Center	40	26.8	160
11	5th Ped	Profile2	Center	30	27.6	22
12	5th Ped	Profile3	Center	30	25	34
13	5th Ped	Profile1	Center	30	17.2	40
14	5th Ped	Profile1	Comer	30	13	45
15	5th Ped	Profile4	Center	40	27.5	177
16	5th Ped	Profile4	Center	30	38.3	77
17	50th Ped	Profile2	Center	40	43.4	113
18	50th Ped	Profile2	Comer	40	26	124
19	50th Ped	Profile3	Center	40	29.3	266
20	50th Ped	Profile1	Center	40	42	99
21	50th Ped	Profile2	Center	30	36	44
22	50th Ped	Profile3	Center	30	16.2	210
23	50th Ped	Profile1	Center	30	28	49
24	50th Ped	Profile4	Center	40	50	180
25	50th Ped	Profile4	Center	30	34.2	33
26	50th Ped	Profile1	Comer	30	35.1	41

Table 8.2.3: Sensitivity of HIC and Head impact angle for variation in pedestrian posture during impact with mid-size car (profile 2) at 40 km/h

	Left leg back, Right leg front, Impacting on Left side		Left leg front, Right leg back, Impacting on Left side		Left leg back, Right leg front, Impacting on Right side	
	Impact Angle (Degree)	HIC	Impact Angle (Degree)	HIC	Impact Angle (Degree)	HIC
5th Percentile	12.5	1298	9	1799	12	1463
50th Percentile	13	650	8	824	12	778
6 YO Child	24.5	393	26	365	21	354

8.3 Discussion

Experimental tests using cadavers, as well as anthropomorphic test devices have greatly advanced our understanding on traumatic injuries related to pedestrian crashes. However, due to the limitation of cadaver resources and the dynamic nature of crashes, only a small fraction of possible vehicle-pedestrian interactions can be examined via physical testing. For this reason, math models are a beneficial alternative to experimental test (Rooij et al., 2003). Application of FE model to a vehicle–pedestrian collision will be helpful in understanding the complexity of dynamic nature of these crash events. In particular, analysis using full human body models may be expected to improve the integrated safety performance of a vehicle design.

Based on pedestrian kinematics presented here, pedestrian was pushed forward along the striking vehicle until a primary head impact with the hood or windshield occurred (Figures 8.2.1-8.2.6). HIC and head impact angle were calculated for each simulation (Tables 8.2.1 and 8.2.2). Head impact angle varied greatly (0° to 40° for the mid-size car, -75° to 40° for the SUV) with changing front-end profile of the vehicles for

same pedestrian size. Results of FE simulation, 5th percentile female striking with the mid-size car of profile2, profile1 and profile3 along centerline at 40 km/h (Runs 10, 12 and 13 respectively, listed in Table 8.2.1), indicate that the head impact angle increased as the front-end profile of the mid-size vehicle was raised. Similarly results of FE simulation, 50th percentile male striking with the mid-size car of profile2, profile1 and profile3 along centerline at 40 km/h (Runs 20, 22 and 23 respectively, listed in Table 8.2.2), indicate that the head impact angle increased as the front-end profile of the mid-size vehicle was raised. In general, as the impact location changed from center of vehicle (Run 7, Table 8.2.2) towards corner of vehicle (Run 8, Table 8.2.2), pedestrian head impact angle decreased and HIC increased. Increased HIC during impact towards corner of the vehicle or along hood edge can be attributed to added stiffness of other interfacing components such as fender, shotgun etc. At impact speed of 40 km/h pedestrian was lifted upward more (Figure 8.2.5) compared to when impacting at 30 km/h (Figure 8.2.6) and traveled more distance before impacting at hood and resulted in higher impact angle. Kinematics comparison for 6 year old child pedestrian indicated that child pedestrian during impact with mid-size vehicle was lifted upward and child's head rotated downward to impact with vehicle hood (Figure 8.3.1a). However, adult pedestrian (5th percentile or 50th percentile) was wrapped around the vehicle profile during impact, and pedestrian became almost parallel to vehicle hood surface (Figure 8.3.1b). It resulted in smaller impact angle for adult pedestrian compared to child pedestrian. While striking with the SUV, child's head was still oriented upwards during primary impact thus resulting in negative head impact angle (Figure 8.3.2).

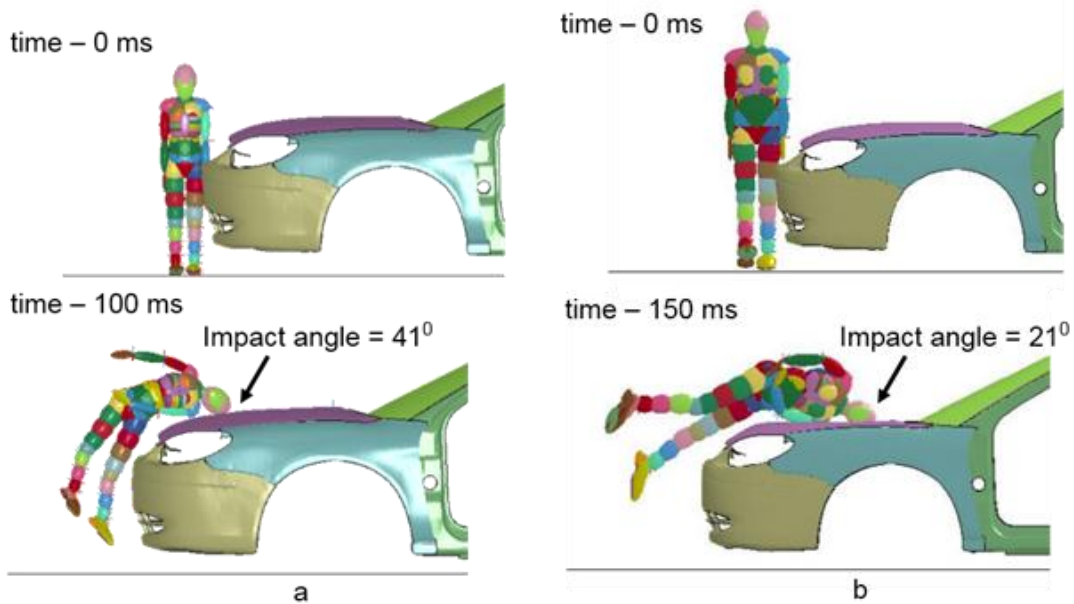


Figure 8.3.1: Pedestrian kinematics comparison (a) 6 year old child pedestrian striking with the mid-size vehicle (profile1) at 40 km/h, and (b) small female (5th percentile) pedestrian striking with the mid-size vehicle (profile1) at 40 km/h

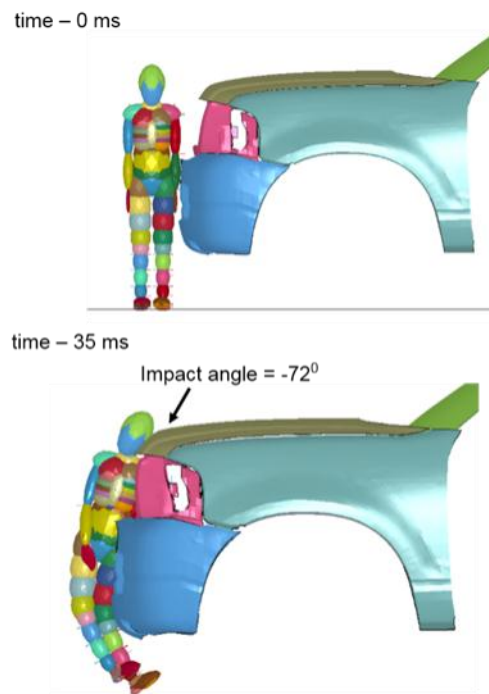


Figure 8.3.2: Pedestrian kinematics of a 6 year old child pedestrian striking with the SUV (profile1) at 30 km/h

At impact speed of 30 km/h all pedestrians had lower impact angle compared to impact speed of 40 km/h (Figure 8.3.3 and Figure 8.3.4). A raised front-end profile (Profile1) had the highest impact angle for all different pedestrians (Figure 8.3.3) with adult pedestrians having an impact angle of around 30° and 6-year old child pedestrian having an impact angle of around 40° .

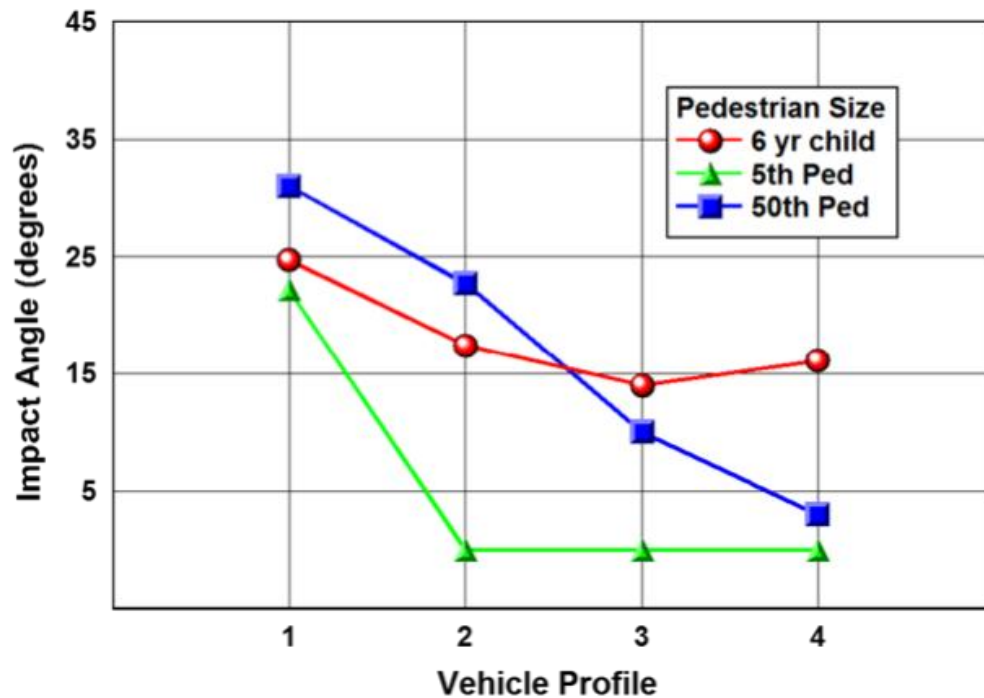


Figure 8.3.3: Comparison of the head impact angles for various pedestrians striking with different front-end profiles of the midsize car at 30 km/h

The average impact angle reported in this study for the child pedestrian (with different front-end profiles of the mid-size car and impact speeds) was 20° with a standard deviation of 9.7° . The average impact angle for adult pedestrians (with different front-end profiles of the mid-size car and impact speeds) was 10° with a standard deviation of 9.5° . For impacts with the SUV vehicle profiles at 30 km/h, the

head impact angle for all pedestrian sizes increased as the slope of hood increased (Figure 8.3.5). For impacts with the SUV vehicle profiles at 40 km/h, head impact angle for adult pedestrian did not change significantly (Figure 8.3.6) but 6 year old child pedestrian head impact angles were negative (upward position).

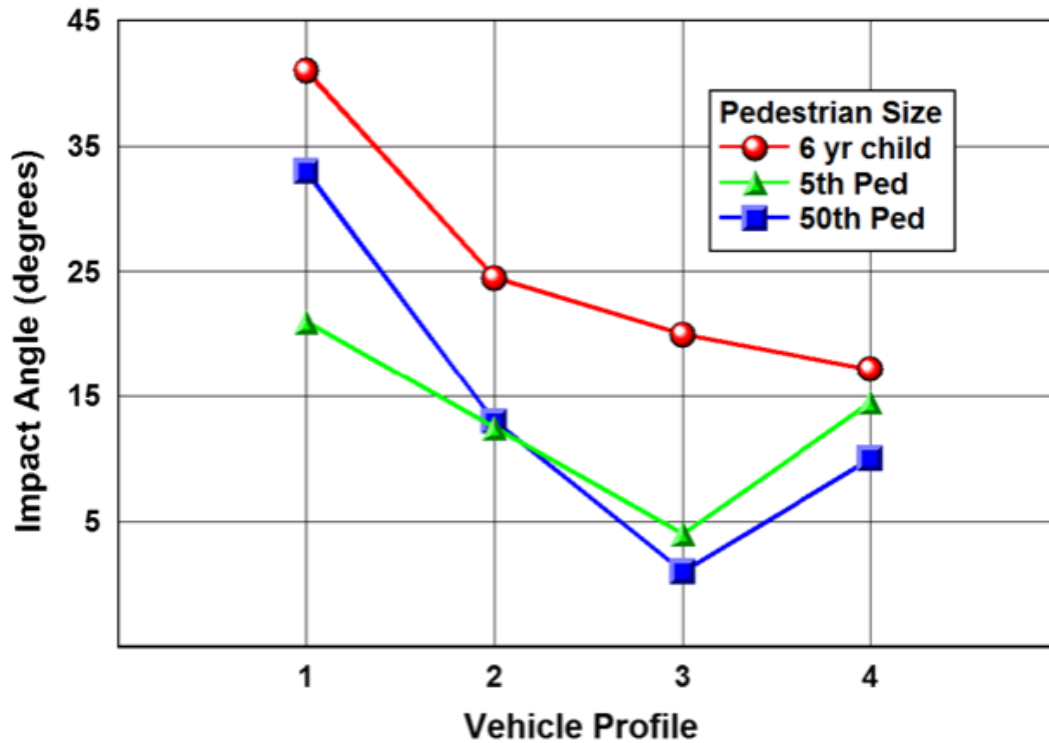


Figure 8.3.4: Comparison of the head impact angles for various pedestrians striking with different front-end profiles of the midsize car at 40 km/h

Head acceleration and thus HIC are generally influenced by impact speed, stiffness of hood or windshield, clearance to under hood package components, impact location (hood center or hood edge, at the boundary of hood rear edge - windshield etc.) (Kerkeling et al., 2005). The stiffness of the hood depends on the hood material, thickness of hood panels, the design of outer panel, inner panel and reinforcements. Other components within the deformation zone add to the overall stiffness. The

clearance to under hood packaging components determine the deformation space available for head during impact. In some cases, higher head impact angle (65° compared to 25°) leads to more vertical travel of head during impact thus causing more scope of coming in contact with under hood package components.

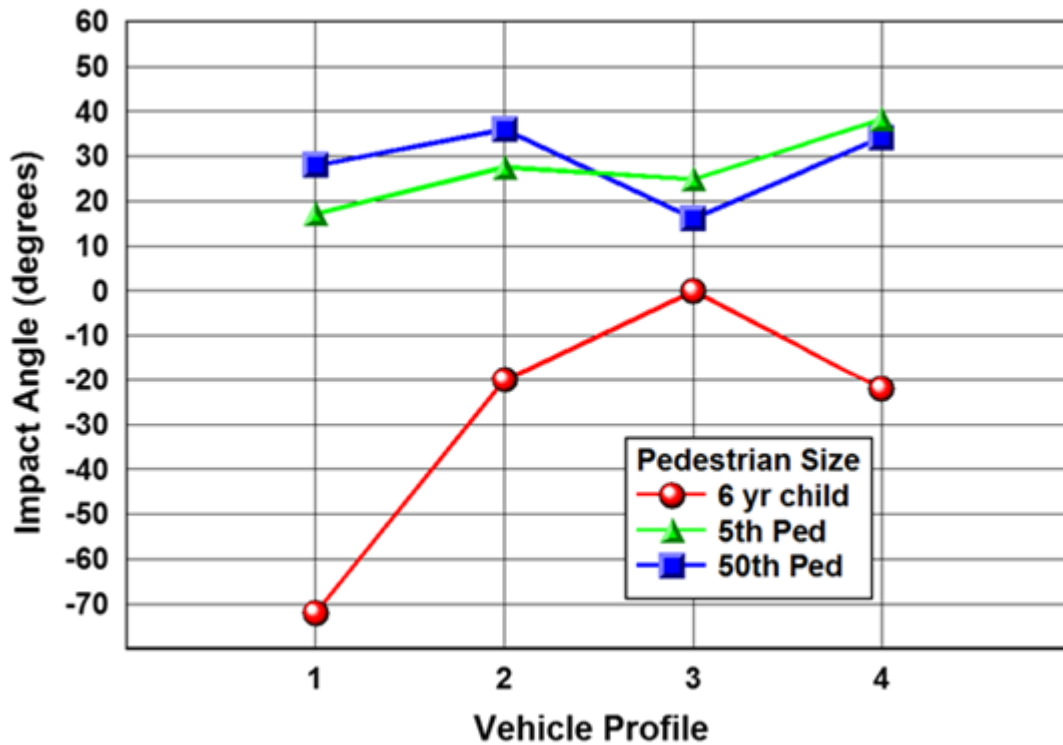


Figure 8.3.5: Comparison of the head impact angles for various pedestrians striking with different front-end profiles of the SUV at 30 km/h

HIC measured during primary head impact for various pedestrian sizes on the mid-size car was higher compared to HIC measured during primary impact with the SUV. For mid-size car, primary impact for 50th percentile pedestrian happened on windshield which doesn't allow any deformation space thus causing higher head acceleration and HIC. In few simulations, much higher HIC was measured (HIC of 3400 in case of 5th percentile pedestrian striking with mid-size car profile1, Run 13 listed in

Table 8.2.1) compared to other test cases. The reason for much higher HIC in this particular case was that head impact happened in the boundary of hood rear edge and windshield. Similar pedestrian test using Post Mortem Human Subjects (PMHS) where pedestrian head impacted on hood rear edge - windshield boundary, reported HIC values in range of 2100-2600 (Kerrigan et al., 2007b). However, GTR does not propose any head impact tests on windshield zone and proposes HIC <1000 for 2/3 of hood zone and HIC <1700 for remaining 1/3 of hood zone (GTR, Technical Report IHRA/Ps/200).

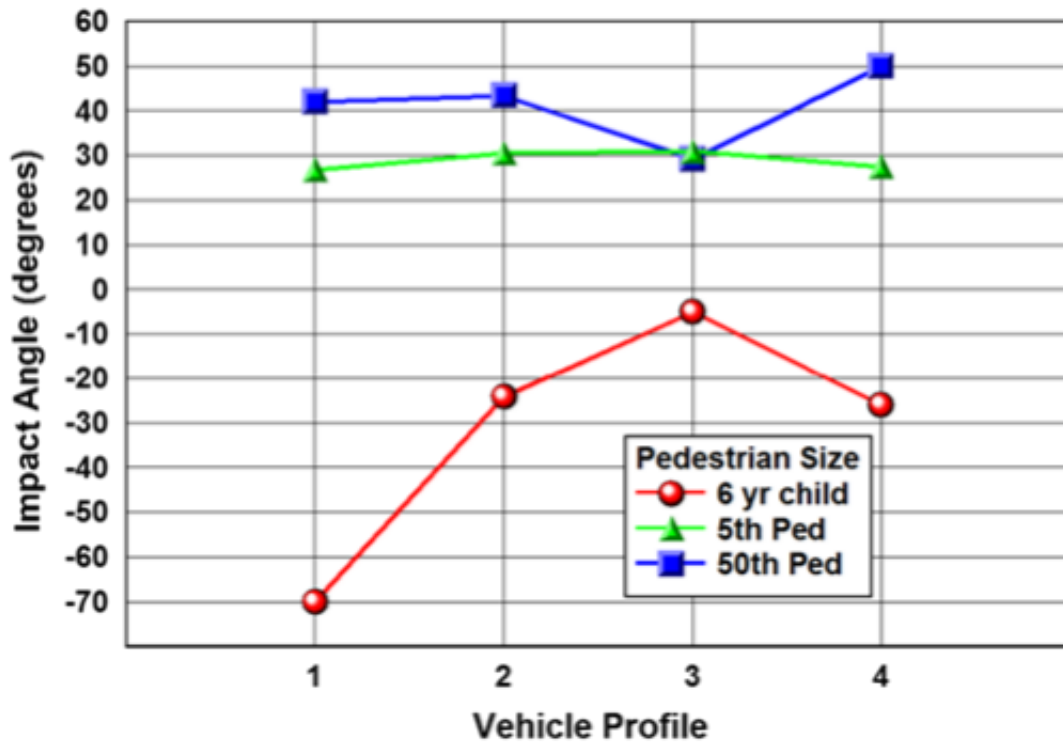


Figure 8.3.6: Comparison of the head impact angles for various pedestrians striking with different front-end profiles of the SUV at 40 km/h

Simulation results of test setups with free motion headform (Table 8.3.1) indicated that the free motion headform when impacted at 65 degrees lead to an overestimation of HIC values. Whereas, when free motion headform was impacted at the model-predicted impact angle, it closely matched HIC prediction with full scale pedestrian model. Head Injury criteria measured by free motion headform when impacted at windshield did not match with HIC calculated by full scale pedestrian model (Run 4, Table 8.3.1).

Table 8.3.1: Comparison of HIC based on full scale pedestrian model (column G) against HIC based on free motion headform at 65 degree (column H) and HIC based on free motion headform at same angle as predicted by full pedestrian model (column I)

A	B	C	D	E	F	G	H	I
Run no	Pedestrian Size	Vehicle Profile	Position	Vehicle Speed (km/h)	Impact angle (degree)	HIC - Full pedestrian model	HIC - Headform at 65 deg	HIC - Hedaform at model-predicted angle (column F)
1	5th Ped	SUV_Profile2	Corner	40	19.6	497	1420	492
2	50th Ped	SUV_Profile3	Center	40	29.3	266	954	282
3	5th Ped	Mid-Size_Profile1	Center	40	21	361	604	266
4	50th Ped	Mid-Size_Profile2	Center	40	13	650	464	238.5

Two PMHS tests under similar conditions as reported by Masson et al. (2007) were compared with simulation results using full pedestrian model and free motion headform (Table 8.3.2). In test01, a PMHS representing a 50th percentile male was impacted with mid-size sedan at impact speed of 39.2 Km/h. In test02, a PMHS representing a 50th percentile male was impacted with big sedan at impact speed of 39.7 Km/h. Results from PMHS test01 were compared with 50th percentile pedestrian

striking with the mid-size car profile² (original vehicle profile) at 40 km/h and results from test02 were compared with 50th percentile pedestrian striking with the mid-size car profile¹ (representing a big sedan) at 40 km/h. PMHS test results as reported by Masson et al. (2007) did not mention HIC but discussed peak head acceleration during impact. For this reason, we have attempted to compare peak head accelerations as reported in FE simulations conducted in this study. Results comparison (Table 8.3.2) indicated that peak head acceleration predicted by pedestrian model matched with peak head accelerations reported in PMHS tests. Head impact angles predicted by pedestrian model were lower compared to head impact angles reported in PMHS tests. But the trend of the head impact angles reported in PMHS tests and simulation results using pedestrian model was similar (higher impact angle during impact with bigger sedan). However, pedestrian kinematics from PMHS test closely matched with kinematics based on simulation (Figure 8.3.7).

Table 8.3.2: Comparison of HIC and Head impact angle based on PMHS test, Pedestrian FE model and free motion headform.

	MADYMO Pedestrian model		PMHS		Head Impactor as per EuroNCAP setup	
	Impact Angle (Degree)	Head Acc (g)	Impact Angle (Degree)	Head Acc (g)	Impact Angle (Degree)	Head Acc (g)
Test01	13	85	33	90	65	118
Test02	33	58	50	67	65	98

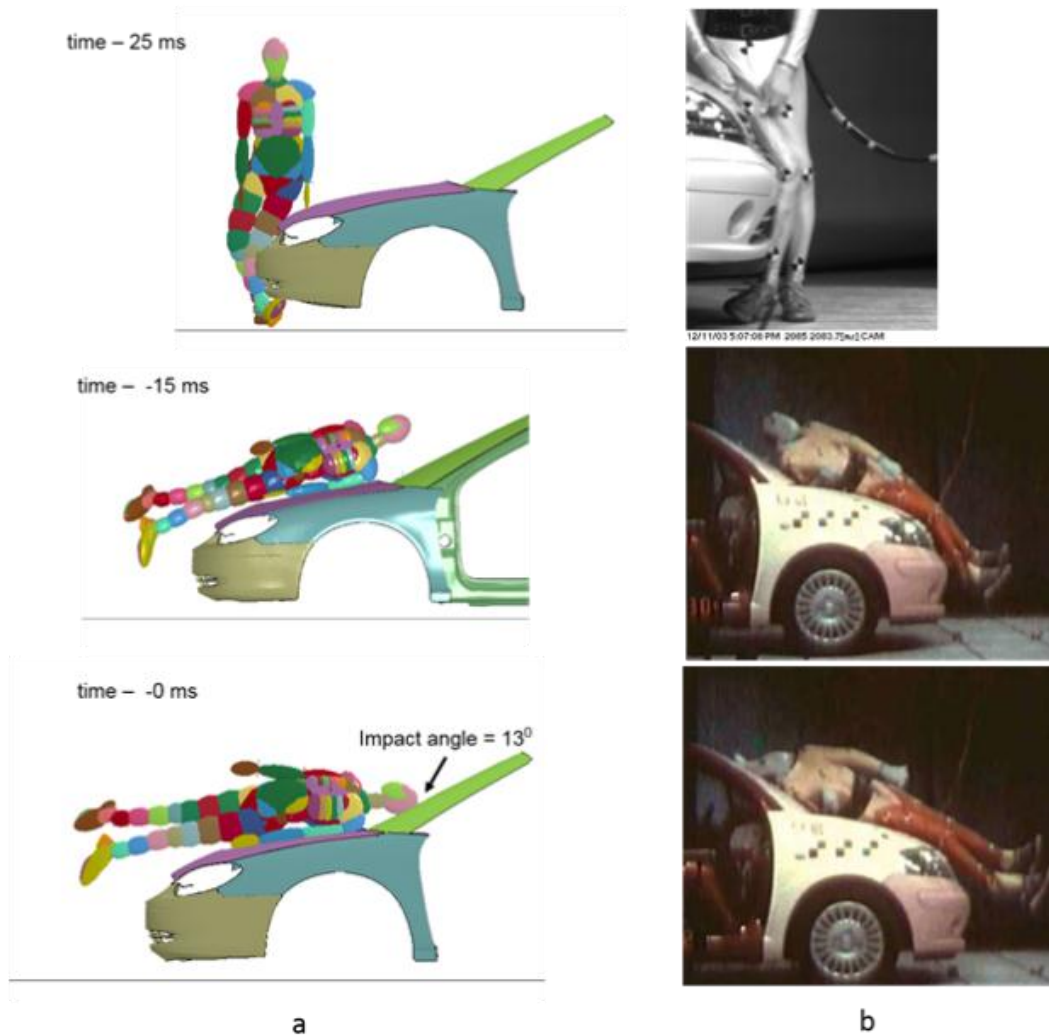


Figure 8.3.7: Pedestrian kinematics comparison (a) 50th percentile pedestrian striking with mid-size car profile2 at 40 km/h, and (b) PMHS test01 (Masson et al., 2007)

Masson et al. (2007) did not report the method used for measuring head impact angle. The reason for difference in head impact angle could be attributed to difference in vehicle front-end profiles under discussion and may be due to different method used for measuring the head impact angle. Free motion headform impactor over-predicted the head acceleration compared to both test cases. The free motion headform impactor lacks connection to other body masses (the neck, thorax, etc.), which could considerably influence impact dynamics by affecting the head effective mass.

Chapter 9: Aim 3 - Effect of vehicle front-end profiles leading to pedestrian secondary head-on impact to ground

In Chapter 8, pedestrian responses were studied using several front-end profiles based off a mid-size vehicle and an SUV that have been validated previously along with several MADYMO pedestrian models. Mesh morphing is used to explore the risk of head injury due to changes to the bumper height, hood leading-edge height, and hood rear reference-line height. But studies highlighted in Chapter 8 were limited to primary impact. In this aim, simulations leading up to pedestrian secondary impact with ground are conducted at impact speeds of 30 km/h and 40 km/h for the same two vehicles with the same number of front-end profiles as discussed in Chapter 8. Again, three pedestrian sizes (50th, 5th and 6 years old child) are used to search for a front-end profile that performs well for *multiple* sizes of pedestrians during secondary impact to ground, not just one particular pedestrian size.

The nature of the injuries sustained by the pedestrian depends very much on the victim's body kinematics. Pedestrian having a secondary head-on impact with ground versus having a secondary impact with lower extremities that are already on ground will lead to different probability and severity of head injuries. After primary impact of pedestrian with vehicle hood or windshield, the pedestrian is thrown away from the striking vehicle due to braking of the vehicle and momentum gained during the impact with vehicle. Under the effect of gravity, the pedestrian finally falls to ground thus leading to secondary impact with ground. The overall body kinematics depends on several factors such as the pedestrian size, initial posture, vehicle front shape and vehicle speed, etc.

9.1 Method

Finite element simulation model: In this study, pedestrian-vehicle crashes were simulated using finite element (FE) vehicle models representing a mid-size car and an SUV (National Crash Analysis Center), and the Madymo human pedestrian models representing a mid-size male (50th percentile), small female (5th percentile) and 6 years old child as discussed in section 8.1.

Apart from vehicle front-end profiles as discussed in Chapter 8, one profile with pop-up hood for the mid-size sedan (Figure 9.1.1) and one profile with pop-up hood for the SUV were developed. To simulate the effect of pop-up hood, the hood rear end (BRRL) was raised by 85 mm and attached to its supports using rigid elements.

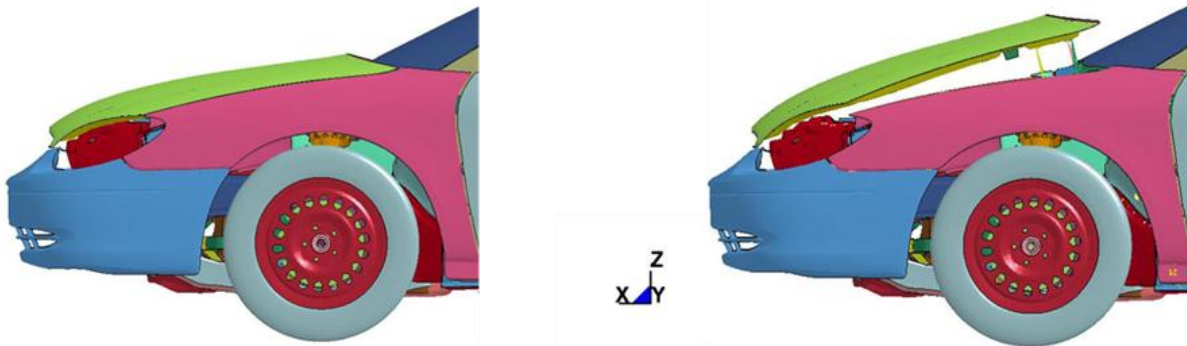


Figure 9.1.1: Front end profile for the mid-size car with and without simulated pop-up hood.

Boundary condition: For each vehicle type and front front-end profile, crash simulations were analyzed with different combinations of the following factors: vehicle velocity at the moment of impact (30 km/h or 40 km/h), pedestrian-vehicle impact location (centerline or corner), and pedestrian size (50th, 5th or 6yr old child). To study the effect of a pop-up hood, three of the simulations were repeated with this feature.

Altogether, for the mid-sized car, 31 crash scenarios were analyzed using these factor combinations (see Table 9.2.1); for the SUV, 27 crash scenarios were analyzed (see Table 9.2.2). Other boundary conditions for pedestrian positioning, contact function, modeling of road surface etc. are considered in the same way as discussed in section 8.1.

Data analysis: Crash simulations were performed for a longer duration (1.5 sec) to capture the pedestrian secondary impact with ground. Simulation results were analyzed for detailed kinematics of pedestrian during impacts with vehicle until it made secondary impact with ground. HIC was calculated at the time of primary impact with the vehicle and at the time of secondary impact with ground.

It was hypothesized that in some cases the secondary impact with ground could happen at the neck or shoulder region rather than direct head-on impact thus giving slightly reduced chance of direct head-on ground impact. Such scenario will also result in predicting a very small HIC value. So, there was a need to clearly distinguish such cases from scenarios of clear secondary impact with lower extremities such as the hip, thus resulting in completely avoiding secondary head-on ground impact. For this purpose, the simulation animations were closely monitored. In the particular simulation cases, where the secondary impact with ground happened at the neck or shoulder region, results were extrapolated by impacting the head with ground at a pre impact velocity calculated at the time of pedestrian secondary ground impact with the neck and shoulder regions.

9.2 Results

In all simulations, overall kinematics showed that pedestrian eventually impacted with ground. In most of the simulations, secondary ground impact occurred at the head/neck/shoulder region. However, there were some front-end profiles that promoted secondary ground impact with pedestrian *lower extremities*, thus avoiding pedestrian secondary *head-on* impact with ground.

Pedestrian kinematics, shown here for a mid-size sedan and 5th percentile female (Figure 9.2.1) indicate that the bumper first hits the lower legs, causing both feet to leave the ground. Further, the hood leading edge hits the upper legs and pelvis, followed by the pedestrian body rotation towards the hood. The lower body gets wrapped around the vehicle front-end structure, and lateral head rotation causes the head to have a primary impact on the hood top surface or on the windshield. After primary head impact with the hood top surface, the lower extremities continued to rotate towards the vehicle. There was an initial phase where the pedestrian body remained in contact with the vehicle such that the struck pedestrian and the striking vehicle moved together. Further, the pedestrian body slid down on the hood surface due to moderate speed reduction of the striking vehicle. Pedestrian was then thrown forward when the impact force finally caused the pedestrian body to move forward in the vehicle traveling direction. Eventually, the pedestrian had a secondary head-on impact with ground. The impact velocity with ground varied in different simulations due to different pedestrian sizes and different front-end profiles of vehicles but in most cases the secondary impact with ground happened at a velocity range from 15 to 22 km/h (4.1-6.1 m/s).

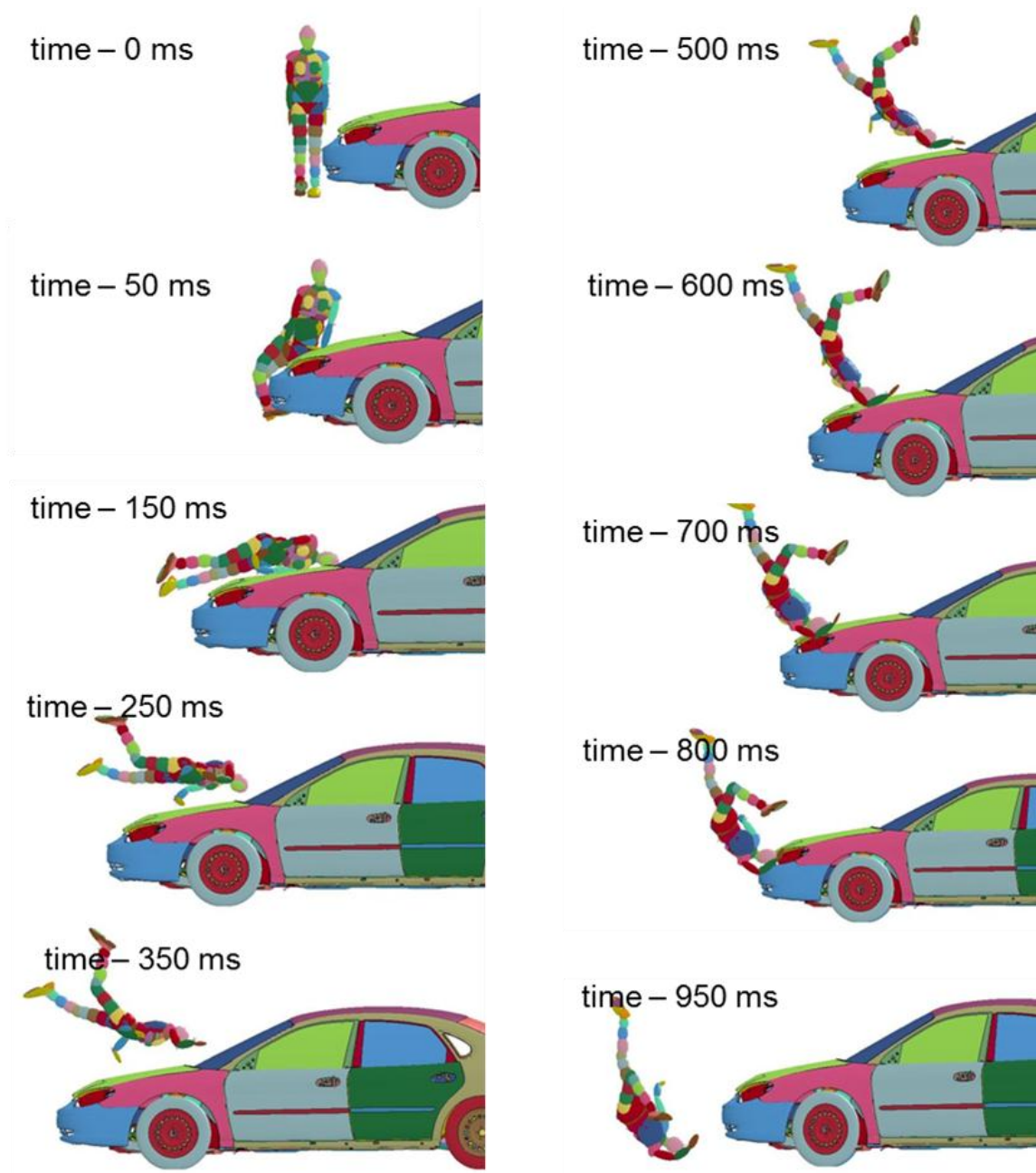


Figure 9.2.1: Pedestrian kinematics during Impact with mid-size car (Profile2)

Based on Average HIC calculated during pedestrian impacts with various profiles of mid-size car at 40 km/h (Figure 9.2.2) and various profiles of SUV at 40 km/h (Figure 9.2.3), the severity of HIC during secondary impact is much higher than HIC during

primary impact. It clearly shows that preventing secondary head-on impact with ground is very important to reduce overall head injury risk during car-pedestrian crashes.

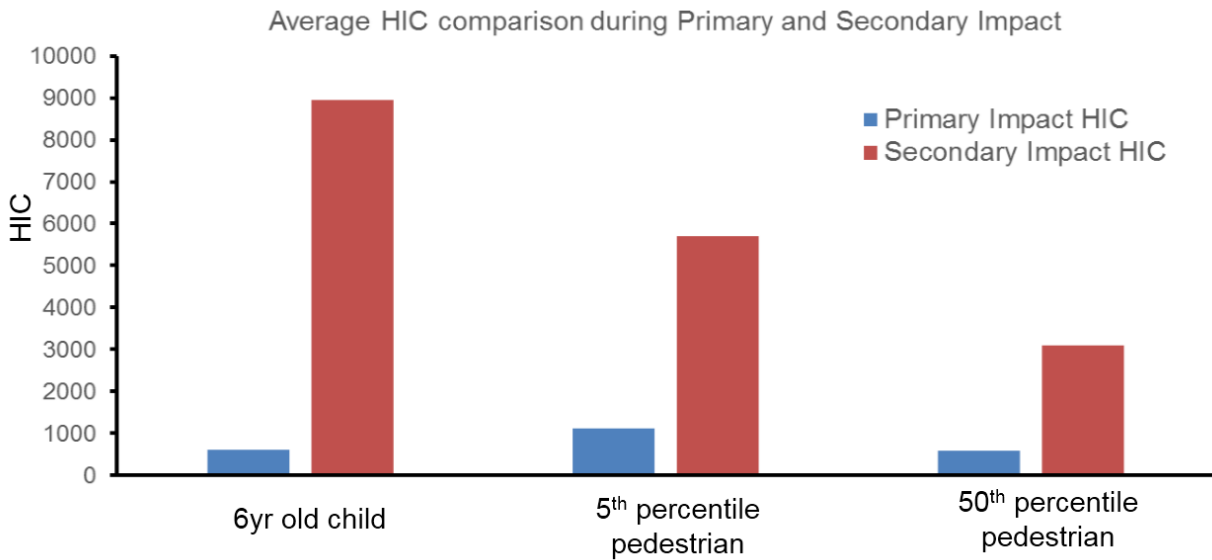


Figure 9.2.2: Average HIC comparison during primary impact and secondary impact for pedestrian striking with various profiles of the mid-size car at 40 km/h

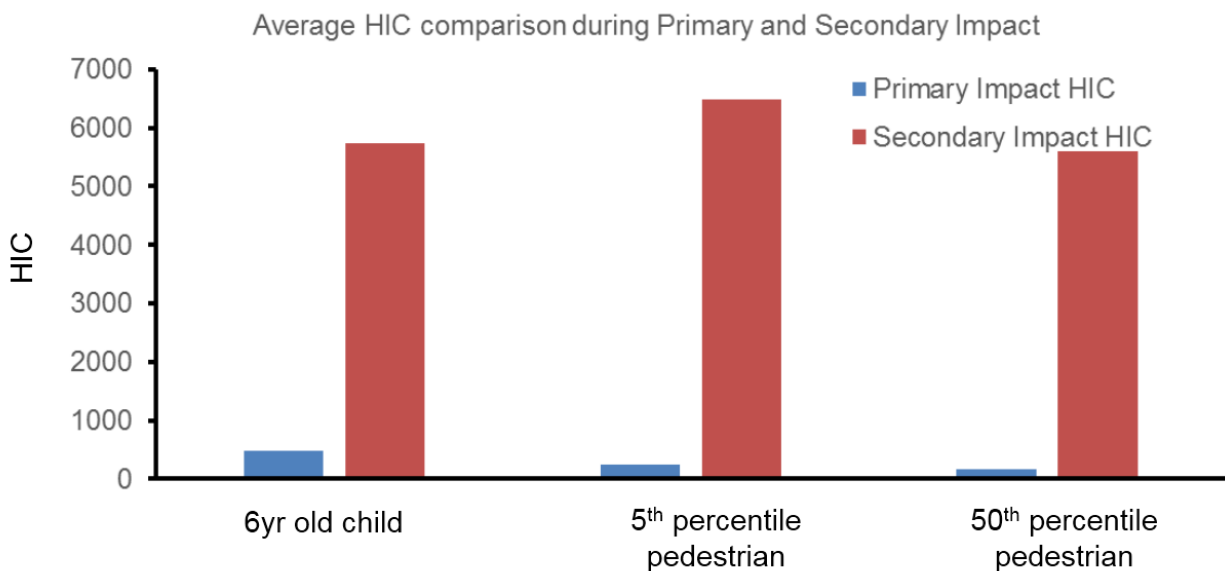


Figure 9.2.3: Average HIC comparison during primary impact and secondary impact for pedestrian striking with various profiles of SUV at 40 km/h

One question needed to be answered in this study was, whether a raised or lowered front-end profile was better for pedestrian secondary impact. As can be seen next, the answer differs depending upon whether the pedestrian is struck by the midsize sedan or SUV simulated in this study.

The pedestrian kinematics of a mid-size male struck by the SUV profile1 (raised front end) at 30 km/h (Figure 9.2.4 a) are compared with the kinematics of a small female struck by the SUV profile3 (lowered front end) at 30 km/h (Figure 9.2.4 b). This comparison for kinematics clearly demonstrates that the SUV with a raised front end, as described by profile1, leads to secondary ground impact with pedestrian lower extremities thus avoiding secondary head impact with ground. In contrast, the SUV with a lowered front end, as described by profile3, leads to direct head-on secondary impact and, hence, higher HIC values and higher chances of serious TBIs.

The pedestrian kinematics of a mid-size male striking with the mid-size car profile1 (raised front end) at 40 km/h (Figure 9.2.5 a) are compared with the kinematics of a mid-size male striking with the mid-size car profile3 (lowered front end) at 30 km/h (Figure 9.2.5 b). This comparison shows that the mid-size car with raised front-end (more like a box type profile) as described by profile1 causes head-on landing of pedestrian with road surface. In contrast, the mid-size car with lowered front-end, as described by profile3, leads to secondary impact between the ground and the pedestrian's lower extremities thus avoiding secondary head impact with ground.

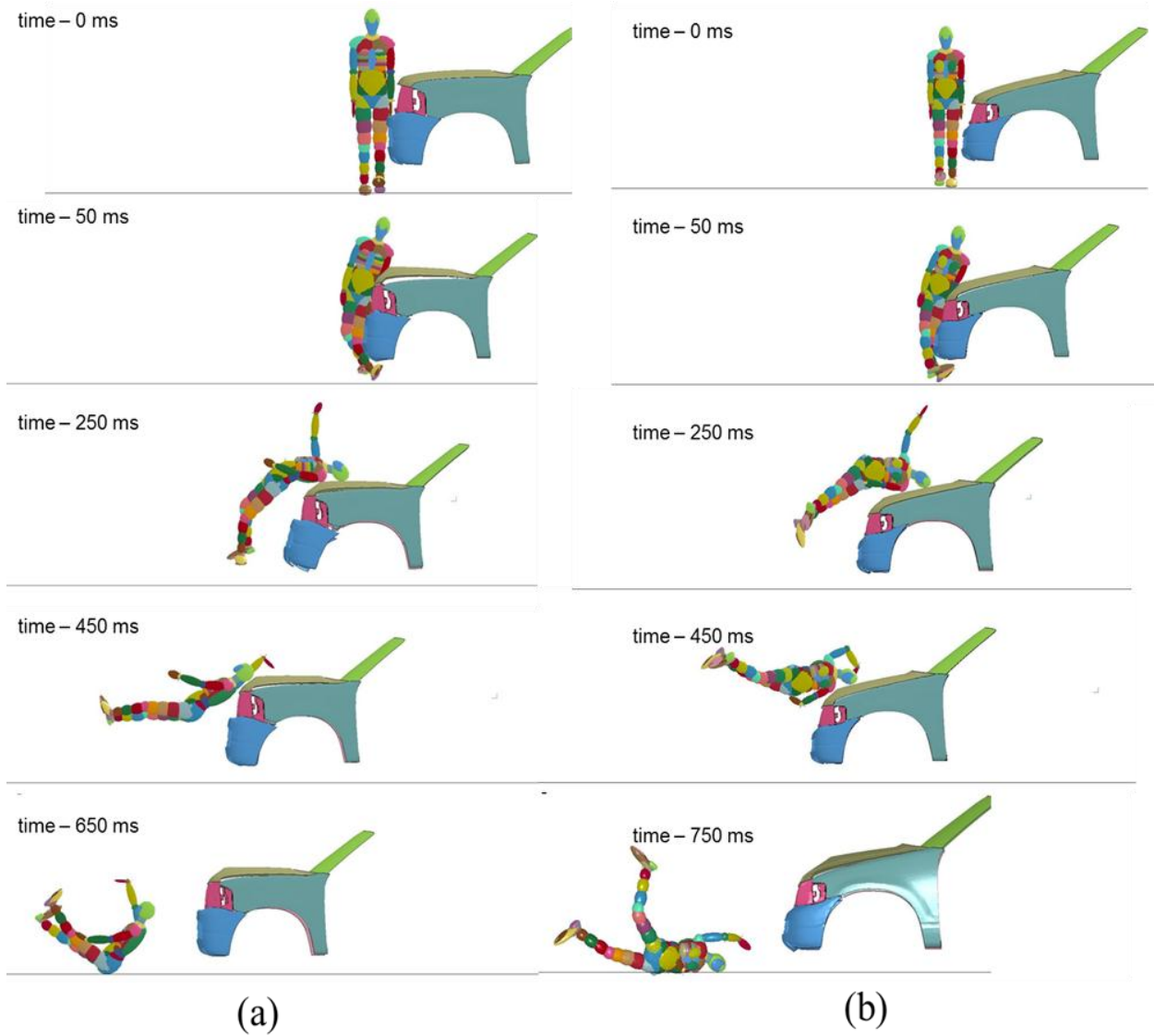


Figure 9.2.4: Comparison of pedestrian kinematics (a) mid-size male striking with the SUV profile1 (raised front end) at 30 km/h (b) small female striking with the SUV profile3 (lowered front end) at 30 km/h.

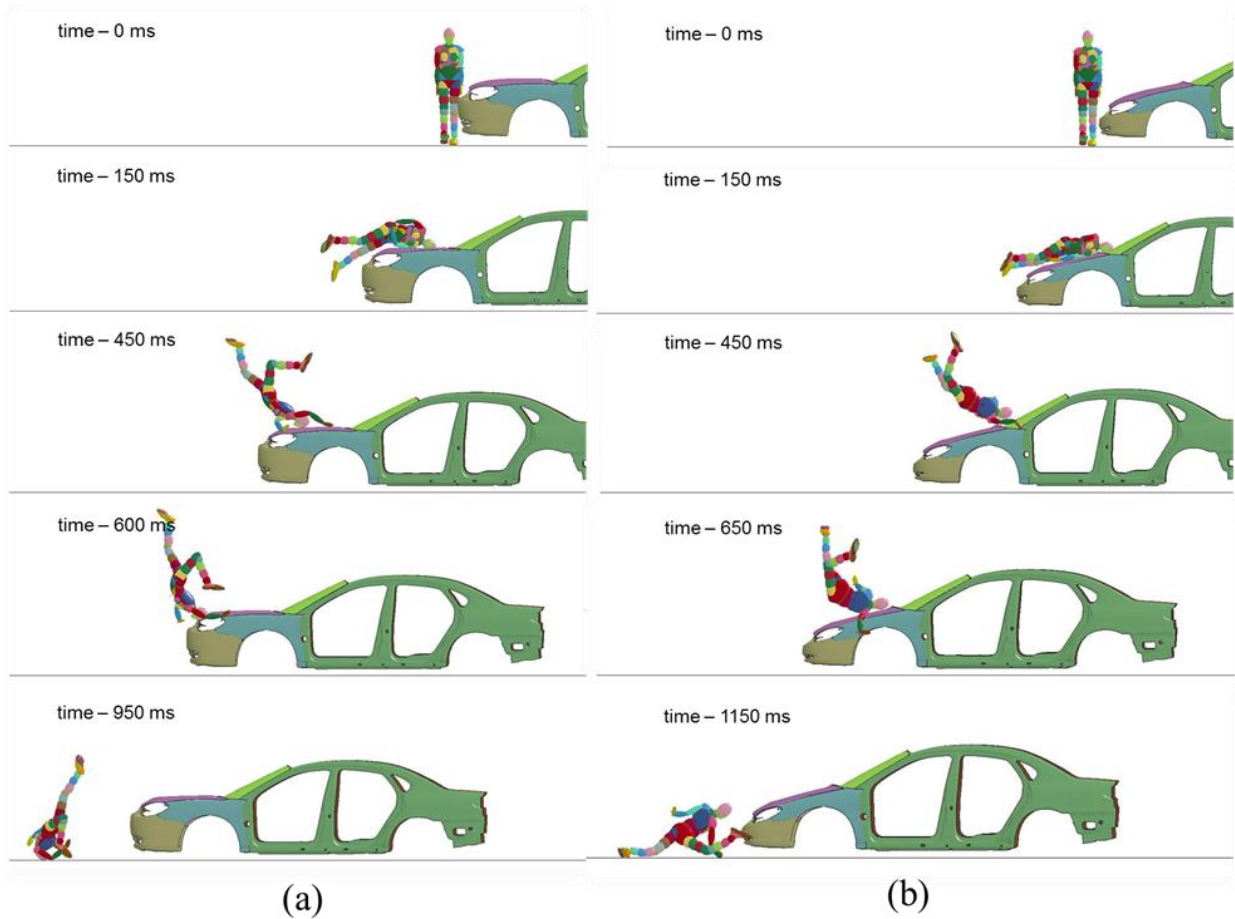


Figure 9.2.5: Pedestrian kinematics (a) mid-size male striking with the mid-size car profile1 (raised front end) at 40 km/h (b) mid-size male striking with the mid-size car profile3 (lowered front end) at 30 km/h.

Table 9.2.1: Mid-size vehicle - simulation setups and results for ground impact

A	B	C	D	E	F	G	H	I
Run no	Pedestrian Size	Vehicle Profile (Hood height in mm)	Position	Speed (km/h)	HIC Primary Impact	HIC Secondary Impact Original	HIC Secondary Impact Extrapolated	% difference b/w secondary and primary impact HIC
1	6 yr Child	Profile2 (650)	Center	40	393	4528	4528	1052
2	6 Yr Child	Profile2 (650)	Corner	40	796	3138	3138	294
3	6 yr Child	Profile1 (795)	Center	40	154	695	4650	2919
4	6 yr Child	Profile3 (585)	Center	40	1144	9442	9442	725
5	6 yr Child	Profile2 (650)	Center	30	174	4835	4835	2679
6	6 yr Child	Profile1 (795)	Center	30	80	2278	2278	2748
7	6 yr Child	Profile3 (585)	Center	30	236	110	110	-53
8	6 yr Child	Profile4 (650)	Center	40	486	1221	22989	4630
9	6 yr Child	Profile4 (650)	Center	30	177	9776	9776	5423
10	5th Ped	Profile2 (650)	Center	40	1298	3936	3936	203
11	5th Ped	Profile2 (650)	Corner	40	302	2451	2451	712
12	5th Ped	Profile1 (795)	Center	40	361	1681	5032	1294
13	5th Ped	Profile3 (585)	Center	40	3459	58	58	-98
14	5th Ped	Profile3 (585)	Corner	40	302	17804	17804	5795
15	5th Ped	Profile2 (650)	Center	30	358	2354	2354	558
16	5th Ped	Profile1 (795)	Center	30	244	1058	1058	334
17	5th Ped	Profile3 (585)	Center	30	1423	32	32	-98
18	5th Ped	Profile4 (650)	Center	40	986	4929	4929	400
19	5th Ped	Profile4 (650)	Center	30	135	2280	2280	1589
20	5th Ped	Profile2_Hood Pop	Center	40	633	946	3980	529
21	50th Ped	Profile2 (650)	Center	40	650	4528	4528	597
22	50th Ped	Profile2 (650)	Corner	40	557	5256	5256	844
23	50th Ped	Profile1 (795)	Center	40	838	4466	4466	433
24	50th Ped	Profile3 (585)	Center	40	420	28	28	-93
25	50th Ped	Profile2 (650)	Center	30	244	49	49	-80
26	50th Ped	Profile3 (585)	Center	30	104	159	159	53
27	50th Ped	Profile4 (650)	Center	40	660	3904	3904	492
28	50th Ped	Profile4 (650)	Center	30	200	2847	2847	1324
29	50th Ped	Profile3 (585)	Corner	40	369	369	369	0
30	50th Ped	Profile3 (585)	Corner	30	125	158	158	26
31	50th Ped	Profile2_Hood Pop	Center	40	1146	5992	5992	423

Table 9.2.2: SUV - simulation setups and results for ground impact

A	B	C	D	E	F	G	H	I
Run no	Pedestrian Size	Vehicle Profile	Position	Speed (km/h)	HIC Primary Impact	HIC Secondary Impact Original	HIC Secondary Impact Extrapolated	% difference b/w secondary and primary impact HIC
1	6 yr Child	Profile2 (980)	Center	40	369	3	2786	655
2	6 Yr Child	Profile2 (980)	Corner	40	319	21	2600	715
3	6 yr Child	Profile1 (1075)	Center	40	733	11832	11832	1514
4	6 yr Child	Profile2 (980)	Center	30	131	10197	10197	7684
5	6 yr Child	Profile3 (885)	Center	30	68	3425	3425	4937
6	6 yr Child	Profile1 (1075)	Center	30	314	12986	12986	4036
7	5th Ped	Profile2 (980)	Center	40	170	3225	3225	1797
8	5th Ped	Profile2_HoodPop	Center	40	258	18956	18956	7247
9	5th Ped	Profile2 (980)	Corner	40	497	3317	3317	567
10	5th Ped	Profile3 (885)	Center	40	161	5459	5459	3291
11	5th Ped	Profile1 (1075)	Center	40	160	7926	7926	4854
12	5th Ped	Profile2 (980)	Center	30	22	45	45	105
13	5th Ped	Profile3 (885)	Center	30	34	2	3499	10191
14	5th Ped	Profile1 (1075)	Center	30	40	52	52	30
15	5th Ped	Profile1 (1075)	Corner	30	45	153	153	240
16	5th Ped	Profile4 (980)	Center	40	177	13348	13348	7441
17	5th Ped	Profile4 (980)	Center	30	77	14905	14905	19257
18	50th Ped	Profile2 (980)	Center	40	113	3776	3776	3242
19	50th Ped	Profile2 (980)	Corner	40	124	2600	2600	1997
20	50th Ped	Profile3 (885)	Center	40	266	7420	7420	2689
21	50th Ped	Profile3 (885)	Center	40	99	45	45	-55
22	50th Ped	Profile2 (980)	Center	30	44	499	499	1034
23	50th Ped	Profile3 (885)	Center	30	210	3620	3620	1624
24	50th Ped	Profile1 (1075)	Center	30	49	53	53	8
25	50th Ped	Profile4 (980)	Center	40	180	14178	14178	7777
26	50th Ped	Profile4 (980)	Center	30	33	16622	16622	50270
27	50th Ped	Profile1 (1075)	Corner	30	41	174	174	324

The simulations, to study the effect of pop-up hood in our current design on overall pedestrian kinematics, indicated that even though pop-up hood helped reducing the HIC during primary impact, it changed the overall pedestrian kinematics in some cases. The specific design evaluated in this study without pop-up hood (Figure 9.2.6) and with pop-up hood (Figure 9.2.7), both resulted in secondary head-on ground impact. The kinematics (Figure 9.2.7) show that pop-up hood changes the overall pedestrian kinematics but eventually pedestrian falls on ground impacting its head with

ground. Vehicle with pop-up hood helped in reducing the HIC at the time of primary impact with hood (Table 9.2.1, run 10 and run 20) but the pop-up hood evaluated in this study did not help in avoiding secondary head-on ground impact.

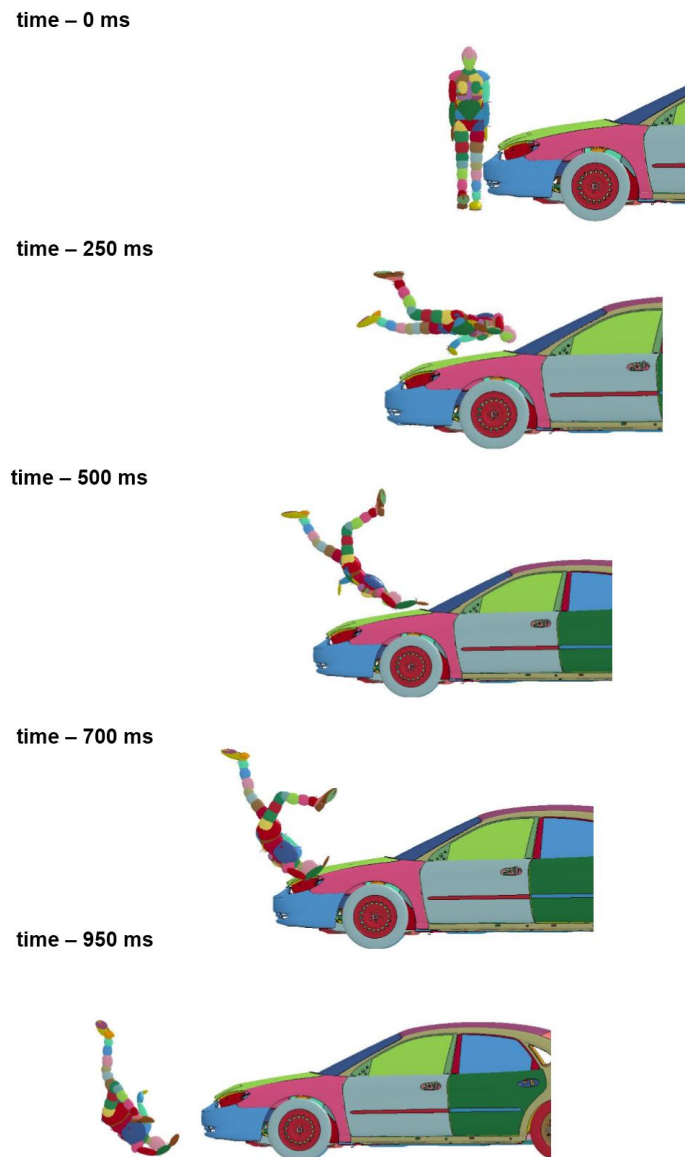


Figure 9.2.6: Pedestrian kinematics of mid-size male striking with the mid-size car profile2 at 40 km/h

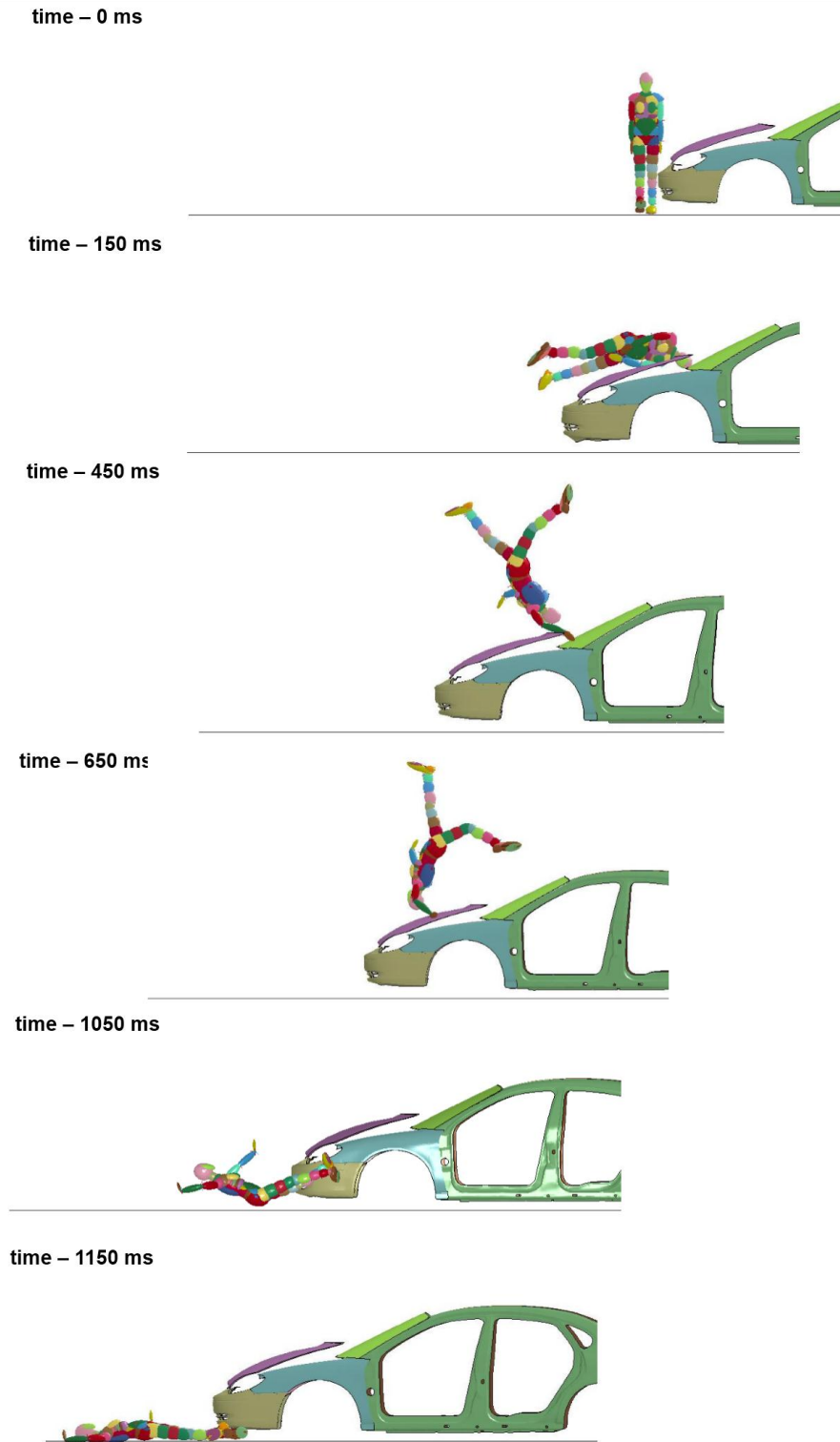


Figure 9.2.7: Pedestrian kinematics of mid-size male striking with the mid-size car profile2 having pop up hood at 40 km/h

9.3 Discussion

Experimental tests using cadavers, as well as anthropomorphic test devices have greatly advanced our understanding on traumatic injuries related to pedestrian crashes. However, due to the limitation of cadaver resources and the dynamic nature of crashes, only a small fraction of possible vehicle-pedestrian interactions can be examined via physical testing. For this reason, math models are a beneficial alternative to experimental test. Application of FE models to vehicle–pedestrian collisions will be helpful in understanding the complexity of dynamic nature of these crash events. In particular, analysis using full human body models can be expected to improve the integrated safety performance of a vehicle design.

Injuries to other body parts are not as severe as head injuries because often head injuries lead to death. The purpose of the current study was to calculate the level of HIC during primary and secondary impacts and investigate if some front-end profile changes such as hood leading edge height, hood slope etc. could help in preventing secondary *head-on* impact with ground. In this computational study, during each of the case simulated here, pedestrian body was pushed forward along the traveling direction of the striking vehicle and ultimately resulted in secondary ground impact. HIC measurements during primary impact and secondary impact (Tables 9.2.1 and 9.2.2) indicate that HIC during secondary impacts is much higher (average 1200% for mid-size car, Table 9.2.1- Column I; average 5000% for SUV, Table 9.2.2- Column I). Comparison of pedestrian kinematics with different front-end profiles on the mid-size car indicated that a lower front-end profile (profile3) can help in avoiding secondary head-on ground impact. As per earlier hypothesis, there were some test cases (highlighted as

yellow, Table 9.2.1), where secondary impact happened with the neck/shoulder region thus causing minor escape of head-on ground impact (Figure 9.3.1). These caused a very low HIC value during the phase of secondary impact. Such cases were extrapolated (to clearly distinguish from cases of secondary impact with lower extremities) by forcing the head to directly impact with ground using head velocity at that moment.

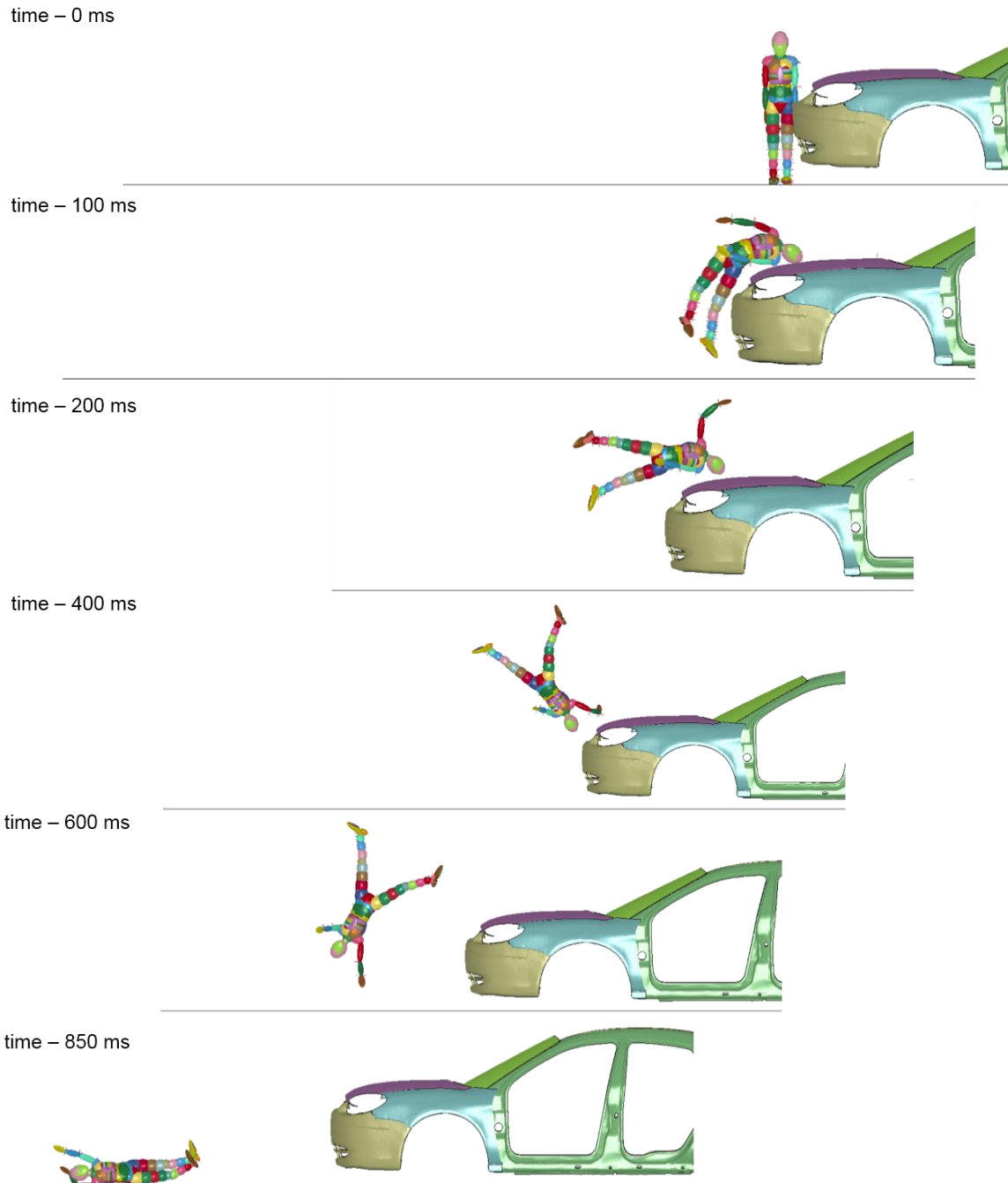


Figure 9.3.1: Kinematics of 6 year old child pedestrian striking with the mid-size car profile1 at 40 km/h

Head trajectories (Figure 9.3.2) indicates that the z-position of 50th percentile pedestrian's head CG (vertical distance of pedestrian's head CG relative to ground)

during impact with different front end profile of the mid-size car. At the start of impact with vehicle, the pedestrian is standing erect and his head is almost at 1.6 m from ground. During the impact with vehicle, the head distance from ground changes and ultimately head impacts with ground leading to almost zero vertical distance with ground. It shows that during impact with a lower front-end (profile3) vehicle, the pedestrian escaped secondary head-on collision with road surface as pedestrian head never approached near to ground. Pedestrian head velocity monitored at the head CG (Figure 9.3.3) indicated that a lower front-end vehicle (profile3) caused an overall lower head velocity and the rate of change of velocity is small during the period when pedestrian is thrown away from vehicle and until it has secondary impact with ground. Our computational study showed that, for the mid-size vehicle (Table 9.2.1), a lowered front profile (profile3) helped in avoiding secondary head-on ground impact for 5th female (run 13), 50th male (run 24). However the lowered front end profile did not help 6 YO child pedestrian in avoiding secondary ground impact (Figure 9.3.4). This particular profile helped 6yr child only at a lower impact speed of 30 km/h (run 7, Table 9.2.1) (Figure 9.3.5). Small stature ATD as 6YO child was predominantly loaded by striking vehicle in pushing mode rather than getting wrapped around the vehicle front end. Also the impact scenario of small female striking with the mid-size car at 40 km/h (run 10, Table 9.2.1) indicated that for a small stature pedestrian (like 5th female), primary impact with mid-size vehicle happened at hood mid zone. For the impact scenario of a mid-size male striking with mid-size car at 40 km/h (Table 9.2.1, run 21) indicated that for a mid-size stature pedestrian (like 50th male), primary impact with the mid-size vehicle happened at windshield.

Simulations in this study using this particular design with pop-up hood indicated that vehicle with a pop-up hood helped only during primary impact with hood thus reducing the HIC from 1298 to 633 but it didn't help in avoiding secondary head impact with ground.

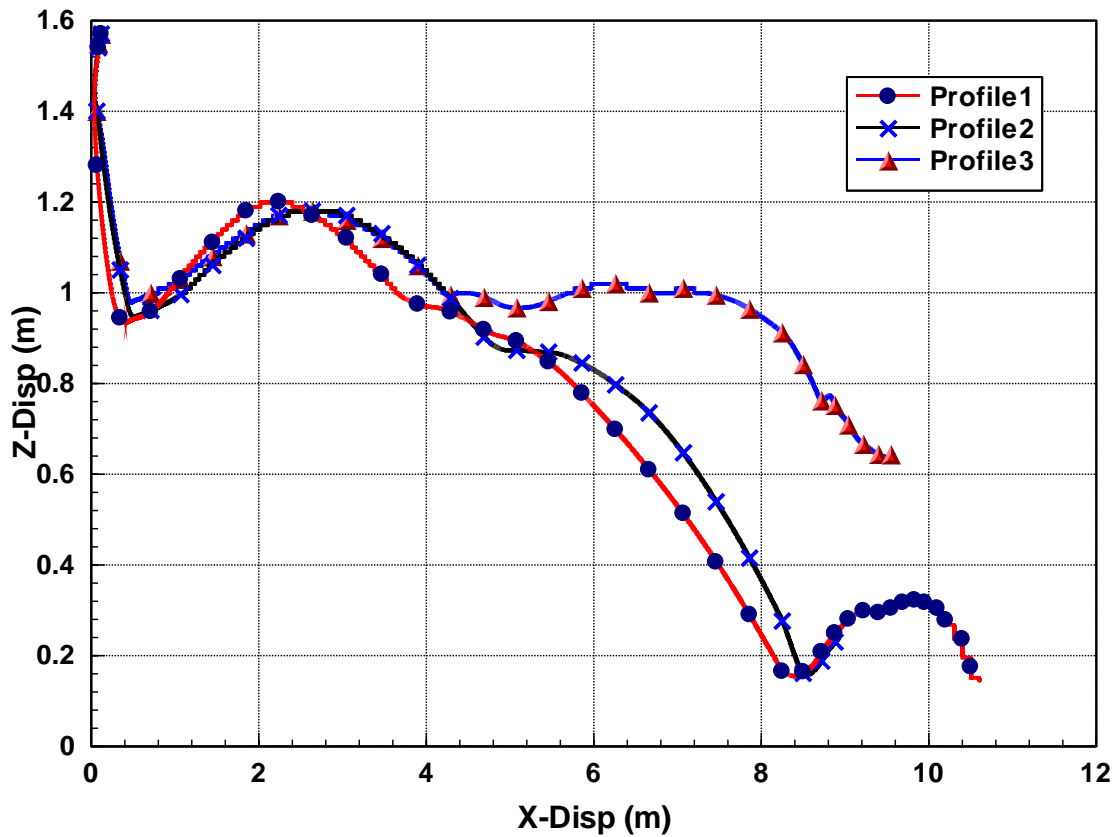


Figure 9.3.2: Comparison of head CG trajectory for 50th percentile pedestrian with three different profiles of the simulated the mid-size car

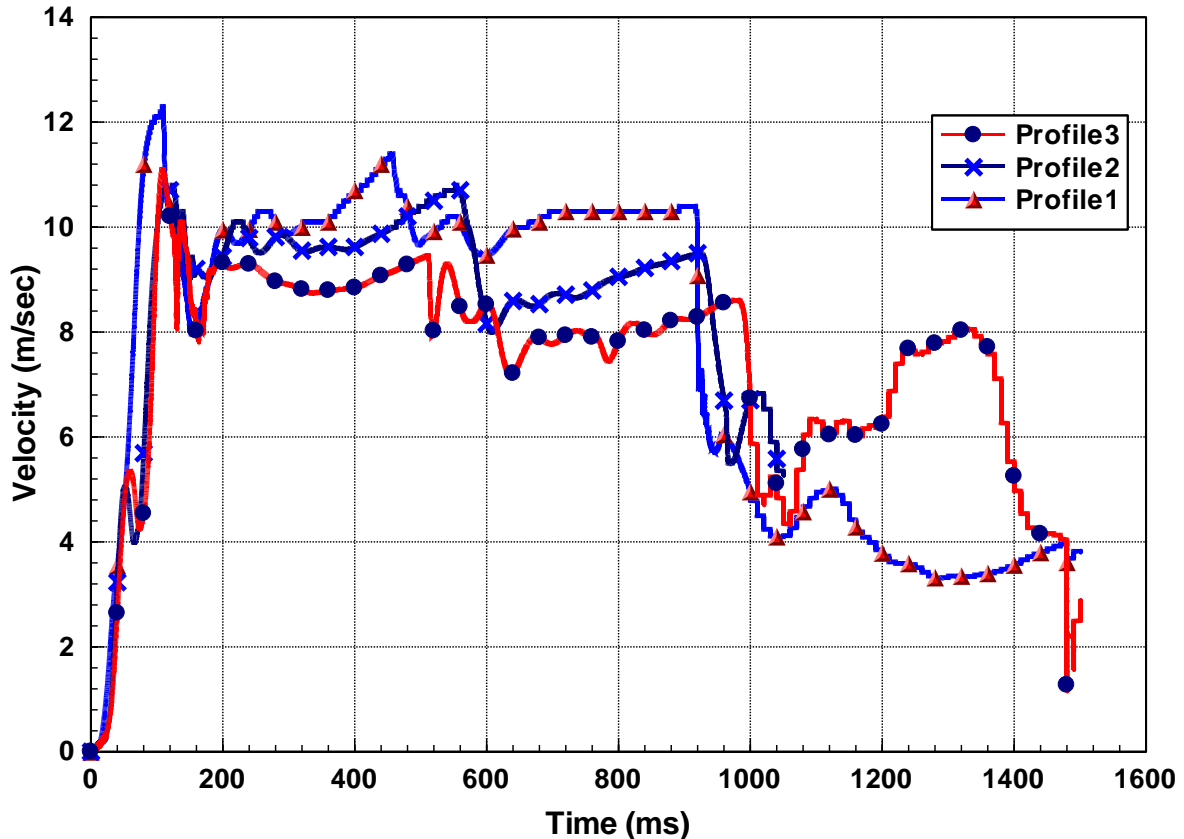


Figure 9.3.3: Comparison of head CG velocity for 50th percentile pedestrian with three different profiles of the simulated the mid-size car

Results for impacts on various profiles of SUV (Table 9.2.2) indicated that at an impact speed of 40 km/h with the SUV, it resulted in secondary head impact with ground irrespective of different front-end profiles. Only one particular front end profile, where the front bumper and hood leading edge were raised (profile1) to make it more 'box type shape,' showed the scope of avoiding secondary head impact with ground at an impact speed of 30 km/h.

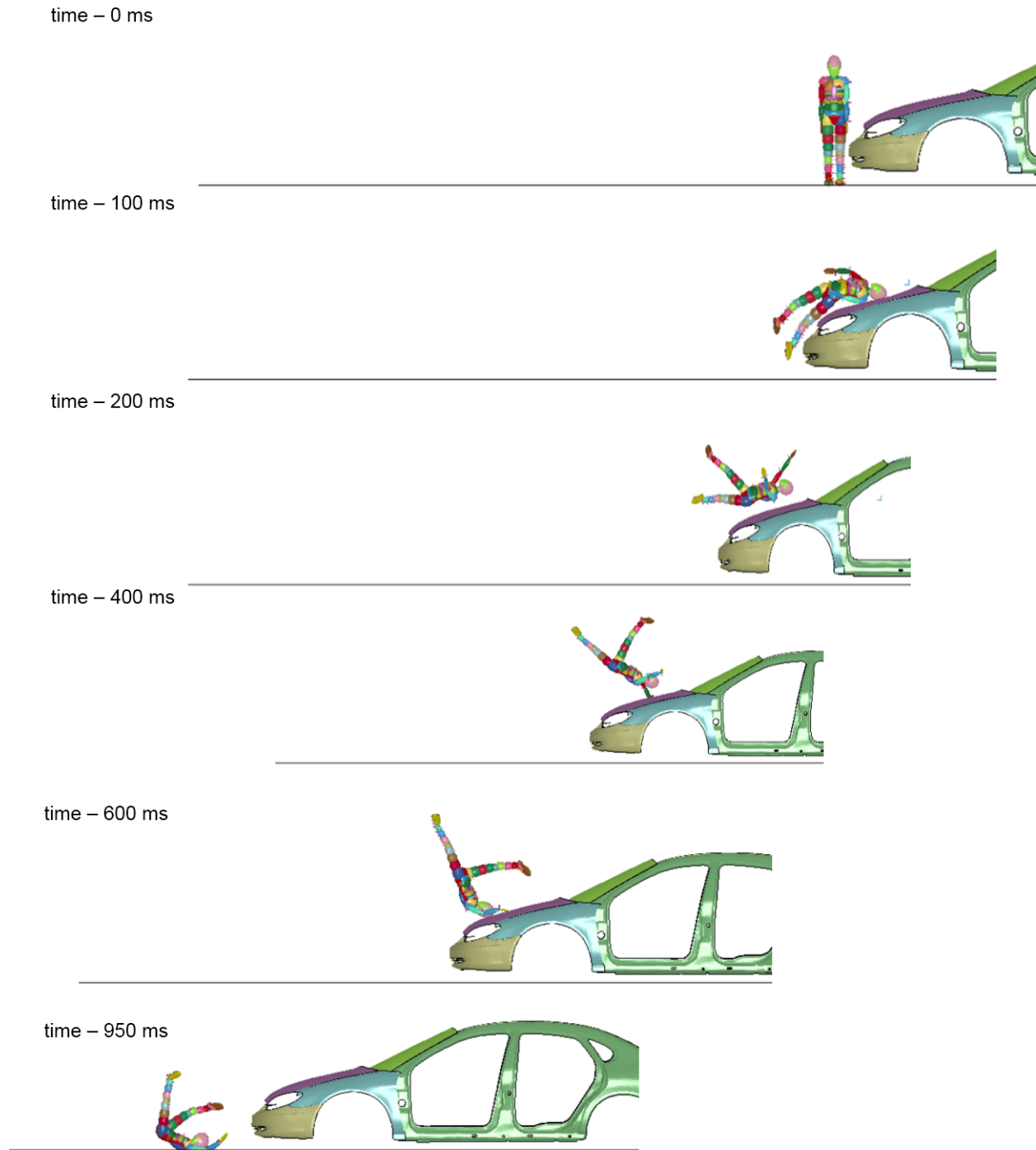
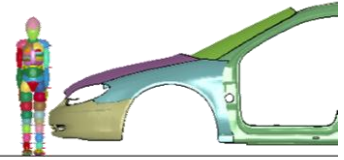
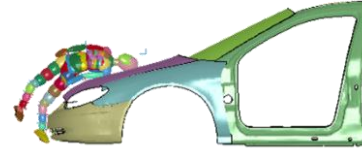


Figure 9.3.4: Kinematics of 6 years old child pedestrian striking with the mid-size car profile 3 (lowered front-end) at 40 km/h

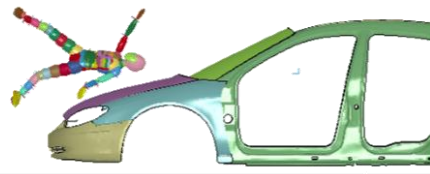
time – 0 ms



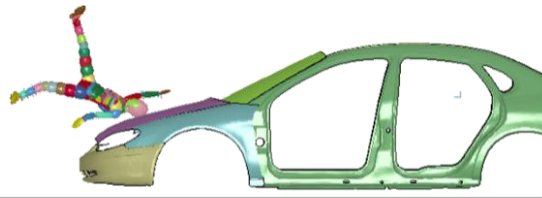
time – 110 ms



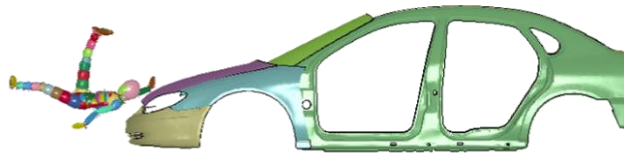
time – 300 ms



time – 500 ms



time – 700 ms



time – 835 ms

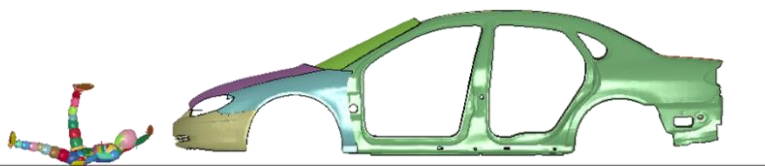


Figure 9.3.5: Kinematics of 6 years old child pedestrian striking with the mid-size car profile 3 (lowered front-end) at 30 km/h

Different front-end profiles for the mid-size car and SUV used in this study were validated for overall crash performance during frontal accident scenario. These validation results (Appendix F) indicated that changing the hood profile without changing major front-end load paths (such as front-rails or sub-frame) didn't make significant difference in vehicle performance during frontal crashes.

This study demonstrates the importance of considering the effect of secondary ground impact in a vehicle–pedestrian accident. Simulation works in this study indicate that the greatest pedestrian ATD HIC estimates can occur if the pedestrian ATD head makes contact with the road surface following primary impact with the striking vehicle. Hence, more attention should be paid to the risk of TBI caused by secondary head-on ground impacts involving vehicles with a higher profile even at a lower impact speed of 30 km/h. Different front-end profiles of vehicle (raised front-end profile or lowered front-end profile) cause pedestrian kinematics to vary a great deal thus leading to secondary ground impact on lower extremities or direct head-on collision. The study shows that a mid-size car with lowered front-end under a limited set of conditions may help reduce the chance of secondary head-on collision for pedestrian size of 5th-percentile female and 50th percentile male. Thus a lowered front-end profile for mid-size cars can be considered much safer for different size of pedestrians in terms of avoiding secondary head-on impact with ground. Whereas, SUV type vehicles, irrespective of front profile shape, almost always lead to secondary head-on ground impact at 40 km/h. This study indicates the need of new speed limit enforcement at 30 km/h in residential areas for SUV type vehicles to be more pedestrian friendly. Our computational study indicate that at 30 km/h, we can find at least one profile that will have low HIC values for the mid-size

car and one profile that will have low HIC values for the SUV for all pedestrian sizes studied.

This computational study indicated that even though active safety measures such as a pop-up hood helped during the primary impact, they didn't help in preventing pedestrian head secondary impact with ground. The numerical simulation studies found one configuration (profile 3) which avoided head-on secondary impact with the ground for the mid-size car for all pedestrian sizes studied. Additional studies similar to this one may find profiles which can reduce the chance of secondary impact while maintaining the stylists' desire to create a stylish front-end.

Chapter 10: Conclusions and Future Works

This dissertation presented the computational work to

- Study the effect of design changes along hood-to-vehicle interfaces for reducing the risk of head injury during primary impact.
- Study the effect of vehicle front-end profiles on pedestrian kinematics and thus evaluate the practicality of current regulatory test setups.
- Study the effect of vehicle front-end profiles in avoiding the chances of pedestrian head-on ground impact.

Based on this work, the following conclusions can be drawn.

- **Significant reduction in HIC is possible during primary impact along hood edges with careful designing of hood edges and hood-to-vehicle interface**

The proposed passive structural change for hood edges and hood-to-vehicle interface (as discussed in Chapter 7) showed significant improvement in HIC on different impact points on the hood and along hood edges. The shape changes for the shotgun-to-fender interface, dividing hood inner panel into two pieces along periphery, under hood clearance, and fender interface low stiffness material proved to be promising designing alternatives to meet pedestrian head impact safety requirement.

- **Head impact test setup as governed by GTR and EuroNCAP may not be representative of real world pedestrian accidents.**

This study demonstrates (as discussed in Chapter 8) that post-impact pedestrian kinematics – especially the angle of primary head impact – vary a great deal based upon the front-end profile of the striking vehicle (e.g., raised front-end profile or lowered front-end profile). Current regulatory tests for pedestrian head impact, however, use a

fixed impact angle which lead to over prediction of HIC during primary impact with vehicle hoods simulated in this study. Because most work to optimize vehicle front-end profiles for pedestrian safety assess the designs using these regulatory test setups, one might think that the use of test setups that over predict injury would lead to vehicle overdesign. On the other hand, the current regulatory setups ignore the secondary impact of the pedestrian's head with the ground – which could be more severe than the primary impact with the vehicle. If current regulatory setups do not fully capture the real world pedestrian impacts, how could they be improved? First, since head impact angle varies significantly with vehicle front-end profile, it is not a good idea to use a fixed head impact angle for all vehicle types and pedestrian sizes. This could be achieved by replacing the use of a free motion headform with the use of full scale pedestrian dummies and full scale pedestrian CAE models. Another improvement could be to assess the risk of pedestrian head injury during secondary impact with ground and thus to design the front end of vehicle which could help in preventing the head-on ground impact.

- **Importance of considering the head injury severity during secondary head impact to ground**

This study demonstrates (as discussed in Chapter 9) the importance of considering the effect of secondary ground impact in a vehicle–pedestrian crash. Simulation works in this study indicate that the highest HIC value calculated from pedestrian ATD's can occur if the pedestrian ATD head makes contact with the road surface following primary impact with the striking vehicle. Hence, more attention should

be paid to the risk of TBI caused by secondary head-on ground impacts involving vehicles with a higher profile even at a lower impact speed of 30 km/h.

Pedestrian safety regulations do not consider the severity of injury during secondary impact with ground. Perhaps, accident investigators only go by evidence of the crash, such as dents on the hood, to indicate where the head made contact with the vehicle. As no dent on road surface can be seen, may be that is why advisory committee do not suggest considering pedestrian ground impact into the regulations.

- **Careful selection of vehicle front-end parameters may help in reducing the risk of fatal head-on impact to ground**

Different front-end profiles of vehicle (raised front-end profile or lowered front-end profile) cause pedestrian kinematics to vary a great deal thus leading to secondary ground impact on lower extremities or direct head-on collision. This study shows that a mid-size car with lowered front-end under a limited set of conditions may help reducing the chance of secondary head-on collision for pedestrian sizes of 5th-percentile female and 50th percentile male. Thus a lowered front-end profile for mid-size cars may be considered much safer for different size of pedestrians in terms of avoiding secondary head-on impact with ground. Whereas, SUV type vehicles, irrespective of front profile shape, almost always lead to secondary head-on ground impact at 40 km/h. This study indicates the need of new speed limit enforcement at 30 km/h in residential areas for SUV type of vehicles to be more pedestrian friendly. This computational study indicates that at 30 km/h, at least one profile was found that works for the mid-size car and one profile works for the SUV for all three pedestrian sizes studied. Additional studies similar

to this one may find profiles which can reduce the chance of secondary impact while maintaining the stylists' desire to create a stylish front end.

For the vehicle design considered in this study, this work indicates that even though active safety measures such as a pop-up hood helped during the primary impact, they didn't help in preventing pedestrian head-on secondary impact with the ground.

10.1 Future Works

Future works could be performed to validate the effect of hood edge design changes (as discussed in chapter 7) on other structural performances such as bending and torsion stiffness, durability etc. Also, Future work could be performed to simulate the pedestrian impact using full human body model to verify the effect of these hood edge design changes in reducing injuries. Also, full frontal impact simulation could be performed after these structural changes to verify performance in event of front crash and to optimize frontal load path gages if required.

The work done for pedestrian primary impact to vehicle (Chapter 8) and secondary impact to ground (Chapter 9) always considered braking effect of vehicle. No case is studied without the braking effect of vehicle during pedestrian crash. Some simulation need to be conducted to compare the results in the event of no-braking of vehicle. This study for pedestrian-vehicle impacts didn't consider the effect of muscle activation during pedestrian impact with vehicle or ground. Future studies could be focused on implementing muscle activation during such impacts.

This study (chapter 9) considered only two impact locations along the vehicle width and only three pedestrian sizes. More impact locations along the vehicle width

(from the centerline to corner of vehicle) and impact with more pedestrian sizes could be investigated for better understanding of the influence of vehicle front-end profile on pedestrian kinematics leading to pedestrian head-on ground impact. The effect of a pop-up hood on overall pedestrian kinematics and thus leading to pedestrian secondary head-on ground impact need to be investigated in more details.

The simulations conducted in this study for pedestrian ground impact had long run time (2-3 days). There is need to develop capability for measuring angular momentum of pedestrian in FE models after initial impact with vehicle and find out how angular momentum can control pedestrian motion after initial impact with vehicle rather than waiting for actual impact with ground. Also, method can be developed to continue simulation without vehicle model after initial impact with vehicle has happened. This also can result in reduced runtime for complete simulation up to pedestrian ground impact.

Further, there is need to conduct experiments to confirm the design changes suggested, for hood-to-vehicle interfaces (Chapter 7) and for vehicle front-end profiles to avoid secondary head impact (Chapter 9), before putting these new ideas into production. As a future study, a statistical model can be derived to discuss the effect of front-end geometry on pedestrian kinematics and injury patterns.

APPENDIX A- VEHICLE FE MODEL DETAILS AND VALIDATION

Vehicle FE models: the full scale SUV FE model is a detailed model consisting of around 800 parts, 630,000 nodes and 620,000 elements. The hood area was further refined in terms of improving the mesh quality and adding missing details in the hood subsystem such as the detailed hinges, latches, adhesives between hood outer panel and hood inner panels, etc. Absence of these details under-predicts the head injury criterion (HIC) by 10-30% (Table A.1). For instance in the absence of the adhesives between hood outer and hood inner panels, the HIC predicted is 590 compared to 870 after modeling the adhesives between the hood inner panel and hood outer panel. The reason for such a difference is that the hood inner panel is set to move independent of hood outer panel during head impact on hood in absence of the mastics thus reducing the overall hood stiffness experienced by the simulated head. These results prove that any pedestrian safety research work undertaken using such vehicle models with missing details could mislead engineers in proposing pedestrian safety countermeasures.

Table A.1: Effect on HIC with missing vehicle details in the FE model at some locations

Impact Location	HIC - After Modeling Missing detail	HIC - With Missing details
1000 WAD Pt3_Frt	1177	1094 (Missing Hood support on Frame)
1000 WAD Pt7_Frt	1195	776 (Missing Front Latch)
1250 WAD Pt3_Rear	870	590 (Missing adhesives between hood Outer and hood inner panel)

Note: Please see Section 7.1 for WAD reference point

Finally, the model was validated for full frontal rigid barrier crash test at 56 km/h as per US New Car Assessment Program (USNCAP) [USNCAP test 3730, <http://www-nrd.nhtsa.dot.gov/database/asp/vehdb/queryvehicle.aspx>]. Velocity time history (Figure

A.1) indicates that a FE model velocity time history matches 98% (based on time for zero crossing of velocity) with actual tests velocity time history. There is only slight difference in velocity time histories during 40 ms to 60 ms duration (Figure A.1). Acceleration time history (Figure A.2) shows acceleration peak of 37g for FE model compared to test prediction of 35g. Energy balance of the FE model (Figure A.3) indicates good stability of the model.

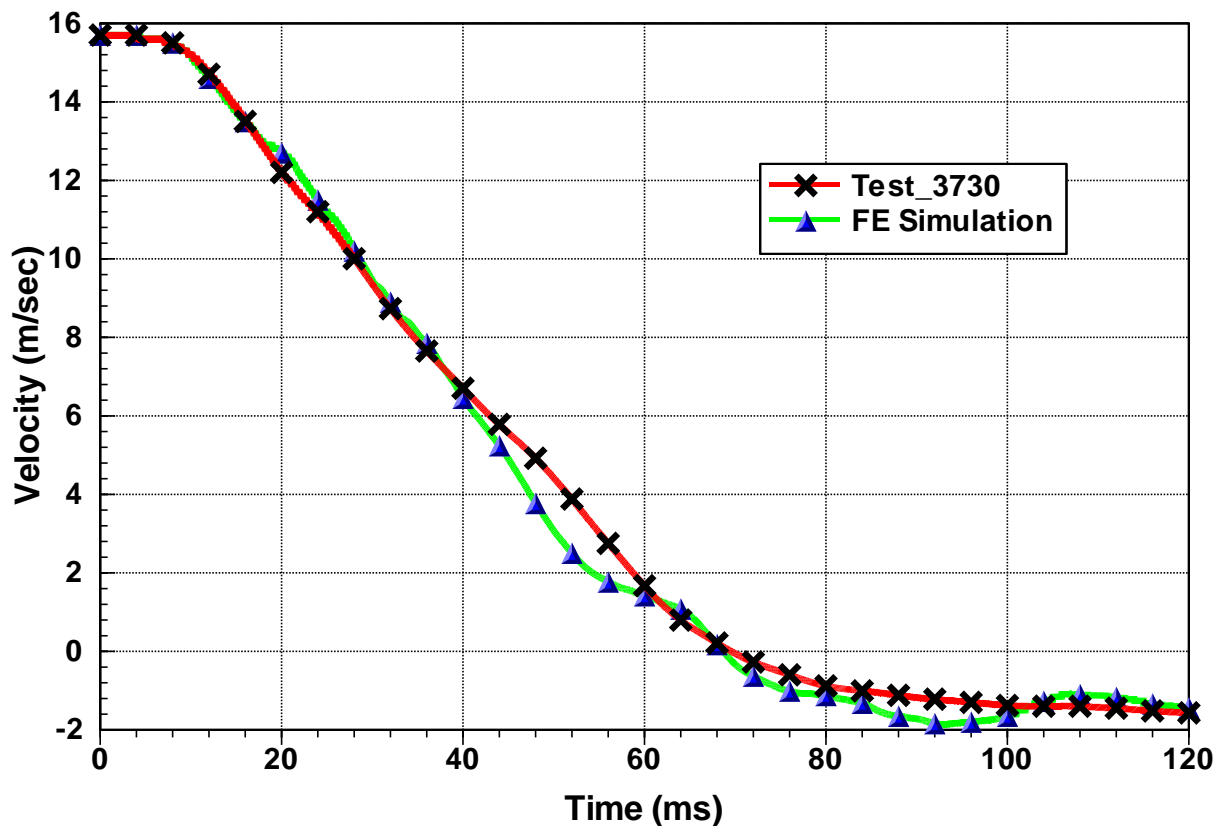


Figure A.1: Velocity comparison- SUV FE simulation vs. test data

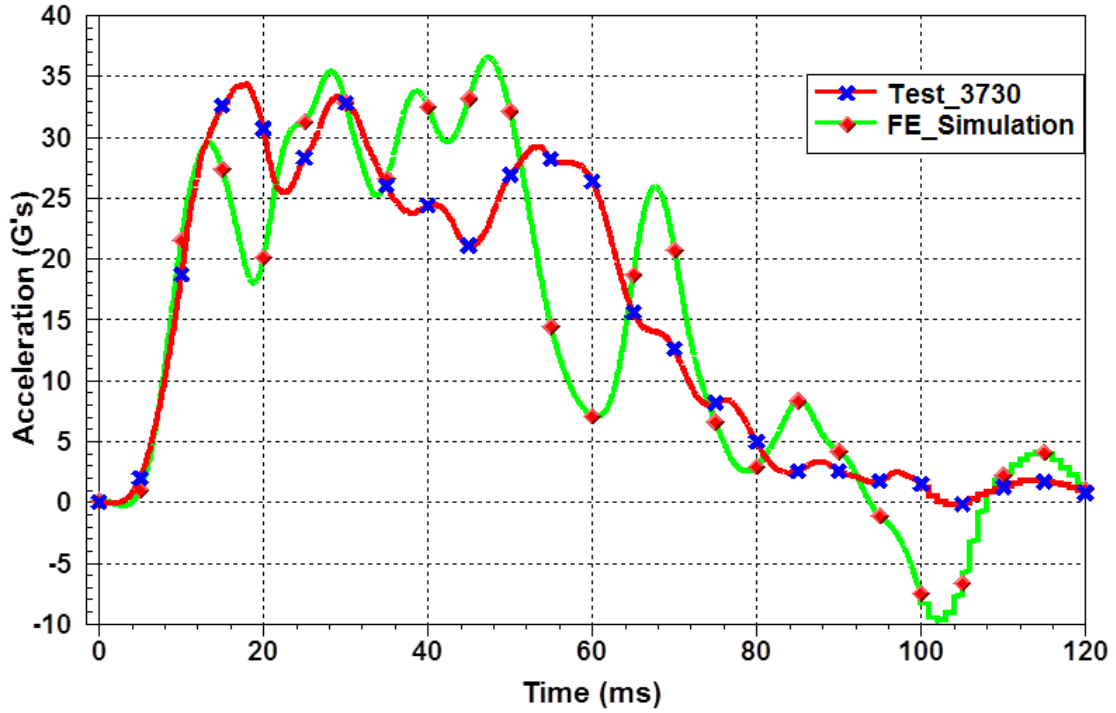


Figure A.2: Acceleration comparison- SUV FE simulation vs. test data

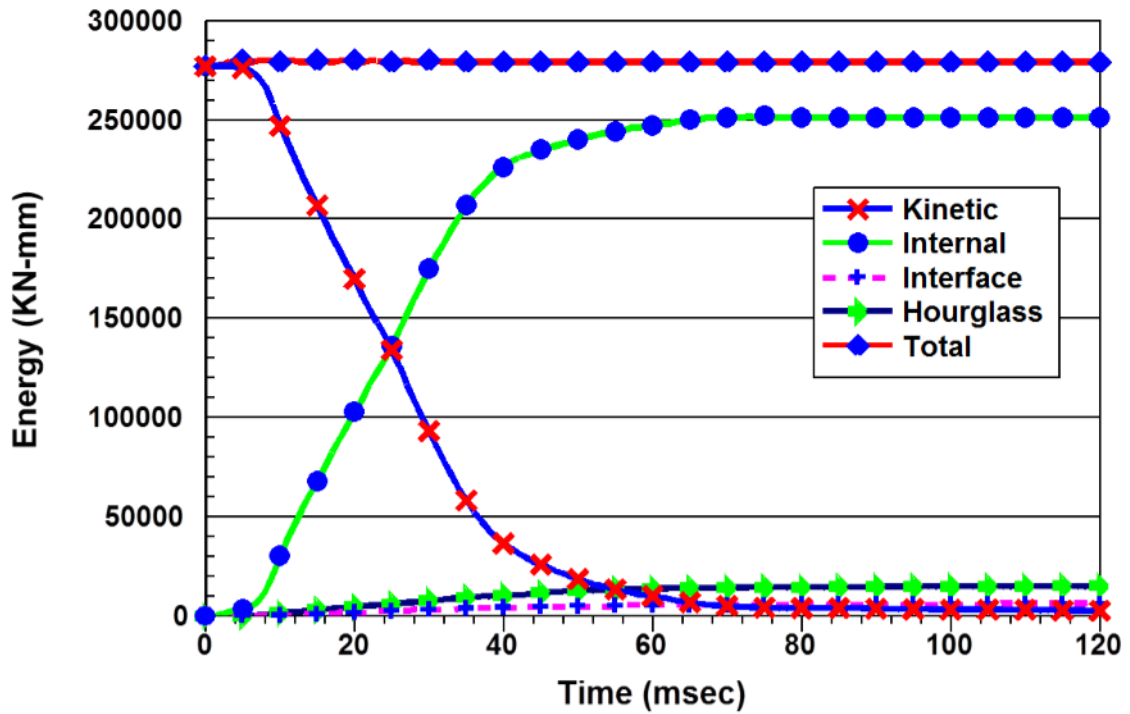


Figure A.3: SUV FE model energy balance

The full scale mid-size vehicle FE model is a detailed model consisting of around 780 parts, 940,000 nodes and 1,060,000 elements. The hood area was further refined in terms of improving the mesh quality and adding missing details in the hood subsystem such as detailed hinges, latches, adhesives between hood outer panel and hood inner panels etc. Finally, the model was validated for full frontal rigid barrier crash test at 56 km/h as per USNCAP (USNCAP test 3248, <http://www-nrd.nhtsa.dot.gov/database/asp/vehdb/queryvehicle.aspx>). Velocity time history (Figure A.4) indicates that a FE model velocity time history matches 87% (based on time for zero crossing of velocity) with actual tests velocity time history. There is only slight difference for zero crossing of velocity in velocity time histories. In FE model, vehicle approaches zero velocity at 88 ms whereas in actual test, vehicle approaches zero velocity at 78 ms (Figure A.4). Acceleration time history (Figure A.5) shows acceleration peak of 36 g for FE model compared to test prediction of 32 g.

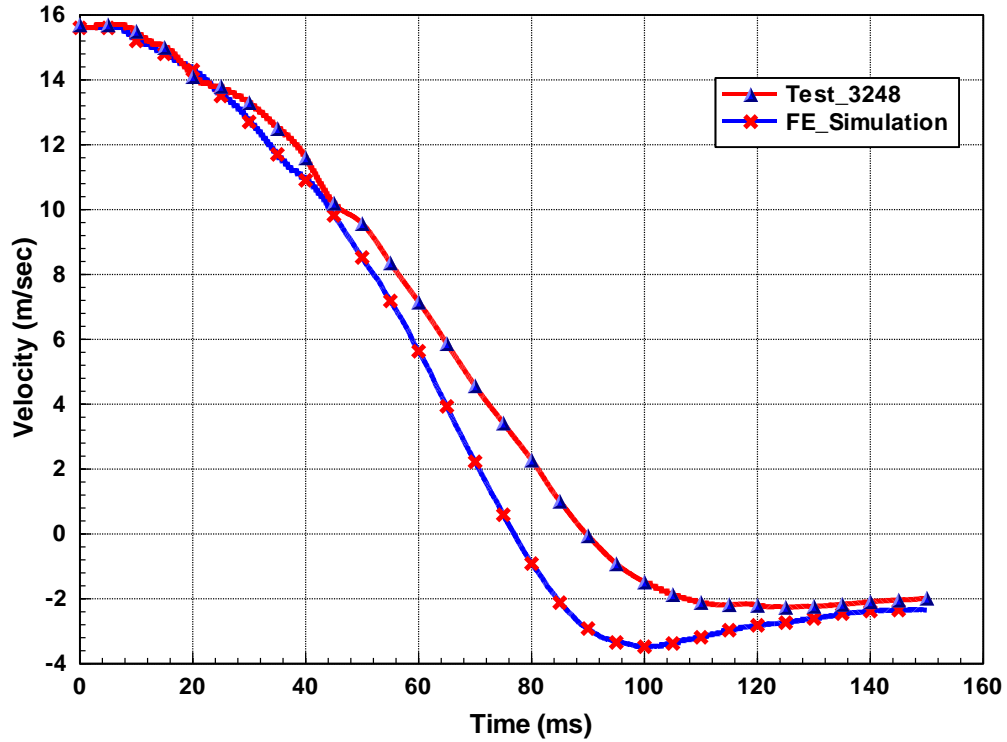


Figure A.4: Velocity comparison- Mid Size Car FE simulation vs. test data

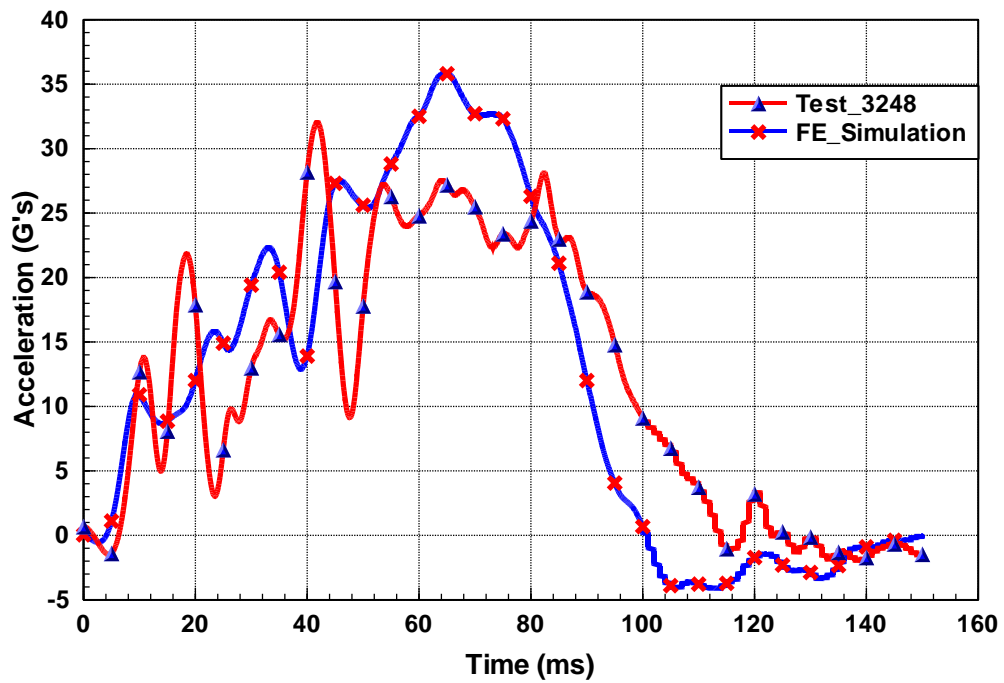


Figure A.5: Acceleration comparison- Mid Size Car FE simulation vs. test data

Validation of vehicle models for high-speed impacts into barriers does not qualify the model to consider suitable for pedestrian impacts because the hood does not absorb much energy in high-speed frontal impacts. More work was done to make this model suitable for pedestrian work.

Some geometry effects such as representation of head lamps, fascia, complete geometry representation of latch and hinges etc. that may be insignificant in high-speed crash are of great importance for pedestrian impact simulations. In regions where fracture plays a role, or complex ribbed anisotropic plastic components, or regions with very complex kinematics like hinge, latch, wiper system etc. are needed to be modeled in detail for pedestrian impact simulation work. For this reason some missing details in the model as headlamps, fascia grill were modeled. Hood panels (inner and outer) were re-meshed, with element size of 5 mm and element formulation number 16, to capture any small deformations. These panels are made of steel and its material law and property are well-established and hence no additional validation was performed. Adhesives were modeled between the hood outer panel and inner panel as shown in Figure A.6. Absence of these adhesives will cause hood inner panel to move independently thus reducing hood stiffness and resulting in predicting lower HIC.

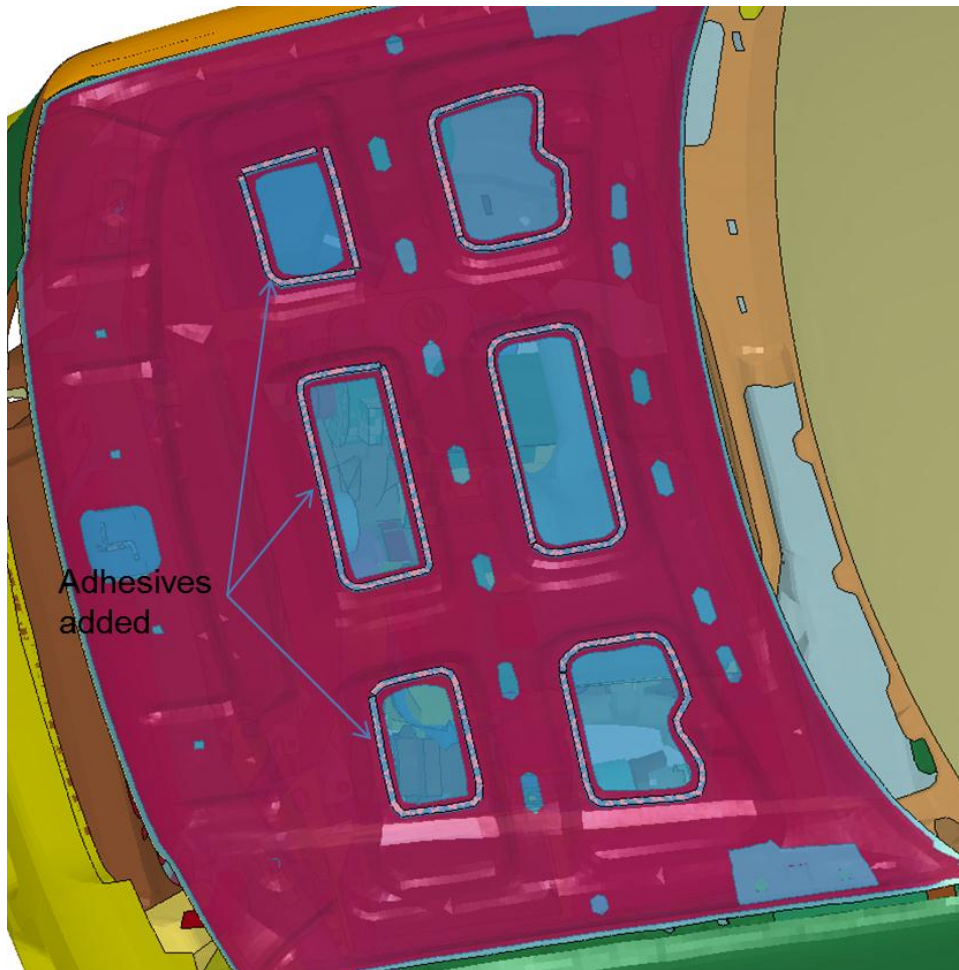


Figure A.6: adhesives modeled between hood outer and inner panels

Originally, Hood hinges and latch were just represented as rigid elements as effects of these geometry are insignificant for full frontal crash but for pedestrian impact simulation work, hinges and latch were modeled in details with modeling the bolts as actual geometry (Figure A.7).



Figure A.7: Rear Hinges modeled in details with actual bolts

APPENDIX B – GLOSSARY OF VEHICLE STRUCTURE

Some of the vehicle structural terms referred in this dissertation are labeled in Figures B.1 - B.3 for clarifications.

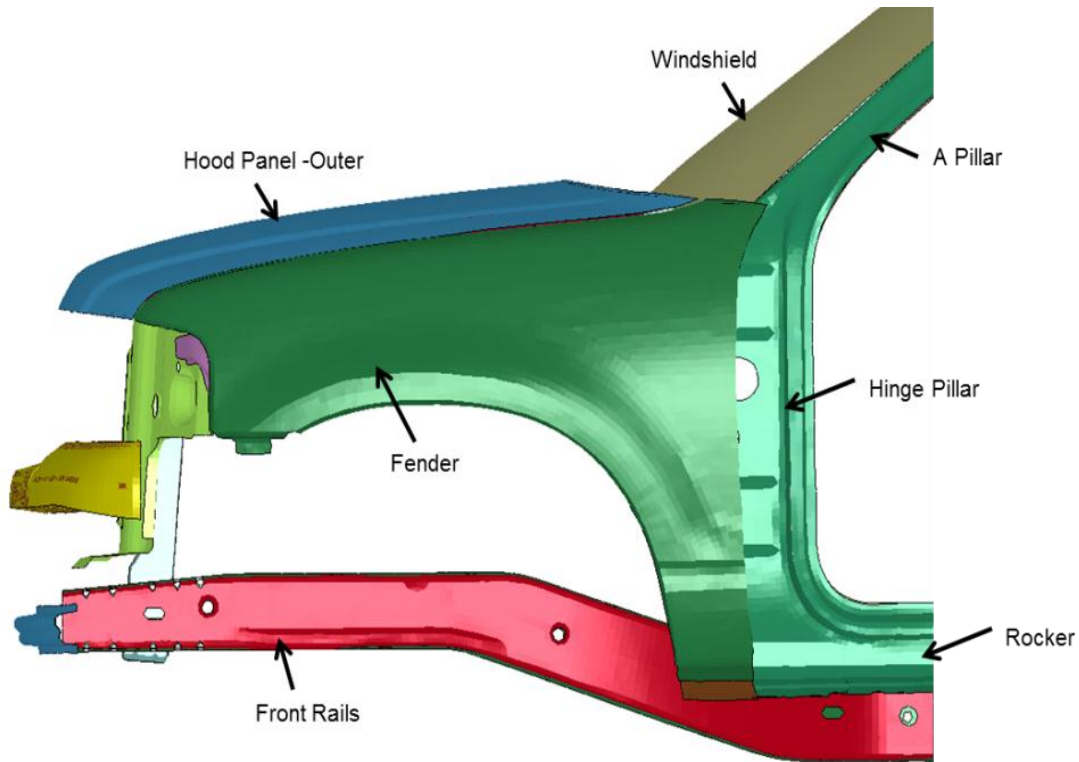


Figure B.1: glossary of vehicle structure terms- Surface A

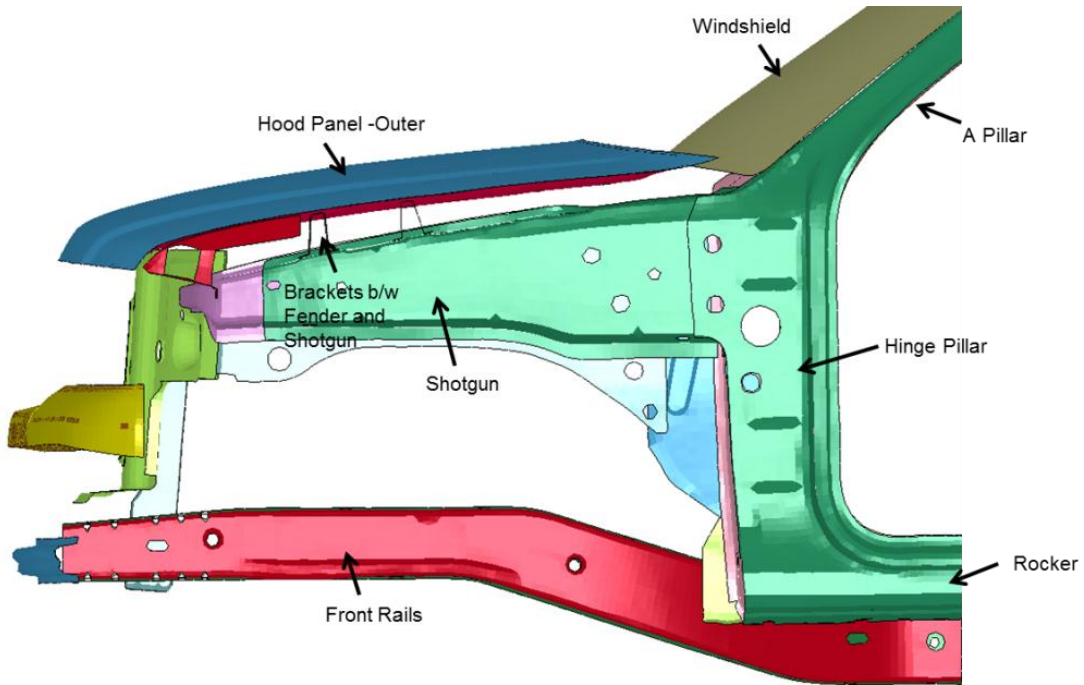


Figure B.2: glossary of vehicle structure terms- Surface B

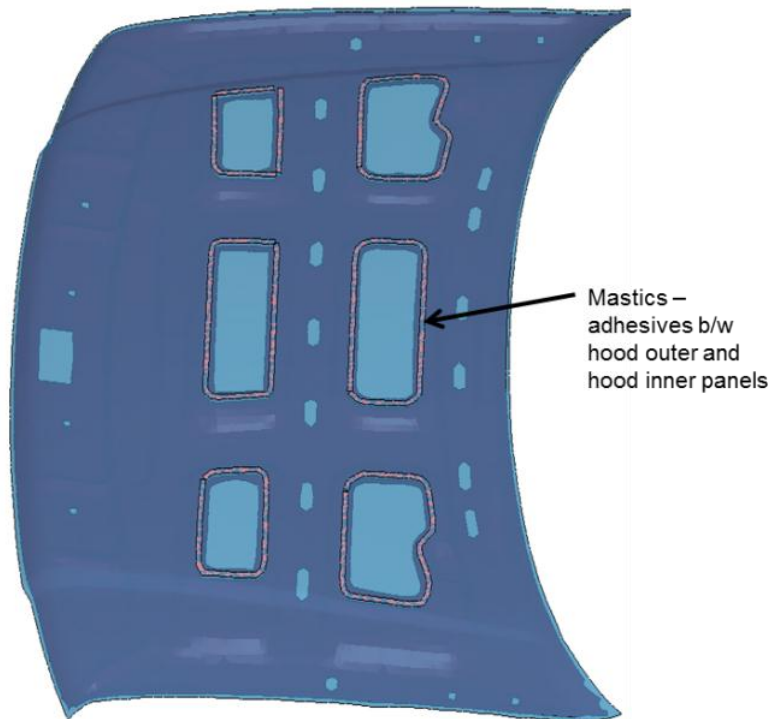


Figure B.3: adhesives between hood outer panel and hood inner panel

APPENDIX C – HEAD ACCELERATION HISTORIES

Resultant head acceleration histories calculated from the original model are compared with the final improved model (Figure C.1 and C.2). Proposed shape changes along hood edges and changes to hood fender interface helped lowering the head acceleration (Figure C.1).

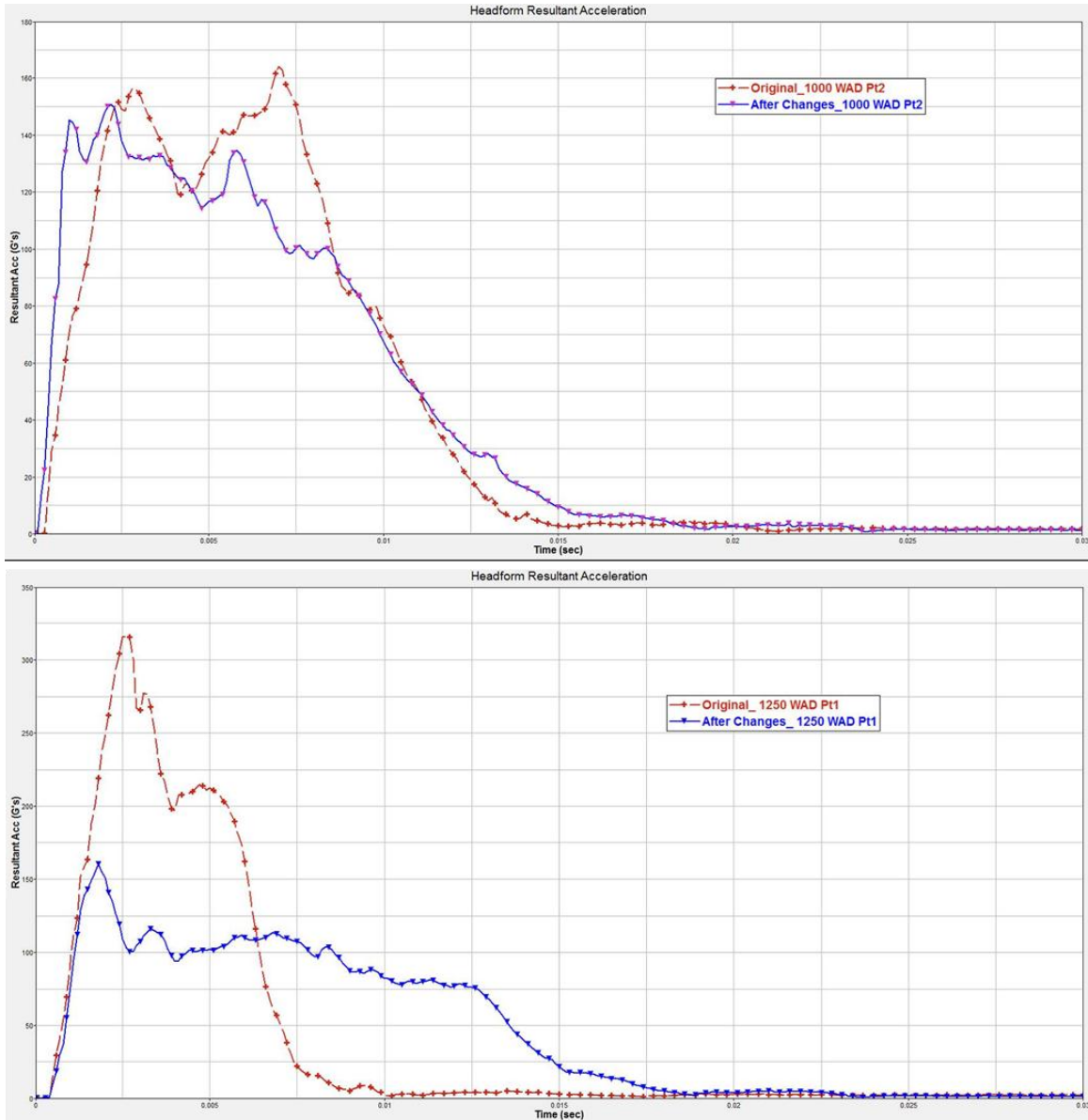


Figure C.1: Comparison of head accelerations – the original model vs. final updated model.

Head acceleration curves for impact location '1700-2100 WAD pt 2' (Figure C.2) indicates a lower peak acceleration but for longer duration which causes a high HIC value. This low acceleration for longer duration is due to coming in contact with under hood structure like hood hinge etc.

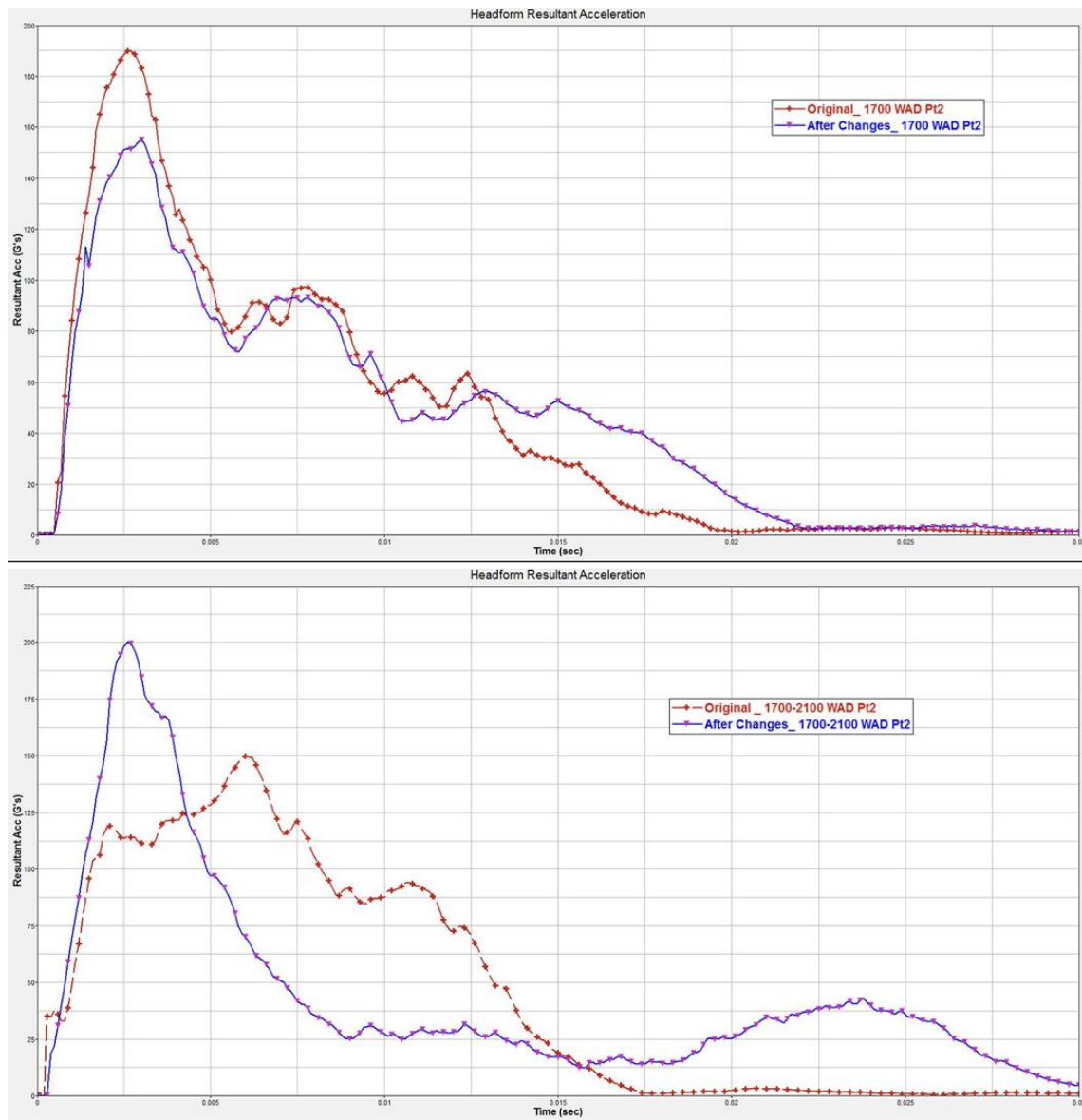


Figure C.2: Comparison of head accelerations – the original model vs. final updated model.

After making proposed shape changes and modifying the fender to shotgun interface, the overall peak acceleration increased but for a very short duration (Figure C.2) which helps lowering the HIC for the same impact location of '1700-2100 WAD point 2'.

The final model, with modified hood shapes or hood to fender interface etc., is tested for frontal impact performances to make sure these changes don't degrade performance during frontal crush. Lowering the shotgun in front region (which changes the upper load path) does not significantly affect the overall frontal impact performance (Figure C.3). It is due to reason that the upper load path (shotgun) does not contribute much to overall load transfer capacity compared to lower load path (main front rails) (Figure C.4).

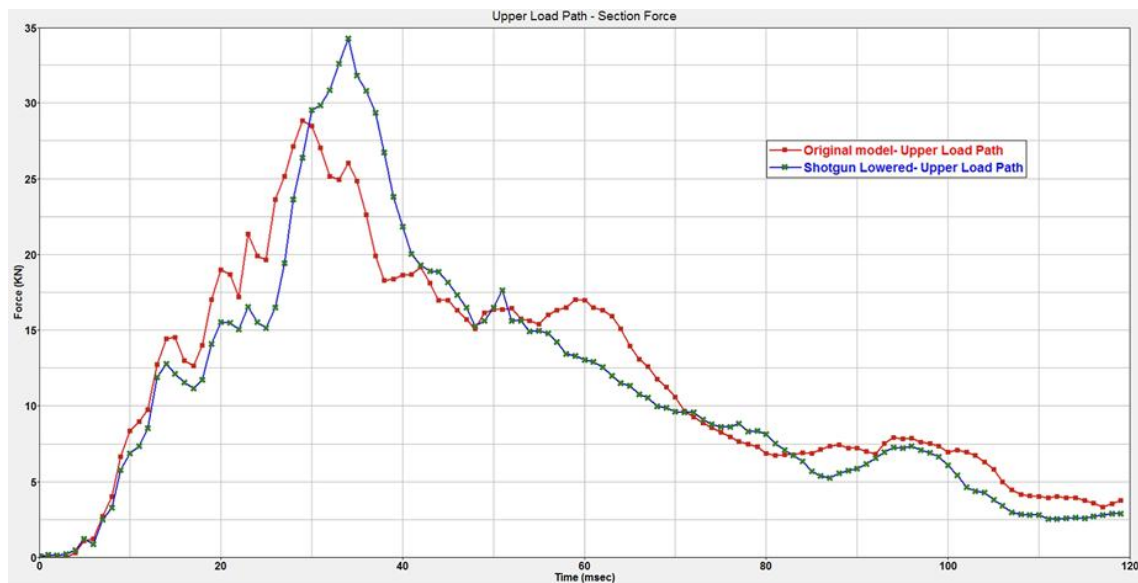


Figure C.3: Comparison of section forces- original vs. modified shotgun (section defined in middle of the shotgun)

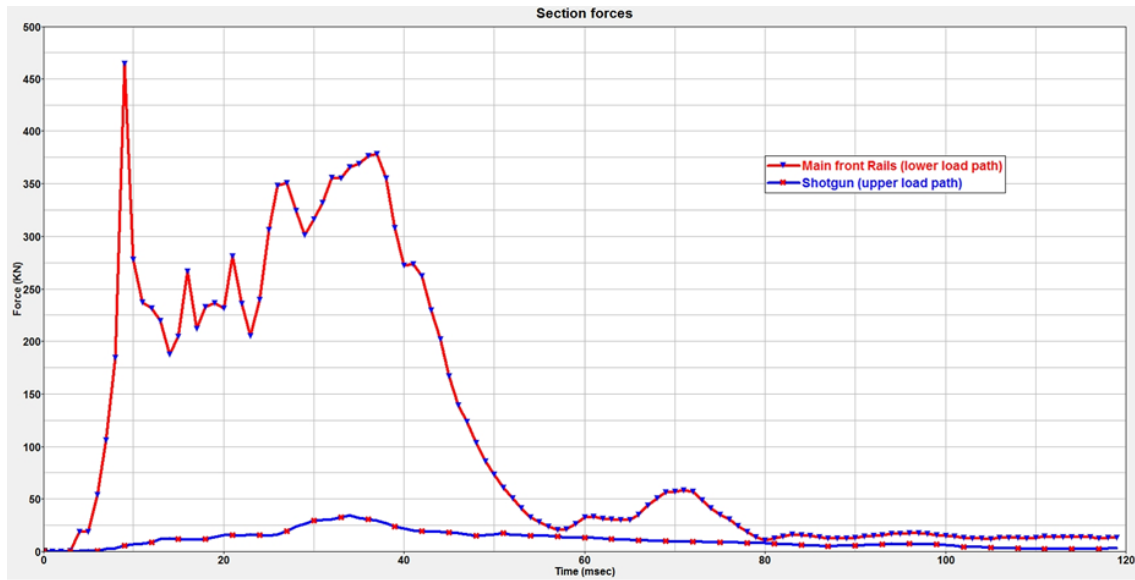


Figure C.4: Comparison of section forces- upper vs. lower load path

Overall acceleration history of vehicle (Figure C.5) indicates no significant difference in vehicle crash pulse during frontal crash. It shows that overall peak acceleration of vehicle is not affected by these structural changes in the hood region and upper load path. The comparison of energy absorption capacity of shotgun (Figure C.6) indicates that there is no significant difference in energy absorbed by shotgun in original model and design improved model. It indicates that shotgun's energy absorption capacity during frontal crash is not compromised due to these design changes.

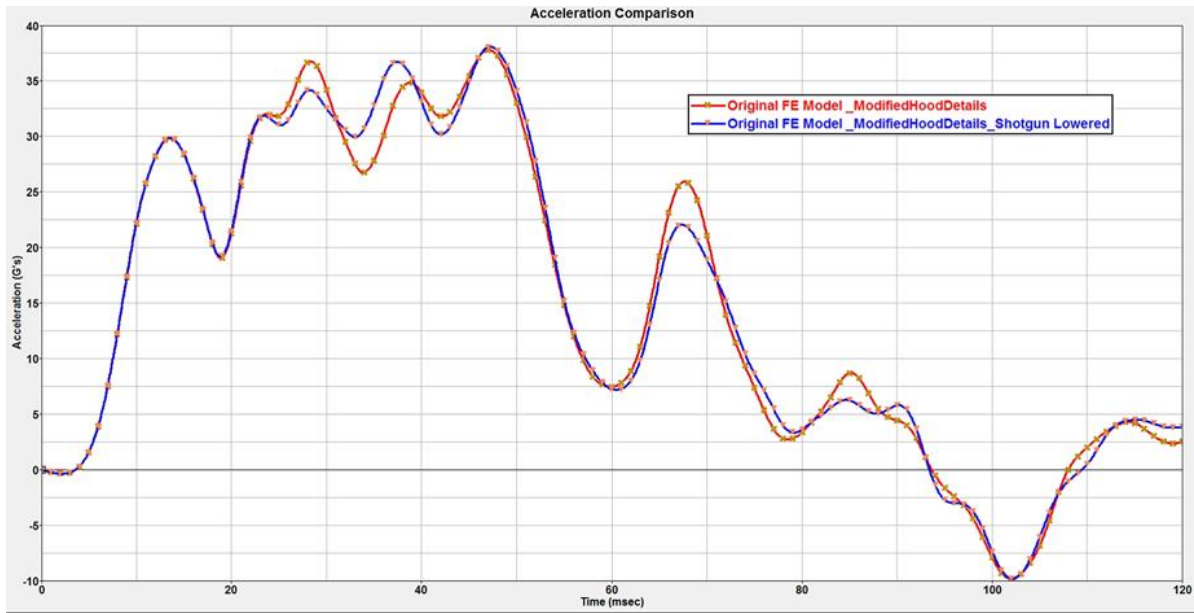


Figure C.5: Vehicle acceleration history- original model vs. modified model (measured at B-Pillar and Rocker Intersection)

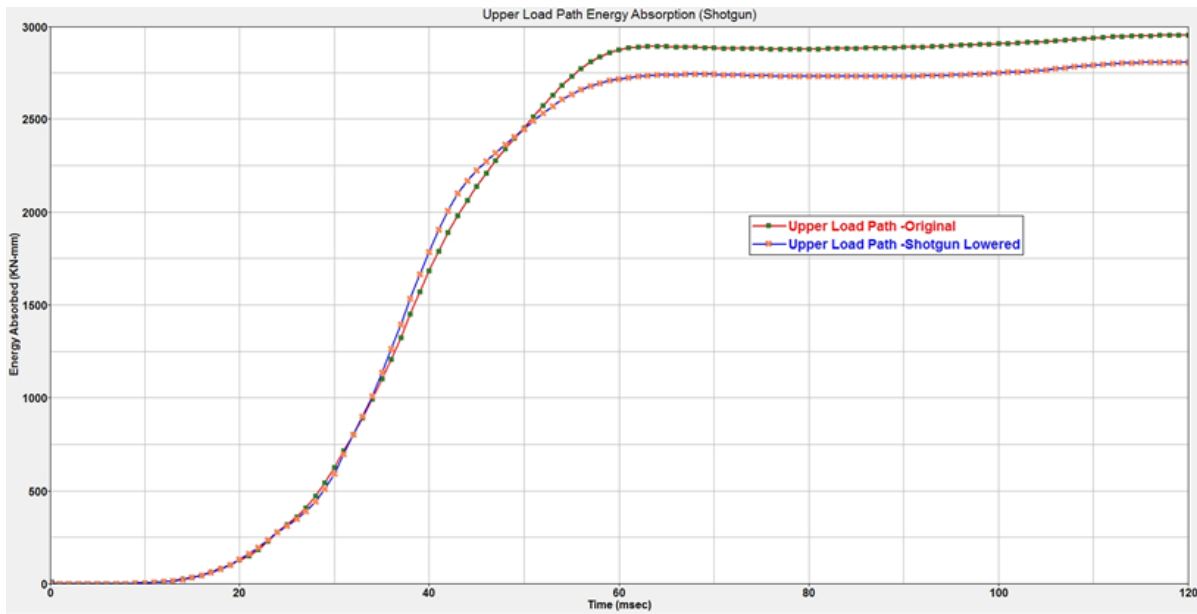


Figure C.6: Shotgun energy absorption capacity- original model vs. modified model

APPENDIX D: MADYMO PEDESTRIAN MODEL VALIDATION SUMMARY

MADYMO pedestrian models were validated against blunt impact test (Figure D.1) (Lange et al. 2001; Hoof et al. 2003; MADYMO Human models manual release 7.2, 2010).

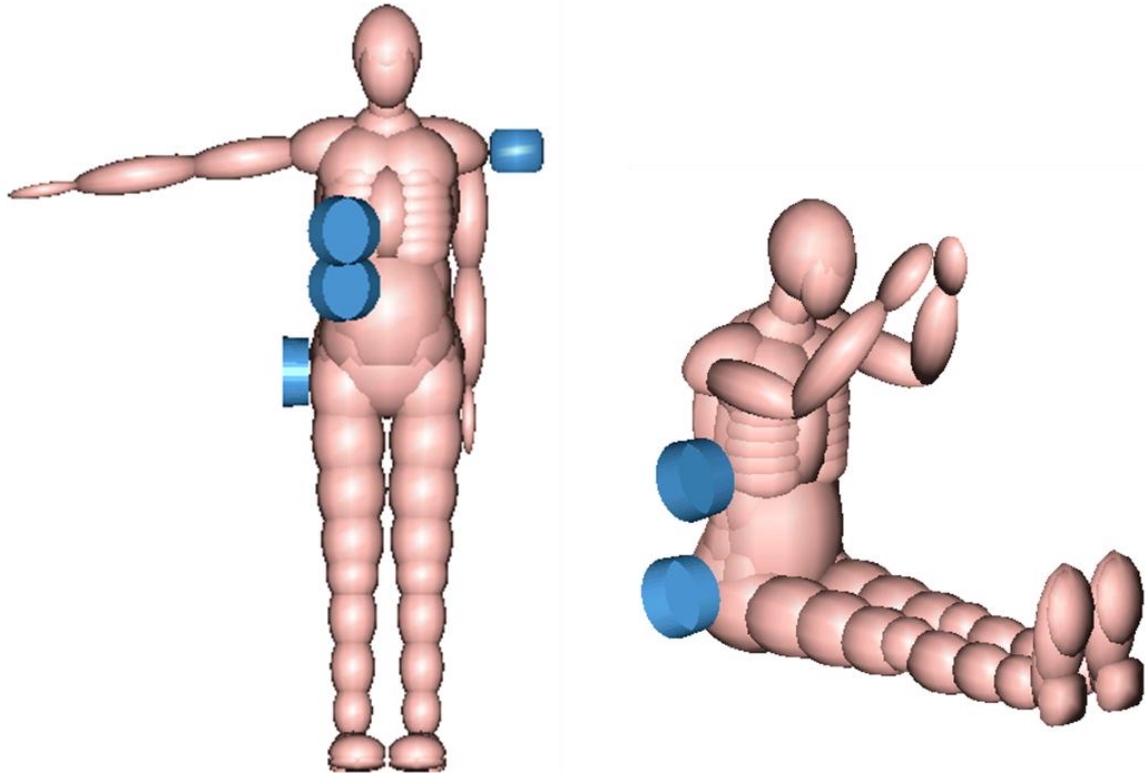


Figure D.1: Different impactor test configurations used for model validation.

In addition, three different sets of Post Mortem Human Subjects (PMHS) vehicle impact tests have been simulated to verify the biofidelity of the pedestrian model (Lange et al. 2001; Hoof et al. 2003; MADYMO Human models manual release 7.2, 2010). Since PMHS subjects of different anthropometries were used in the tests, the pedestrian model was scaled to the specific body dimensions of each PMHS subject prior to simulating the corresponding test. In total 18 subjects (16 male, 2 female) were

used in these tests (Table D.1), ranging in height from 160-192cm and in weight from 53-90 kg.

Table D.1: car-pedestrian impact tests used for validation of the pedestrian models

Model	Description	Test Object	Specifications
Mid-size male scaled to PMHS size	5 tests, large family car	5 PMHSs	32-40 km/h, deceleration of 4.7 - 5.7 m/s ²
Mid-size male scaled to PMHS size	10 tests, 3 different cars	10 PMHSs	25, 32, 39, 40 km/h
Mid-size male scaled to PMHS size	3 tests, small family car	3 PMHSs	25, 32, 39 km/h

APPENDIX E: METHOD FOR CALCULATING VEHICLE LOWERING AMOUNT RELATIVE TO GROUND

The actual vehicle tires lose their roundness because of tire compression due to the vehicle's own weight. FE vehicle model does not take into account of the tire out-of-roundness (Figure E.1) due to vehicle weight. To calculate tire compression amount, data from 20 similar SUV and 20 similar mid-size vehicles was measured and average tire compression amount was used for each vehicle type. Also based on Global Technical Regulation (GTR) test setup for legform to bumper impact, legform is raised by 25 mm due to pedestrian leg uplifting during walking stance. To consider that, pedestrian human model also needs to be raised by 25 mm.

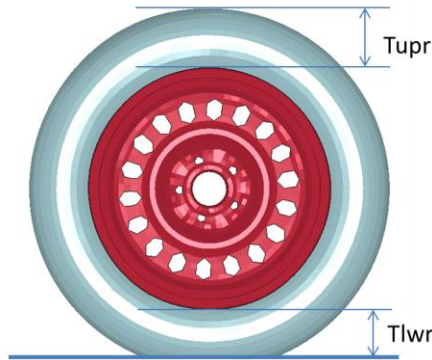


Figure E.1: Tire compression measurements

$$T_{cmp_i} = T_{upr_i} - T_{lwr_i}$$

$$\overline{T_{cmp}} = 1/n \sum T_{cmp_i}$$

$$V_{low} = \overline{T_{cmp}} + 25$$

As a combined effect of pedestrian raise and vehicle tire compression, entire vehicle model was lowered by 60 mm for the SUV and 40 mm for the mid-size car.

APPENDIX F – EFFECT OF FRONT-END PROFILE CHANGES ON FRONTAL CRASH PERFORMANCE

The mid-size car model with lowered front-end profile (profile2) and raised front-end profile (profile1) is tested for frontal crash performances (USNCAP 56 km/h) to make sure these changes don't degrade vehicle's performance during frontal crash. Overall acceleration history of vehicle (Figure F.1) indicates no significant difference in vehicle crash pulse (measured at B-Pillar and Rocker Intersection) during frontal crash. It shows that overall peak acceleration of vehicle is not affected by these structural changes in the front-end profile. The comparison of overall vehicle velocity during frontal crash (Figure F.2) also shows that it remains unaffected by these structural changes.

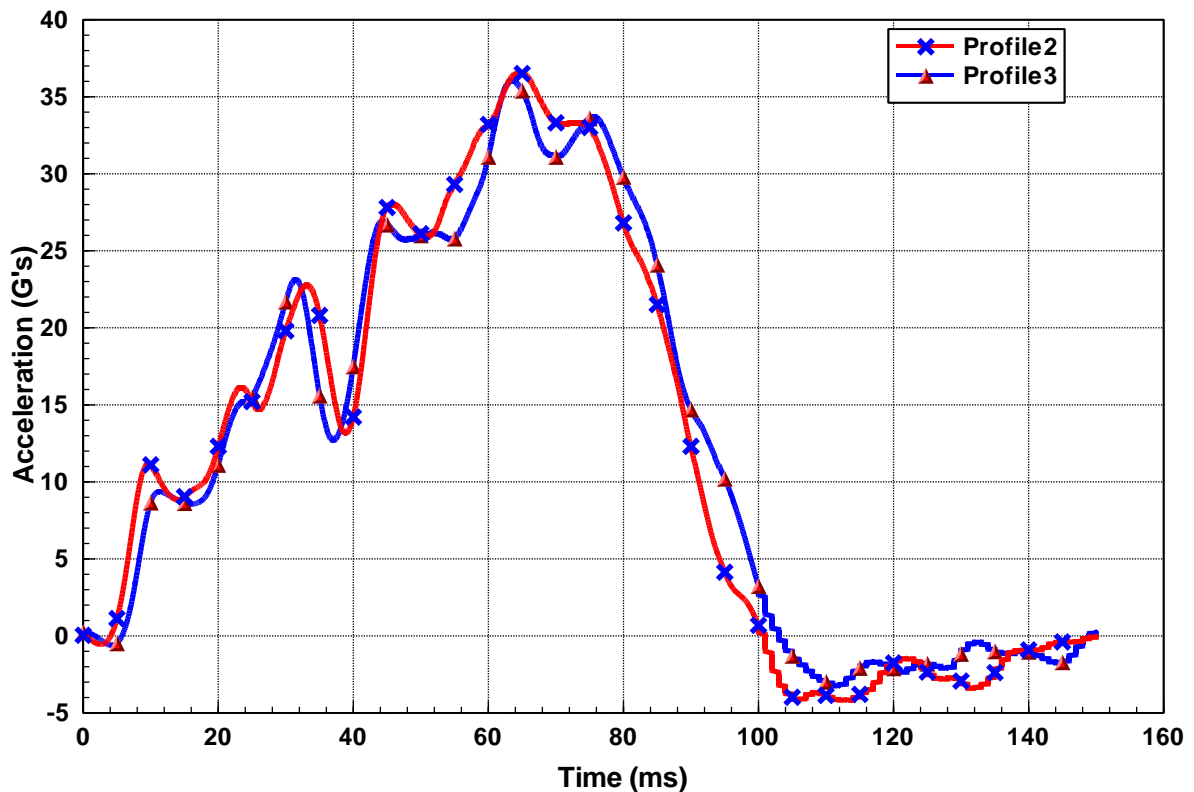


Figure F.1: Mid-size car acceleration comparison for different front-end profiles during frontal crash

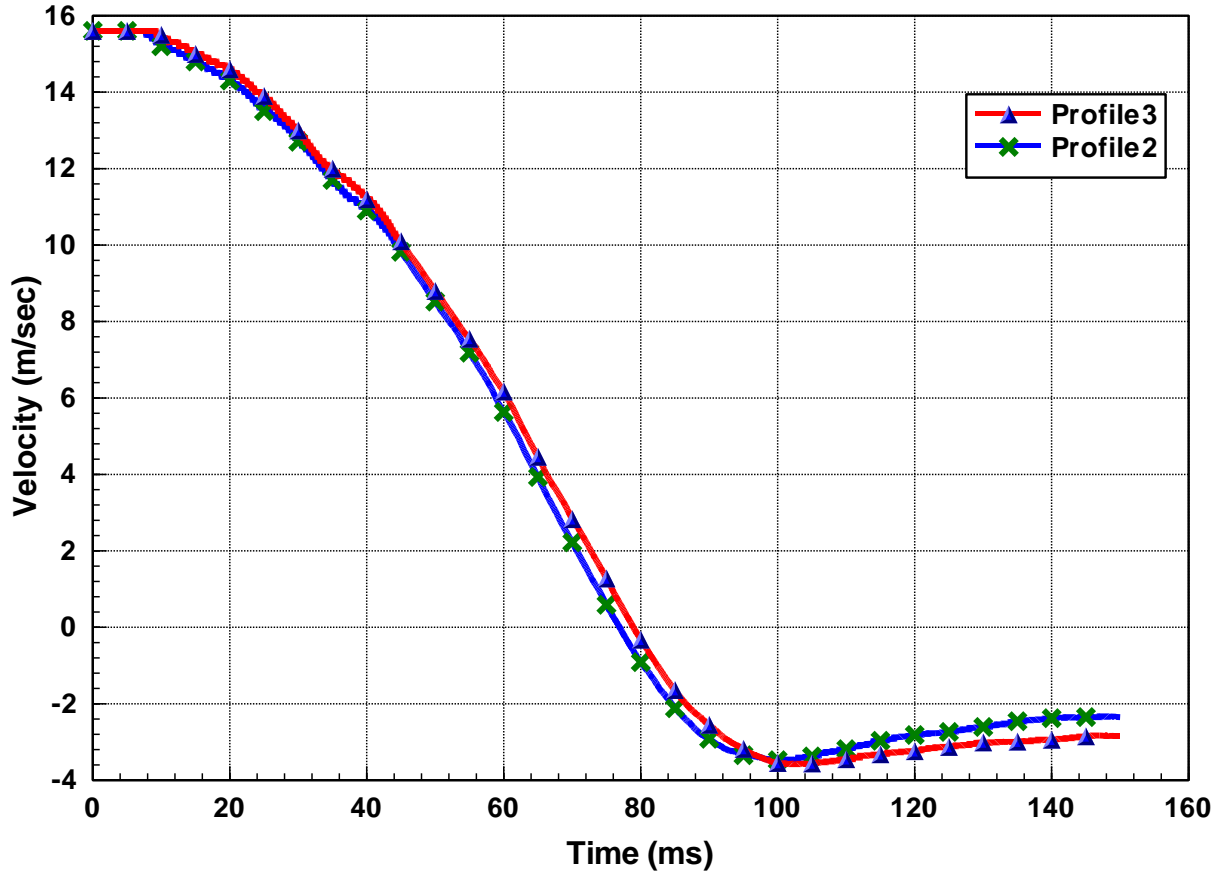


Figure F.2: Mid-size car velocity comparison for different front-end profiles during frontal crash

The SUV model with raised front-end profile (profile1) and lowered front-end profile (profile2) is also tested for frontal crash performances (USNCAP 56 km/h) to make sure these changes don't degrade vehicle performance during frontal crash. Overall acceleration history of vehicle (Figure F.3) indicates no significant difference in vehicle crash pulse (measured at B-Pillar and Rocker Intersection) during frontal crash. It shows that overall peak acceleration of vehicle is not affected by these structural changes in the front-end profile. The comparison of overall vehicle velocity during frontal crash (Figure F.4) also shows that it remains unaffected by these structural changes.

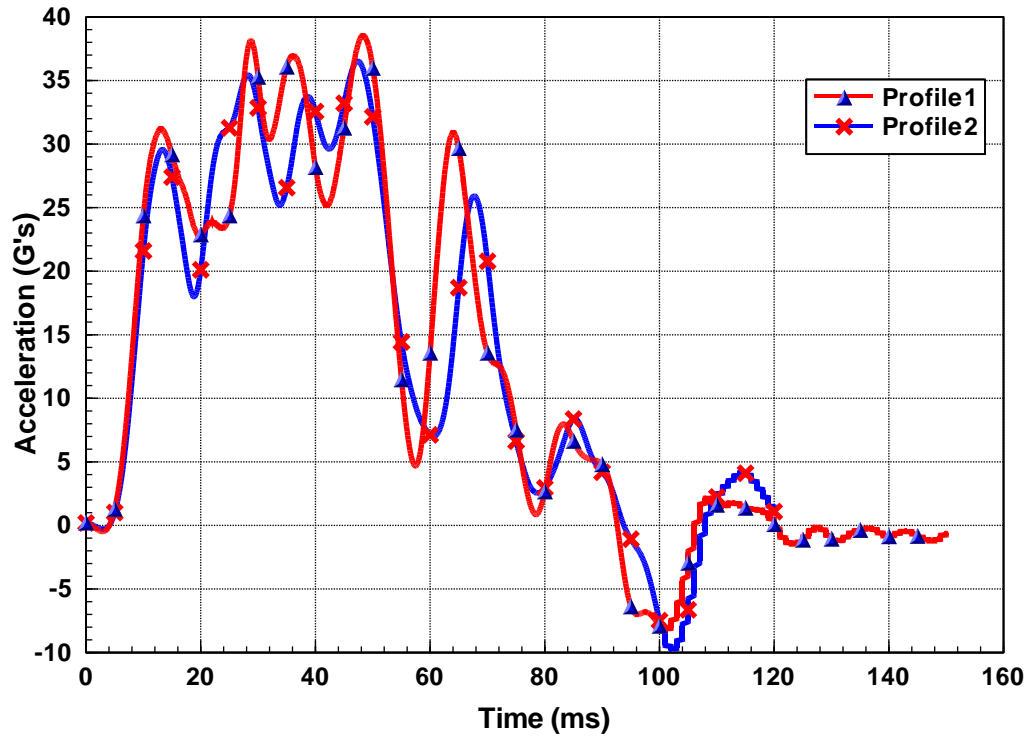


Figure F.3: SUV acceleration comparison for different front-end profiles during frontal crash

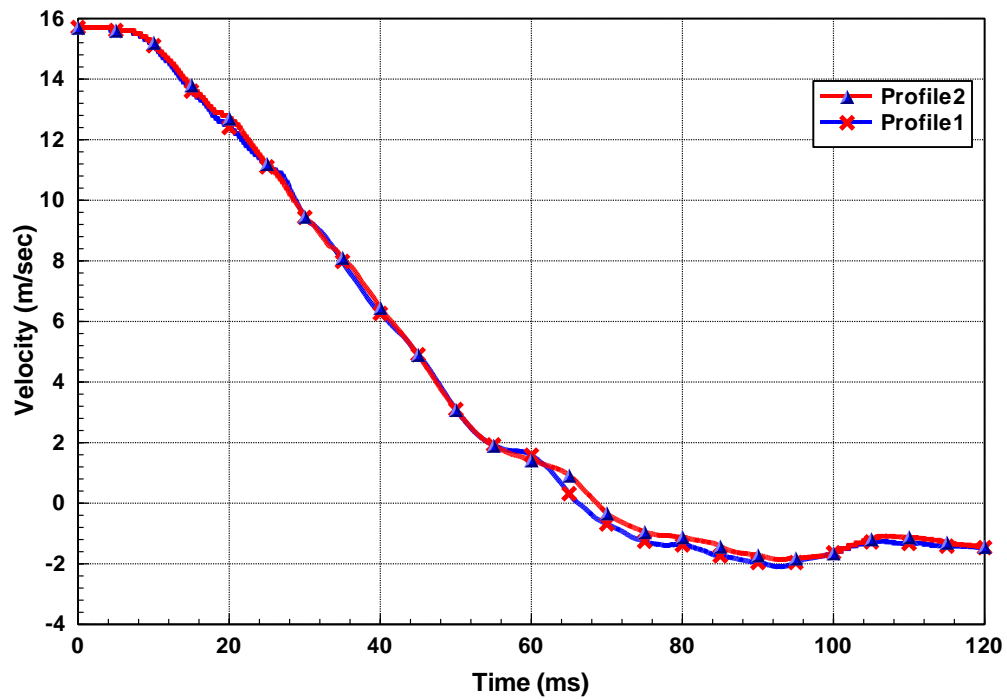


Figure F.4: SUV velocity comparison for different front-end profiles during frontal crash

REFERENCES

- Akiyama, A., Yoshida, S., Matsushashi, T., Rangarajan, N.; Development of Simulation Model and Pedestrian Dummy. SAE paper No. 1999-01-0082.
- Anderson R, McLean J. Vehicle Design and Speed and Pedestrian Injury: Australia's Involvement in the Harmonised Research Activities. Pedestrian Safety Expert Group, 2001
- Atsuhiro K.; Japan Automobile Research Institute, Development of Flexible Pedestrian Legform Impactor (Flex-PLI) and Introduction of Flex-PLI Technical Evaluation Group Activities 2008.
- Bae, H., Jung, H., Lee, K., 2007. The study on developing active hood lift system for decreasing pedestrian head injury. In: 20th International Technical Conference on the Enhanced Safety of Vehicles, Lyon, France.
- Ballesteros, M.F., Dischinger, P.C., and Langenberg, P. (2004) Pedestrian injuries and vehicle type in Maryland, 1995–1999, Accident Analysis and Prevention, Vol. 36 pp. 73–81.
- Barrios J., Aparicio A., Davila A., Miguel J., Modrego S., Olona A., Badea A., Furones A., Paez F., Martin J. (2009) Evaluation of the effectiveness of pedestrian protection systems through in depth accident investigation, reconstruction and simulation.
- Beillas, P.; P.C. Bageman; K.H. Yang; A.I. King; P.J. Arnoux; H.S. Kang; K. Kayvantash; C. Brunet C.; C. Cavallero and P. Prasad P.,2001, Lower Limb: Advanced FE Model and New Experimental Data.
- Bermond, F.; M. Ramet; R. Bouquet and D. Cesari (1994). A finite element model of the

pedestrian leg in lateral impact

- Bjorklund M, Zheng Q (2001) Development and evaluation of a pedestrian anthropomorphic test device [MSc Thesis]. Dept. of Machine and Vehicle Design, Chalmers University of Technology, Göteborg, Sweden.
- Cesari D., Ramet M., Clair P. (1980), Evaluation of Pelvic Fracture Tolerance in Side Impacts. Proceedings 24th Stapp Car Crash Conference.
- Cheng, C.-S., Wang, J. T., 2002, "An Analytical Study of Pedestrian Headform Impacts Using a Dual Asymmetrical Triangle Function," GM R&D Publication No. R&D-9326; Conference Proceedings of Crashworthiness, Occupant Protection and Biomechanics in Transportation Systems, the 2002 ASME International Congress, New Orleans, La.
- Chidester, A., Isenberg, R. 2001. Final Report – The Pedestrian Crash Data Study. National Highway Traffic Safety Administration. United States of America. Paper Number 248.
- Coley, G., Lange, R. de, Oliveira, P. de, Neal-Sturgess, C., Happee, R., Pedestrian Human Body Validation Using Detailed Real-World Accidents, Proc. Int. IRCOBI Conf. Biomechanics of Impact, October 10-12 2001, Isle of Man, United Kingdom, 2001
- Danner, M., Langwieder, K., and Wachter, W. (1979) Injuries to pedestrians in real accidents and their relation to collision and car characteristics. In Society of Automotive Engineers, SAE Paper No. 791008
- Lange, R. de; Happee, R.; Yang, J.K.; Liu X. (2001) Development and validation of full body human pedestrian models, TNO Automotive, The Netherlands

- EEVC (2002) Improved Test Methods to evaluate pedestrian protection afforded by pedestrian cars. Technical Report, European Enhanced Vehicle-Safety Committee, Working Group 17.
- EEVC Working Group 17 Report - Improved Test Methods to Evaluate Pedestrian Protection Afforded By Passenger Cars (December 1998 with September 2002 updates)
- Engin A.E. Measurement of resistive torques in major human joints. Aerospace Medical Research Laboratory, Report AMRL-TR-79-4, 1979
- European New Car Assessment Program (Euro NCAP) - Pedestrian Testing Protocol Version 5.2.1
- European New Car Assessment Program (Euro NCAP) - Pedestrian Testing Protocol Version 6.0
- Fisher, A., Hall, R. (1972) The influence of car frontal design on pedestrian accident trauma. *Accident Analysis and Prevention* **4**, 47–58.
- Genneralli, T.A. (1985) The State of the Art of Head Injury Biomechanics – a Review, Proc. of the 29th Annual American Association for Automotive Medicine (AAAM) Conf.
- Giesen, E.B.W., Van Eijden, and T.M.G.J. (2001) The three-dimensional cancellous bone architecture of the human mandibular condyle. *Journal of Dental Research* **79**: 957-963.
- Glaeser K.P. (1991), "Development of a Head Impact Test Procedure for Pedestrian Protection," BAST Report under contract N° ETD/89/7750/M1/28 to the E.C. (INF GR/PS/150)

Global Technical Regulation No.9, Pedestrian Safety, **ECE/TRANS/180/Add.9**

Gray's Anatomy, 2000

Happee R., Janssen, A.J., Fraterman E., Monster J.W.; Applications of Madymo Occupant Models in Ls-Dyna/Madymo Coupling. 4th European Ls-Dyna User Conference 2003.

Hayamizu, N., Sakuma, S., Hayashi, S., Kozato, A. (2002) Experimental Study of Child Pedestrian Injury – Development of Prototype 6-Years-Old Pedestrian Dummy, proc. of 2002 JSAE Annual Congress.

Hoof J. Van, Lange R. De, Wismans S.H.M. Jac (2003) improving pedestrian safety using numerical human models. Stapp Car Crash Journal, Vol. 47 (October 2003), pp. 401-436

Huang, S., Yang, J. (2009); Optimization of a reversible hood for protecting a pedestrian's head during car collisions

Huang, S., Yang, J. (2010); A reversible bumper system for protecting pedestrian lower limbs from car collisions , International Journal of Vehicle Design, vol. 53, no. 4, pp. 288-299

IHRA (2001) Pedestrian Safety Working Group, Technical Report IHRA/Ps/200, International Harmonized Research Activities.

Ikeda, K., Ishitobi, H., (2003), Development of Aluminum Hood Structure for Pedestrian Protection.

Institute of Traffic Accident Research and Data analysis (ITARDA), Traffic accident statistics annual report, 2007

- Jacobs G., Thomas A. (2002) Africa Road Safety Review: Final Report, US Department of Transportation, Federal Highway Administration, 2002
- Kaneta, Y., Sasahara, N., Kusama, I., Suzuki, D., Ohkawa, H., Hara, T. Injury tolerance of knee joint subjected to dynamic three point bending, Journal of Biomechanical Science and Engineering, 2010.
- Kang, H.S., Willinger, R., Diaw, B., Chinn, B. (1997) Validation of a 3D anatomic human head model and replication of head impact in motorcycle accident by finite element modelling, Proc. of the 41th STAPP Car Crash Conf., pp. 329-338.
- Kendall, R., Meissner, M., and Crandall, J. (2006) The causes of head injury in vehicle pedestrian impacts: comparing the relative danger of vehicle and road surface, SAE Paper 2006-01-0462.
- Kerkeling, C., Schaefer, J., Thompson, G. (2005); Structural hood and hinge concept for pedestrian protection. 2005 ESV, Paper Number: 05-0304
- Kerrigan R. J., Crandall R. J., Deng B.; (2007a) Pedestrian kinematic response to midsize vehicle impact. International Journal of Vehicle Safety.
- Kerrigan, R. J., Crandall R. J., Deng B. (2007b); A Comparative Analysis of the Pedestrian Injury Risk Predicted by Mechanical Impactors and Post Mortem Human Surrogates. Stapp Car Crash Journal, Vol. 52, pp. 527-567
- Klinich K.D., Schneider, L. (2003) Biomechanics of pedestrian injuries related to lower extremity injury assessment tools: a review of the literature and analysis of pedestrian crash database.
- Krieger K.W., Padgaonkar A.J., King A.I. (1976) Full scale experimental simulation of pedestrian-vehicle impacts.

- Lange R. de, Rooij Van L., Happe R., Liu X.J. (2001) Validation of Human Pedestrian Models Using Laboratory Data as well as Accident Reconstruction
- Langlois, J.A., Rutland, W., Wald, M. (2006) The epidemiology and impact of traumatic brain injury: A brief overview.
- Li Y., Qiu J., Liu G., Zhou J., Zhang L., Wang Z., Zhao X., Jiang Z. (2008) Motorcycle Accident in China, Chinese Journal of Traumatology.
- Lissner H. R., Lebow M., Evans F.G. (1960) Experimental Studies on the Relations between acceleration and intracranial pressure changes in man, surgery, Gynecology and Obstetrics Vol 111, PP 329-338.
- Liu Qi, Xia Yong, Zhou Qing, Wang J.T (2009) Design analysis of a sandwich hood structure for pedestrian protection. 2009 ESV, Paper Number: 09-0356
- Longhitano D. (2005a) Torso Injury trends for pedestrian struck by cars and LTVs, proceedings of 19th ESV Washington Dc, USA, Paper 411, 2005.
- Longhitano D, Henary B, Bhalla K, Ivarsson J, Crandall J. (2005b) Influence of vehicle body type on pedestrian injury distribution. SAE world congress 2005
- Lopez Ad, Mathers CD, Ezzati M, Jamison DT, Murray CJ. Global and regional burden of disease and risk factors, 2001: Systematic analysis of population health data.
- MADYMO Human Models Manual release 7.2, January 2010
- Ma D., Obergefell A., Rizer A. (1995): Development of human articulating joint model parameters for crash dynamics simulations. Stapp Car Crash Conference, SAE 952726, 1995.

- Mao H, Zhang L, Jiang B, Genthikatti VV, Jin X, Zhu F, Makwana R, Gill A, Jandir G, Singh A, Yang KH. (2013) Development of a finite element human head model partially validated with thirty five experimental cases. *Journal of Biomechanical Engineering*: 111002-15
- Margulies S.S., Thibault L.E. (1992) A Proposed Tolerance Criterion for Diffuse Axonal Injury in man. *Journal of Biomechanics* 25(8), pp. 917-923.
- Masson C., Serre T., Cesari D. (2007) Pedestrian-Vehicle Accident: Analysis of 4 Full Scale Tests with PHMS, Proceedings of 20th International Technical Conference on the Enhanced Safety of Vehicles, Lyon, France.
- Matsui Y., Ishikawa H., Sasaki A. (1998) Validation of Pedestrian Upper Legform Impact Test- Reconstruction of Pedestrian Accidents, Proc of the 16th Int. Technical Conf. on the enhanced safety of Vehicles, Washington, United States.
- Matsui Y, W. A., Konosu A. Comparison of Pedestrian System Safety Tests Using Impactors and Full-Scale Dummy Tests. *Automotive Crash Research Side Impact, Rollover and Vehicle Aggressivity, SEA 1671, 2002*
- McLean, A. J., Anderson, W. G. (1997); *Biomechanics of Closed head Injuries*.
- Melvin J.W., James W lighthall, Kazunari Ueno. *Brain Injury Biomechanics*.
- Meissener, M., Van, Looij L., Bhalla, K., Crandall, J., Longhitano, D., Takahashi, Y., Dokko, Y., and Kikuchi, Y. (2004) A multi-body computational study of the kinematic and injury response of a pedestrian with variable stance upon impact with a vehicle, *Society of Automotive Engineers Transactions, SAE Paper 2004 01-1607*
- Mohan D. (2002) *Traffic Safety and Health in Indian Cities, Journal of Transport and*

Infrastructure.

Nahum, A.M., Smith, R., Ward, C.C. (1977) Intracranial pressure dynamics during head impact, Proc. of the 21th STAPP Car Crash Conf., pp. 339-366.

National Highway Traffic Safety Administration (NHTSA), "Traffic Safety Facts 2003 Pedestrians", DOT HS 809 769, 2003.

National Highway Traffic Safety Administration (NHTSA), "Traffic Safety Facts 2007 Pedestrians", DOT HS 810 993, 2007

Newman, J.A., "A Generalized Model for Brain Injury Threshold (GAMBIT)", International Conference on the Biomechanics of Impact (IRCOBI), 1986

Nyquist, Gerald W. (1985) Tibia Bending: Strength and Response. SAE #851728

Ommaya A.K., Hirsch A.E., (1971) Tolerance for cerebral concussion from head impact and whiplash in Primates, Journal of Biomechanics 4, pp13-31.

Ono, K., Kikuchi, A., Nakamura, M., Koyabashi, H., Nakamura, N. (1980) Human head tolerance to sagittal impact reliable estimation deduced from experimental head injuries using subhuman primates and human cadaver skulls. Proceedings of 24th Stapp conference, 1980.

Otte, D., and Pohlemann, T. (2001) Analysis and load assessment of secondary impact to adult pedestrians after car collisions on roads. IRCOBI Conference.

Pritz, H., Hassler, C., Herridge, J., and Weis, E.J. (1975) Experimental study of pedestrian injury minimization through vehicle design. Society of Automotive Engineers.

Rooij Van L., Meissner, M., Bhalla, K., Crandall, J. (2003) The evaluation of the kinematics of the MADYMO human pedestrian model against experimental tests

and the influence of a more biofidelic knee joint.

Roudsari, B.S., Mock, C.N., and Kaufman, R. (2005) An evaluation of the association between vehicle type and the source and severity of pedestrian injuries, *Traffic Injury Prevention*, Vol. 6 pp. 185–192.

Ruan, J.S., Khalil, T.B., and King, A.I. (1993) Finite element modeling of direct head impact. Proc. 37th Stapp Car Conference, SAE Paper No.933114. Society of Automotive Engineers, Warrendale, PA.

Schwarz, D., Bachem, H., Opbroek, E. (2004), Comparison of Steel and Aluminum Hood with same design in view of Pedestrian Head Impact.

Stammen JA, Saul RA, Ko B. (2001) Pedestrian Impact Head Testing and PCDS Reconstructions. *ESV*, June 2001

Takahashi Y., Y. Kikuki; F. Mori, and A. Konosu (2003); Advanced FE Lower Limb for Pedestrians

Tamura, Atsutaka (2010) A numerical study of traumatic brain injury due to ground impact in an SUV-pedestrian crash using full-scale finite element model. ASME International Mechanical Engineering Congress and Exposition.

Teresinski G., and Madro R. Ankle joint injuries as a reconstruction parameter in car-to pedestrian accidents, *Forensic Science International* 118 (2001), pp. 65–73

The traffic accident white paper 2002 edition, Japan

The World Bank Group, Road safety.

www.worldbank.org/html/fpd/transport/roads/safety.htm. 2002.

Tomoyuki, M., Junji, H. (2001) Development of a finite element model of the total human body for safety (THUMS) and application to car-pedestrian impacts. 17th

- international ESV conference 2001.
- Trosseille, X., Tarriere, C., Lavaste, F., Guillon, F., and Domont, A. (1992) Development of a F.E.M. of the human head according to a specific test protocol. Proc. 36th Stapp Car Crash Conference.
- Van Hoof, R. de Lange, J. Wismans (2003) Improving pedestrian safety using numerical human models, proceedings of the 47th Stapp Car Crash Conference.
- Versace J. (1971) A Review of the Severity Index. Proceedings of the Fifteenth Stapp Car Crash Conference SAE Paper No. 710881
- Vik, A., Kvistad, K.A., Skandsen, T., Ingebrigtsen, T, (2006); Diffuse axonal injury in traumatic brain injury.
- Wismans, J., Janssen, E., Beusenbergh, M., Koppens, W., Happee, R., Bovendeerd, P. (2000) Injury Biomechanics, Eindhoven University of Technology, Netherlands.
- Yamada, H. Strength of Biological Materials, The Williams & Wilkens Co., Baltimore, 1970.
- Yang, J. 1995. Computer Simulation of Shearing and Bending Response of the Knee Joint to a Lateral Impact. Proc. 39th Stapp Car Crash Conference, SAE Paper No. 952727, pp 251-264.
- Yao, J., investigations of Head impact dynamics, Injury Mechanisms and countermeasures in car to pedestrian accidents [PhD thesis 2010], Chalmers University of Technology, Göteborg, Sweden.
- Yoganandan, N. (1994) Biomechanics of Skull Fracture. Proceedings of Head Injury 94 Symposium, Washington DC.
- Zhang, L., Yang, K.H., and King, A.I. A Proposed Injury Threshold for Traumatic Brain Injury. Journal of Biomechanical Engineering 2004.

Zhou, C., Khalil, T.B., and King, A.I. (1995) A new model comparing impact responses of the homogeneous and inhomogeneous human brain. Proc. 39th Stapp Car Crash Conference, SAE Paper No. 952714. Society of Automotive Engineers, Warrendale, PA.

ABSTRACT**PEDESTRIAN HEAD PROTECTION DURING CAR TO PEDESTRIAN ACCIDENTS: IN THE EVENT OF PRIMARY IMPACT WITH VEHICLE AND SECONDARY IMPACT WITH GROUND**

by

VISHAL GUPTA**May 2014****Advisor:** Dr. King H. Yang**Co-advisor:** Dr. Trilochan Singh**Major:** Mechanical Engineering (Biomechanics)**Degree:** Doctor of Philosophy

Current regulations for assessing pedestrian safety use a simplified test setup that ignores many real-world factors. In particular, the level of protection is assessed using a free-motion headform impacting the vehicle's hood at a fixed angle. As such, this test setup does not capture the effect due to the vehicle front-end profile, nor does it comprehend injury due to a possible secondary impact of the pedestrian's head with ground. This thesis aims to numerically simulate vehicle to pedestrian crashes to develop knowledge that may suggest ways to improve safety above and beyond the regulatory tests. Inputs to the simulations include the vehicle front-end profile, impact speed, and pedestrian size. Outputs include the angle of primary head impact to the hood, the extent of head injury (HIC), and whether or not there is a secondary head impact with the ground.

One key finding is that head impact angles, and hence head injury measures, vary greatly due to changes in vehicle front-end profile. This suggests that the current test

setup for assessing pedestrian head impact, which assumes a fixed head-impact angle, could be improved to better capture the kinematics of real-world pedestrian crash events. One improvement could be the use of a full scale pedestrian dummy or human body model rather than a free motion headform. A second finding is that severity of head injury is much greater in a secondary head impact with ground than in the primary impact with the hood. Moreover, it is possible to avoid the secondary head impact with ground by careful designing of vehicle front-end profile. More research needs to be carried out to prove that concepts developed through numerical simulations also works in physical tests.

AUTOBIOGRAPHICAL STATEMENT

VISHAL GUPTA

EDUCATION

06/2000	B.E., Mechanical Engineering, Punjab Technical University, India
08/2007	M.S., Mechanical Engineering, Wayne State University, MI
05/2014	PhD., Mechanical Engineering, Wayne State University, MI

EXPERIENCE

09/2001-07/2003	Mechanical Engineer, Abhishek Industries Limited, Trident Group of Industries, India
08/2003-08/2005	Lecturer, Mechanical engineering Department, Guru Gobind Singh College and Baba Banda Singh Bahadur Engineering College affiliated to Punjab Technical University, India
08/2006-08/2007	Graduate Teaching Assistant, Mechanical Engineering department, College of engineering, Wayne State University, MI
08/2007-08/2008	Automotive CAE Engineer, Detroit Engineered Products (DEP), Troy, MI
08/2008-03/2010	Automotive CAE Engineer, Engineering Technology Associates (ETA), Troy, MI
03/2010-10/2011	Automotive CAE Engineer, Detroit Engineered Products (DEP), Troy, MI
11/2011- till date	Automotive CAE Engineer, Vehicle Optimization Methods, General Motors, Warren, MI

PUBLICATION AND PRESENTATION

Gupta V, Yang KH. "Effect of vehicle front end profiles leading to pedestrian secondary head impact to ground". Stapp Car Crash J. 2013 Nov;57:139-155.